Graduate Theses and Dissertations   Graduate School

January 2015

Experimental Investigation of Encapsulated Phase Change Materials for Thermal Energy Storage

Tanvir E. Alam
University of South Florida, tanvir@mail.usf.edu

Experimental Investigation of Encapsulated Phase Change Materials for Thermal Energy Storage

by

Tanvir E Alam

A dissertation submitted in partial fulfillment
of the requirements for the degree of
Doctor of Philosophy
Department of Mechanical Engineering
College of Engineering
University of South Florida

Co-Major Professor: D. Yogi Goswami, Ph.D.
Co-Major Professor: Ajit Mujumdar, Ph.D.
Jaspreet Dhau, Ph.D.
Elias Stefanakos, Ph.D.
Muhammad M. Rahman, Ph.D.
Manoj K. Ram, Ph.D.
Abdul Malik, Ph.D.

Date of Approval:
June 28, 2015

Keywords: Packed Bed, Latent Heat, Spherical Capsule, Macroencapsulation, Polymer Coating, Metal Coating

DEDICATION

I dedicate this dissertation to my parents, my wife and my brothers for their support,
inspiration, encouragement, and patience.

ACKNOWLEDGMENTS

First and foremost, I would like to express the deepest gratitude and most sincere appreciation to my advisor, Dr. D. Yogi Goswami, for giving me the opportunity to pursue research in the field of solar energy engineering. His encouragement, guidance, and support helped me to learn and think more about the clean and green planet. I would also like to thank my co-major professor Dr. Ajit Mujumdar for all the assistance he provided throughout these years. Especial credit goes to Dr. Jaspreet Dhau who guided me from beginning to the end of my Ph.D. program. I would also like to thank my advisory committee, Drs. Elias Stefanakos, Muhammad M. Rahman, Manoj K. Ram, and Abdul Malik for their support and suggestions.

I am grateful to Dr. Chand K. Jotshi, Dr. Burton Krakow, Mr. Charles Garretson, Mrs. Barbara Graham, and Mrs. Ginny Cosmides who helped me in the course of my stay in Clean Energy Research Center (CERC). I would like to thank my friends in CERC, Chatura Wickramaratne, Rachana Vidhi, Abhinav Bhardwajh, Rajeev Kamal, Philip Myers, Saeb Besarati, Jamie Trahan, Yanyang Zhang , Mehdi Zeyghami, Antiono Ramos, Barry Osterman-Burgess and Francesca Moloney for their support and help.

I am grateful to my parents and my brothers for their unconditional support throughout my life. Last but not the least, I would like to acknowledge my wife, Farhana, for her patience, understanding and encouragement throughout my studies.

TABLE OF CONTENTS

LIST OF TABLES

LIST OF FIGURES

vii

ABSTRACT

Thermal energy storage (TES) is one of the most attractive and cost effective solutions to the intermittent generation systems like solar, wind and other renewable sources, compared to alternatives. It creates a bridge between the power supply and demand during peak hours or at times of emergency to ensure the continuous supply of energy. Among all the TES systems, latent heat thermal energy storage (LHTES) draws lots of interests as it has high energy density and can store or retrieve energy isothermally. Two major technical challenges associated with the LHTES are low thermal conductivity of the phase change materials (PCMs), and corrosion tendency of the containment vessel with the PCMs. Macro-encapsulation of the PCM is one of the techniques to encounter the low thermal conductivity issue as it will maximize the heat transfer area for the given volume of the PCM and restrict the PCMs to get in contact with the containment vessel. However, finding a suitable encapsulation technique that can address the volumetric expansion problem and compatible shell material are significant barriers of this approach.

In the present work, an innovative technique to encapsulate PCMs that melt in the 100-350 ^{o}C temperature range was developed for industrial and private applications. This technique did not require a sacrificial layer to accommodate the volumetric expansion of the PCMs on melting. The encapsulation consisted of coating a non-reactive polymer over the PCM pellet followed by deposition of a metal layer by a novel non-vacuum metal deposition technique. The fabricated spherical capsules were tested in different heat transfer fluid (HTF) environments like air, oil and molten salt (solar salt). Thermophysical properties of the PCMs were investigated by

ix

DSC/TGA, IR and weight change analysis before and after the thermal cycling. Also, the constrained melting and solidification of sodium nitrate PCM inside the spherical capsules of different sizes were compared to explore the charging and discharging time. To accomplish this, three thermocouples were installed vertically inside the capsule at three equidistant positions. Low-density graphene was dispersed in the PCM to increase its conductivity and compared with pure PCM capsules.

A laboratory scale packed-bed LHTES system was designed and built to investigate the performance of the capsules. Sodium nitrate (m.p. 306°C) was used as the PCM and air was used as the heat transfer fluid (HTF). The storage system was operated between 286°C and 326°C and the volumetric flow rate of the HTF was varied from 110 m^3/h to 151 m^3/h. The temperature distribution along the bed (radially and axially) and inside the capsules was monitored continuously during charging and discharging of the system. The effect of the HTF mass flow rate on the charging and discharging time and on the pressure drop across the bed was evaluated. Also, the energy and exergy efficiencies were calculated for three different flow rates.

Finally, a step-by-step trial manufacturing process was proposed to produce large number of spherical capsules.

x

CHAPTER 1:

INTRODUCTION

1.1 General Background

A drastic change in the climate due to the emission of greenhouse gasses, growing need of energy and diminishing reserves of the fossil fuel inclines the mankind towards sustainable and clean energy resources such as solar energy. Even though it is available in abundance, its intermittent nature hinders the widespread implementation as a cost effective and reliable energy resource. Efficient energy storage is essential to overcome this problem. Out of all available energy storage techniques, thermal energy storage shows the greatest potential as it is a simple, cost effective, efficient and reliable method [1].

Three types of TES systems are being investigated, especially for concentrated solar power (CSP) plants [2]. Sensible heat thermal storage (SHTES) is the most frequently used and commercially available TES technology [2, 3], however, LHTES is fast emerging as a viable alternative to SHTES [2]. This is partly due to the fact that the LHTES has a higher energy storage density than the SHTES [4-6]. The high energy storage density implies a smaller storage tank leading to a substantial decrease in the overall cost of the storage system. One of the major drawbacks associated with the LHTES is the longer charging and discharging times potentially leading to inefficient energy retrieval from the system. The main reason for this is the low thermal conductivity of the PCMs [7, 8]. Various methods have been presented to increase the PCM thermal conductivity. Insertion of nano or expanded graphite mixture [9, 10] and metal particles into the PCM matrix increases the thermal conductivity of the PCM. Micro- and macro-

1

encapsulation of PCMs have also been shown to improve the heat transfer rate [11-16]. Recently, in packed bed thermal storage systems, macroencapsulation technique has been considered as one of the heat storage approaches to encounter the low thermal conductivity problem of the PCMs [14-16].

1.2 Research Objective

The main goal of the investigation is to develop a macroencapsulated spherical capsule to enhance the heat transfer rate of the PCM for LHTES system in a temperature range between 50 and 350°C. The capsule must withstand the highly corrosive environment of molten alkali metal nitrate based salts and their eutectics, must exhibit good compatibility with the Heat Transfer Fluid (HTF), as well as have the ability to survive thermal cycles at elevated temperatures. Later, thermal and cyclic performances of these spherical capsules are tested in a packed-bed latent heat storage system. Brief descriptions of the content in the chapters are mentioned below:

Chapter one highlights the general background of the storage system and the research objective of the present work.

Chapter two presents the literature survey of the past works associated with thermal energy storage, heat transfer rate enhancement techniques, macroencapsulation, and melting and solidification inside a spherical capsule.

Chapter three discusses about an innovative technique to spherically encapsulate PCMs. It does not need a sacrificial layer to accommodate the volumetric expansion of the PCM on melting. The spherical capsules are tested in different heat transfer fluid (HTF) environments like air, oil and molten salt (solar salt) and their thermophysical properties are investigated using DSC/TGA, IR and weight change analysis before and after thermal cycles.

Chapter four provides a description of the construction of a laboratory scale packed-bed LHTES setup with encapsulated PCM and the performance of the spherical capsules inside the packed-bed. Temperature profiles at various axial positions in the storage system are determined for three different flow rates. The pressure drop across the bed is measured and compared with the theoretical analysis. Also, the energy and exergy efficiencies of the system are calculated for three different flow rates.

Chapter five discusses the melting and solidification of different size spherical capsules filled with sodium nitrate PCM. Also, 5 wt% and 7 wt% of graphene is used as the high conductive dispersion particle to enhance the heat transfer rate during solidification and compared with pure PCM capsules.

Chapter six discusses the manufacturing process steps of the encapsulated PCM for latent heat storage systems.

Finally, chapter seven summarizes the conclusions based on the experimental study and also suggests future recommendations for further studies in this area.

3

In this chapter, a literature survey of recent studies associated with thermal energy storage, storage materials, heat transfer rate enhancement techniques, macroencapsulation, laboratory scale latent heat packed-bed storage system with encapsulated PCMs and melting/solidification inside a spherical capsule are discussed.

2.1 Thermal Energy Storage

TES can be utilized to minimize the difference between supply and demand of the periodic sources of generation. Three processes are involved in a TES system: charging, storing, and discharging/ retrieving [17]. For instance, consider a TES system combined with a concentrated solar power plant. At daytime, the parabolic trough collects energy from the sun and transmits it through the HTF. During the charging stage, a fraction of the high temperature HTF is pushed through the heat exchanger of TES and heat is conveyed from the HTF to the storage media. During the night the discharge mode starts, and a low temperature HTF is pumped through the TES in the reverse direction. As it passes through the TES, it absorbs the thermal energy from the system.

Zalbe et al. [18] and Fernandes et al [19] mentioned certain characteristics and requirements for design of an efficient TES in the literature. These are summarized as follows.

---

[1]The content of 2.5 was published in T.E. Alam, J. Dhau, D.Y. Goswami,, E. Stefanakos, "Macroencapsulation and characterization of phase change materials for latent heat thermal energy storage systems," Applied Energy. 2015, 154, 92-101. DOI: 10.1016/j.apenergy.2015.04.086. Permission is included in Appendix C.

[2]The content of 2.6 was published in TE Alam, J Dhau, D.Y. Goswami, M.M. Rahman, and E.. Stefankos. "Experimental Investigation of a Packed-Bed Latent Heat Thermal Storage System With Encapsulated Phase Change Material,". In ASME 2014 International Mechanical Engineering Congress and Exposition. (2014, November). Permission is included in Appendix C.

a) TES materials should have high energy density to make the TES compact in size

b) Storage material should be mechanically and chemically compatible with the TES

c) Maintained in suitable operating temperature range with appropriate storage medium

d) TES should store/retrieve relatively high energy at a shorter temperature gradient

e) Prolonged lifespan with stable performance of the system and no degradation of the storage capacity

f) Easy controlling option

g) Well insulated to minimize the heat loss and degradation in the storage capacity

h) Cost effective system

2.2 Categories of Thermal Energy Storage

TES can be classified into three different categories. These are mentioned in figure 2-1 and discussed in the following sections.
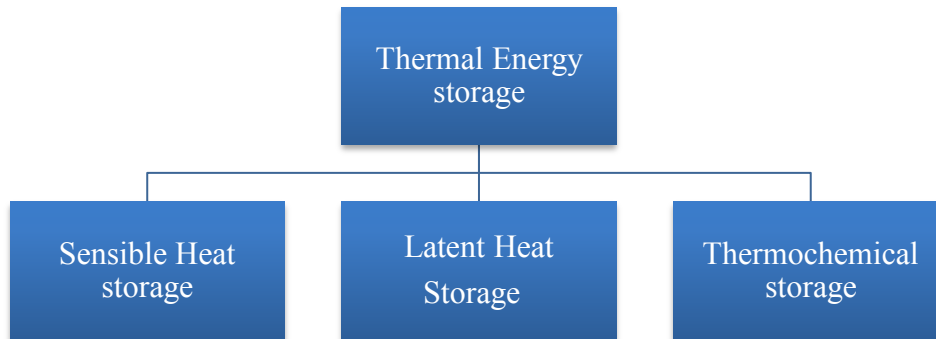
Figure 2-1: Category of thermal energy storage

2.2.1 Sensible Heat Storage

The energy storage capacity of the sensible heat storage (SHS) depends on the temperature difference of the inlet and outlet, specific heat capacity of the storage material and the total mass of the storage media. [20]. This type of storage is extensively investigated and used commercially in the power plants [2, 3]. It is expressed by the formula

$$Q = \int_{T_i}^{T_f} mC_p dT = mC_p(T_f - T_i) \qquad (1\text{-}1)$$

Q = amount of heat (kJ)

m = mass of storage material (kg)

C_p = specific heat capacity (kJ/ kg^{o}C)

T_i = initial temperatures of SHS (°C)

T_f = final temperatures of SHS (°C)

Depending on the storage medium, the SHS is classified in solid or liquid base system (rock, concrete, metal, molten salt, synthetic oil and mineral oil).

2.2.2 Latent Heat Storage

Latent heat storage (LHS) stores energy by absorbing or releasing the latent heat of fusion or vaporization of the storage material at the phase change temperature. LHS can store a large amount of energy compared to SHS in same volume for a smaller temperature range [20]. It is expressed by the formula

$$Q = \int_{T_i}^{T_m} mC_p dT + mL + \int_{T_m}^{T_f} mC_p dT = m[C_{sp}(T_m - T_i) + L + C_{lp}(T_f - T_m)] \quad (1\text{-}2)$$

Q = amount of heat (kJ)

m = mass of storage material (kg)

C_{sp} = specific heat capacity in solid state (kJ/ kg^{o}C)

C_{lp} = specific heat capacity in liquid state (kJ/ kg^{o}C)

T_m = melting temperatures of storage material (°C)

T_i = initial temperatures of LHS (°C)

T_f = final temperatures of LHS (°C)

L= latent heat of fusion (kJ/kg)

Due to the difficulty in handling high-pressure gases, and due to the high costs associated with the construction of storage systems for the liquid-vapor transition, most of the investigation and research has been conducted on solid- liquid transition of the material. According to Stekli et al. [1], LHS can be categorized into tank PCM TES and encapsulated PCM TES.

Regin et al. [21] summarized three basic components to develop an effective LHS. These are presented as follows.

a) Low-cost suitable storage material with higher latent heat of fusion for desired temperature range

b) Durable storage material containment system

c) Larger surface area to transfer the heat from the source to the storage material and from storage material to the heat sink efficiently.

2.2.3 Thermochemical Storage

The core component of the thermochemical storage system is the reversible endothermic chemical reaction. To achieve the high efficiency, the reversibility of the chemical reaction needs to be ensured. As the heat from the heat source is brought to exhilarate the endothermic chemical reaction, it will absorb the heat. If the reaction is reversible, the heat can be extracted. The energy density of this type of storage system is higher compared to other two storage systems. However, this technology is still at a very premature stage to go for commercialization.

2.3 Phase Change Material for LHTES

Numerous researchers have conducted investigations on wide range of organic and inorganic PCMs. Lane et al. [20], Zalbe et al. [18], Abhat [22], Farid et al. [23] Regin [21], Sharma et al. [24] have summarized the characteristics of PCMs needed for efficient TES system design. These are presented as follows.

7

a) High latent heat of fusion, high specific heat both in solid and liquid state, and high energy density to reduce the size of the storage system. It should also show insignificant volume of expansion and low vapor pressure during the phase change period.

b) A desirable melting/solidification temperature corresponding with the operating temperature limit.

c) High thermal conductivity to achieve required heat transfer between the HTF and the storage media and insubstantial supercooling during solidification.

d) Congruent melting to avoid segregation of the component.

e) Chemically stable, non-toxic, non-explosive and non-corrosive to protect the containment vessel.

f) Abundantly available and cheap.

Zalbe et al. [18] presented a comparison between organic and inorganic PCMs. Organic materials such as waxes or paraffin, terpenes, and low molecular weight alkanes have been studied by many researchers [25-29] for low temperature applications (below 100°C). The problem associated with the organic PCMs, compared to inorganic PCMs, is that they have lower latent heat of fusion, lower thermal conductivity, and higher flammability [18]. In general, inorganic PCMs possess higher energy density than the organic PCMs and also have higher temperature utilization ranges [7].

Salt hydrates can be used as a potential PCM as they show higher latent heat of fusion [18, 24]. The main problem associated with salt hydrates is their incongruent melting and subcooling of the PCM during freezing. To neutralize the subcooling effect, various nucleating agents need to be added which leads to a rise in the overall cost of the TES system [30].

8

Organic and hydrate PCMs have high chance of oxidation and formation of PCM solution that can reduce the storage density. Encapsulating the PCM can solve this problem.

In this research, inorganic PCMs and their eutectic, having temperature range of 100° C to 400° C, will be discussed as most of the Rankine cycle based solar plants (maximum temperature limit of synthetic oil is 400^oC) and waste heat recovery systems use this range [3,7,31] of temperature. The PCMs used for the research are listed in table 2-1.

Table 2-1: Inorganic PCM with melting point ranging from 100^oC to 400^oC [7, 32-34]

Phase Change Material (wt%)	Melting Point (^{o}C)	Latent Heat of fusion (kJ/kg)
$LiNO_3$(30%) –$NaNO_3$(18%)-KNO_3(52%)	122	140.6, (140)*
$LiNO_3$(33%) –KNO_3(67%)	133	170, (172)*
$LiNO_3$(57%) –$NaNO_3$(43%)	193	248
$LiNO_3$(49%) –$NaNO_3$(51%)	194	265, (267)*
KNO_3(54%) –$NaNO_3$(46%)	222	100, (120)*
$LiNO_3$	253	373(362)*
$NaNO_3$	306	177, (172)*
KNO_3	335	88, (92)*
NaCl(34.81)-KCl(32.29)-LiCl(32.90)	346	281, (130)*
$MgCl_2$(60)- NaCl(19.6)-KCl(20.4)	380	400, (232)*

* Measured in CERC, University of South Florida

Nitrate based PCM and their eutectics have considerably high latent heat of fusion at the same time these are chemically stable and low cost. The chloride-based eutectics in table 2-1 are hygroscopic.

2.4 Heat Transfer Enhancement Techniques

As it is mentioned earlier, low thermal conductivity is the major problem associated with the PCM-based LHTES. Thermal conductivity of the most PCMs falls in the 0.3-0.6 W/m.K range [35]. During charging of the system, melting of the PCM is faster as it is a natural

9

convection dominated process. However, heat transfer rate during solidification is low between the capsule and the HTF as it forms a high resistance solid layer on the inner wall of the capsule. As it starts creating the solid layer, conduction becomes dominant and consequently discharging takes a longer time. Jegadheeswaran et al. [36], Agyenim et al. [37] and Cárdenas et al. [31] reviewed different techniques to enhance the heat transfer rate of the PCM based LHTES system. The following techniques presented in figure 2-2 are adopted to elevate the heat transfer rate in the PCM based LHTES.
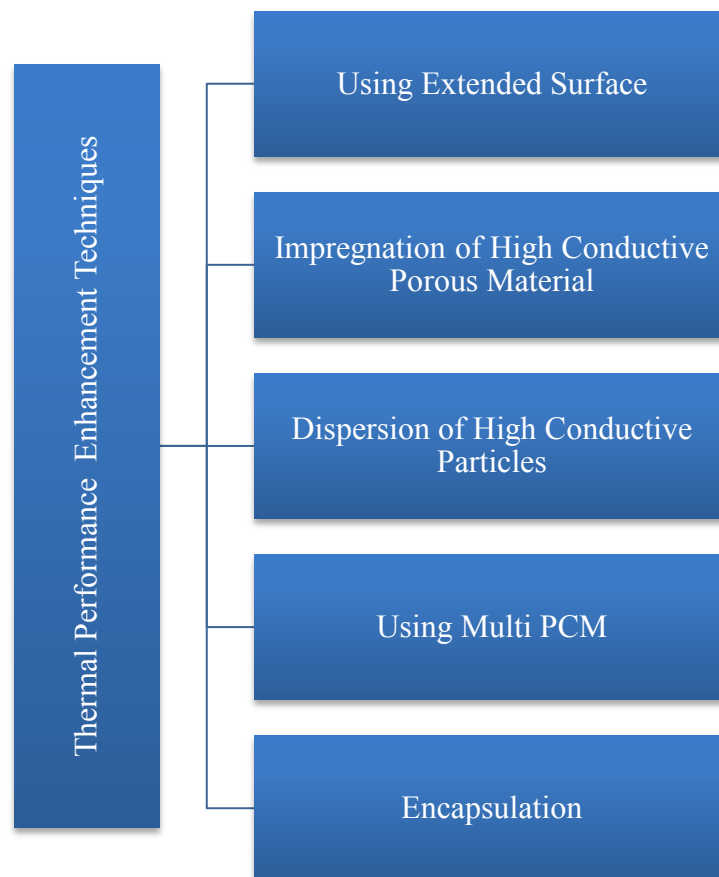
Figure 2-2: Various categories to enhance the heat transfer rate in the PCM based LHTES

Figure 2-3 summarizes various methods employed by the researchers to enhance the heat transfer rate [37].
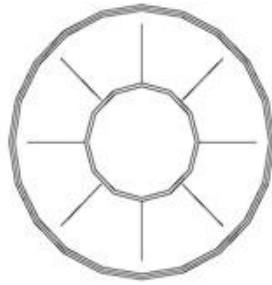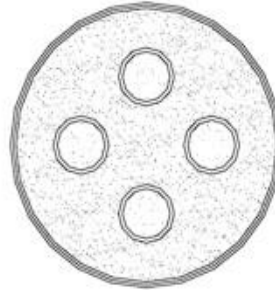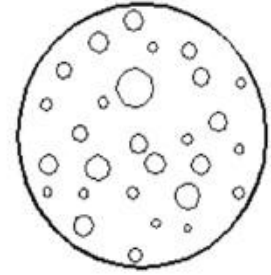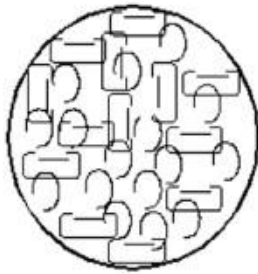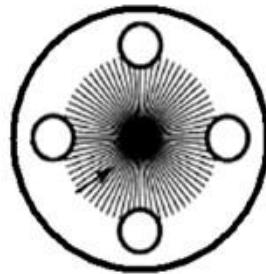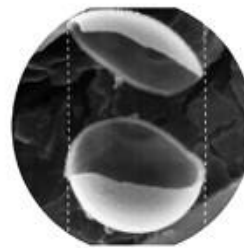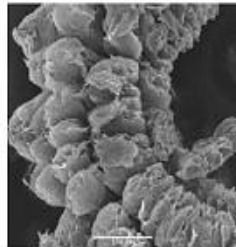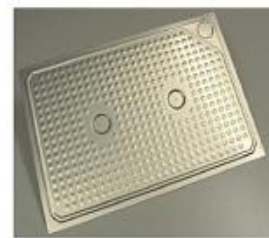
Figure 2-3: Various methods employed by the researchers to enhance the heat transfer rate [37] (permission is in Appendix C)

11

To maximize the heat transfer area in the TES fins or extended surfaces are employed. If the conductivity of the PCM is lower than HTF, the fin will be placed in the PCM side or vice versa [38]. Melting and solidification process dynamics has the influence of the configuration and orientation of the fin [36]. Lacroix and Benmadda [39] conducted a research on the horizontal fin configuration in rectangular box and concluded that instead of having a larger number of short fins, it is more effective to have fewer long fins in the system. Optimization of the number of fins depends on the wall temperature. Shatikian et al. [40] found that the performance of the enhancement depends upon optimization of both number of fins and thickness. Steinmann [41] tested aluminum fins in $NaNO_3$ PCM for 400 hours and found that aluminum fins are compatible with $NaNO_3$. Other materials like graphite foil, steel and copper can also be employed as the fin material.

Porous matrices made of steel, stainless steel, aluminum, copper, and graphite can be impregnated in the PCM based LHTES to enhance the heat transfer rate. Mesalhy et al. [42] numerically investigated a horizontal cylindrical annulus structure and concluded that the performance of enhancement technique depends upon the pore size and the thermal conductivity of the material in the matrix. Recently, Fiedler et al. [43] compared aluminum and copper based porous matrices and found that the copper matrix had approximately 80% more effective thermal conductivity than the aluminum matrix. Even though melting and solidification time of the storage material reduces by employing the metal structures significantly, compatibility of the PCM and the porous structure has always been an issue.

Multi-PCM-based LHTES refers to using a number of PCMs with various melting points in the storage system. Employing multiple PCMs with decreasing melting points ensures a higher temperature difference between the HTF and the PCM in the flow direction, which will lead to

12

higher heat transfer performance of the system [36]. Wang et al. [44] were the first group to introduce a novel technique to enhance the heat transfer rate. Michels and Pitz-Paal [34] conducted an experimental exploration on multiple PCMs in shell and tube configuration. Synthetic oil was used as the HTF and allowed it to go through the tube and three PCMs were placed in the shell side. It was found from the experiment that single PCM storage with a higher melting point has a lower storage/retrieval capacity compared with a multi-PCM storage with three PCMs. Charging and discharging experiments were demonstrated with three different melting point PCMs by Farid and Kanzawa [45]. They observed an improvement of ten percent in the heat transfer rate. Cylindrical enclosures were used to load three different PCMs and air was used as HTF. In case of multi-PCM system, all the PCM started melting at the same time whereas for single capsules, it started at different time. Multi PCM system is one of the more efficient ways to improve the performance of the system by enhancing the heat transfer rate. However, selection of right combination of PCMs is still a challenge [31].

Dispersing particles in the PCM is one of the most efficient and simplest ways to enhance the conductivity of the PCM [31]. Hoover [46] is the pioneer of conducting research on particle impregnation technique to improve the thermal conductivity. Khodadadi et al. [47] conducted an extensive review on the enhancement of the heat transfer rate by dispersing particles in the PCM. Lots of materials have been employed as the particles such as metals (Ag, Cu, and Al), metal oxides (Al_2O_3, MgO, CuO and TiO_2), carbon nano tubes, graphite, silver nanowires, and carbon based nano particles (graphene flakes) [47]. Mettawee and Assassa [48] conducted an experimental investigation to improve the thermal conductivity of PCM by dispersion of micro aluminum particles. It was found that there was a sixty percent reduction in the charging time as compared to pure PCM by adding the particle Zeng et al. [49] investigated the effect of silver

13

nanoparticles in 1-tetradecanol and found that silver nanoparticles did not show any strong reaction with 1-tetradecanol. Overall, the thermal conductivity of the PCM increased with the increase of silver nanoparticles. Xie et al.[50], Hong et al.[51] , Weinstein et al. [52] , Zeng et al. [53], and Kim and Drzal [54] employed alumina (Al_2O_3), MgO, graphite nanofibers, multi-walled carbon nanotubes, and exfoliated graphite nanoplatelets, respectively and all observed the enhancement of the heat transfer rate. Recently, researchers have shown great interest in graphene to improve the thermal conductivity of PCM [55-57]. Some important properties of graphene are presented in table 2-2. As most of the works have been conducted with low temperature PCMs, this area has much open space for future work.

Table 2-2: Important properties of graphene for thermal conductivity improvement

Material	Thermal Conductivity $(W \cdot m^{-1} \cdot K^{-1})$	Specific surface area $(m^2 \cdot g^{-1})$
Graphene	~5000 [58]	~2630 [58]

Khodadadi and Hosseinizadeh [59] reported that overall latent heat of the PCM composite decreased with the increasing wt% of the particles, though the thermal conductivity of the composite increased. Hence, optimization of the mass fraction of the particle and latent heat of the PCM is quite important.

2.5 Encapsulation[1]

Another method to enhance the heat transfer rate is by utilizing micro- (capsule size ~1-1000 μm) or macroencapsulated (capsule size above 1000 μm) PCMs [60]. Considerable work has been carried out on microencapsulation of the low melting point (50-120°C) inorganic salt hydrates and organic materials such as waxes, terpenes, low molecular weight polymers, etc [61-66]. Compared to macroencapsulation, the microencapsulation of PCMs provides faster charging

14

and discharging rates because of the shorter distance for heat transfer. However, the lower PCM-to-coating mass ratio (~1:1) greatly reduces the energy storage density of the storage media and increases the storage capital cost [20]. Recently, Zhang *et al.* [67] encapsulated $NaNO_3/KNO_3$ PCM in AISI 321 tubular capsules. Zheng *et al.* [68] fabricated spherical capsules with copper as the PCM and chromium-nickel as the shell material. The fabricated capsules have been shown to withsand 1000 thermal cycles. Vincent and Silva [69] tested parafin wax in rectangular steel shell in horizontally hollow brick for 8 days. Zhao [70] and Zheng *et al.* [71] have reported an encapsulation technique that uses stainless steel/carbon steel as the shell material. The process follows a post-formed approach where cylindrical steel capsules are fabricated first and then filled with PCM followed by welding a cap at the top. The major challenge in this approach is countering the corrosion of the metal cans from the molten salt at high temperatures. Mathur *et al.* [72] have demonstrated a ceramic-based macroencapsulation technique for the sodium nitrate pellets (5-15 mm in diameter). The technique involves the decomposition of a sacrificial polymer layer to provide a void in between the coating and core PCM, which is needed for accommodating expansion of the PCM during the phase transition period. Some of the other techniques [73, 74] reported in the literature are tabulated in Table 2-3.

Table 2-3: Macroencapsulation techniques and materials

S. No	Core (PCM) Material	Shell material	Core to Shell ratio	Temperature of operation (^{o}C)	Geometry of capsules	Average size of capsules	Thermal Cycles	Ref.
1.	$NaNO_3$-KNO_3	AISI 321	-	160-270	Cylindrical	27.3/39/75 mm*	5000	[67]
2.	Copper	Chromium-Nickel	4:1	1050-1150	Spherical	2 mm	1000	[68]
3.	Paraffin wax	Steel	-	0-36	Rectangular	(30×18×2.8 cm)	8 days	[69]
4.	$NaNO_3$, NaCl-$MgCl_2$, $MgCl_2$, Al	Stainless steel, carbon steel	-	300-450/ 300-750	Cylindrical		60 / (480 h)	[70, 71]

15

Table 2-3 (Continued)

S. No	Core (PCM) Material	Shell material	Core to Shell ratio	Temperature of operation (^{o}C)	Geometry of capsules	Average size of capsules	Thermal Cycles	Ref.
5.	NaNO$_3$, molten salt	Ceramic – metallic	-	300-550	Spherical	5-15 mm	2500	[72]
6.	Hydrated salts, paraffin, fatty acids, bio PCM	Polyolefin	-	(-64)-120	Spherical	98 mm	-	[73]
7.	Paraffin, salt hydrate	Aluminum, plastics	-	(-10)-100	Box, bag	-	-	[74]
8.	NaNO$_3$, KNO$_3$, NaNO$_3$-KNO$_3$, NaNO$_3$-KNO$_3$-LiNO$_3$	PTFE-Nickel	8:1/12:1	120-350	Spherical	27.43 mm	2200 (5133 h)	[16]

*same diameter and height

2.6 Heat Transfer Study in Latent Heat Packed-Bed Storage[2]

A latent heat packed-bed storage system uses a single tank. The benefit of using this type of storage is the low cost of the system. As the PCM (filler material) needs to be non-reactive with the HTF in the packed-bed containment, it is better to encapsulate the PCM. Numerous studies have been conducted to analyze the overall performance of this type of storage by many research groups [21,75-86]. Saitoh [75] observed the effectiveness of spherical capsules over other geometries. Ozturk [76] used paraffin as PCM to experimentally investigate the thermal effect of the LHTES on greenhouse heating. Regin [21, 77] presented a review on utilizing organic PCM base capsules in a latent heat thermocline system and exhibited a numerical analysis of the system. Michel and Pitz-Paal [34] reported an experimental and numerical investigation of a shell and tube type cascaded LHTES system using alkali metal nitrates as PCMs. Recently, Esakkimuthu et al. [81] employed 75 mm spherical containers containing a low

16

temperature inorganic salt (melting point of 55°C) PCM in a packed-bed system integrated with a solar air heater. Xiao and Zhang [82] performed experiments with low temperature organic PCMs in cylindrical capsules and investigated the charging and discharging time, efficiency, and temperature profile of the PCM in a packed-bed environment. Zheng et al. [83] experimentally and numerically discussed the thermal energy storage using sodium nitrate (NaNO$_3$) PCM contained in cylindrical steel containers (25.4 cm $\times$ 3.81 cm (h $\times$ r)). Bellan [84] worked on the numerical investigation of the encapsulated NaNO$_3$ LHTES system and optimized the main parameters of the storage tank. Peng [85] also carried out a numerical analysis of a LHTES system containing sodium nitrite as the PCM, examined the temperature distribution inside the bed, and established the relationship of charging and discharging efficiency with the HTF flow rate and capsule size. Nithyanandam et al. [86] investigated the dynamic response of a thermocline energy storage system and provided guidelines for constructing an encapsulated PCM-based packed bed storage for CSP plant operation.

2.7 Melting and Solidification in Spherical Capsules

Melting and solidification within the spherical containers can be classified into constrained and unconstrained categories. In the presence of a thermocouple, the solid PCM clasps itself to the thermocouple and restrain it from sinking or rising inside the capsule due to density difference of two phases of the PCM. This is called fixed or constrained melting. On the other hand, in the absence of a thermocouple, direct contact melting next to the capsule wall is observed as the solid PCM sinks or rises up inside the capsule due to density difference of two phases of the PCM. This is called unconstrained or unfixed melting [87].

Saitoh [75] explored a thermal storage system with various geometrically shaped capsules filled with organic PCM and concluded that spherical capsules exhibited the best

17

storage performance. Moore and Bayazitoglu [88] conducted a numerical and experimental investigation with low temperature PCM in a spherical glass enclosure considering unconstrained melting. The numerical result had shown good agreement with the experimentally investigated data. Roy and Sengupta [89] conducted further study on melting in spherical geometry. This analysis was assumed to have constant wall temperature and high solid density and the analytical modeling was adopted from Bareiss and Beer's [90] model for cylindrical geometries. The predicted results of the numerical solution were compared with the experimental data presented by Moore and Bayazitoglu [88] and showed good agreement. Bahrami and Wang [91] also employed the same model [90] of unconstrained melting in the spherical geometry with a modified assumption. Roy et al. [92] later proposed a gravity-assisted model for melting PCM in a sphere with an isothermal boundary condition, in which they considered the natural convection effect during unconstrained melting. Saitoh et al. [93] presented a numerical and experimental investigation of spherical capsule using n-octadecane and water considering inner wall temperature distribution. Fomin and Saitoh [94] considered the wall temperature of a spherical capsule as a sinusoidal function and developed a numerical model for the unconstrained melting process. The obtained results were in good agreement with a discrepancy not more than ±15%. Cho and Choi [95] reported an experimental investigation of paraffin and paraffin-water mixture as the PCM in a spherical capsule for observing the melting and solidification and heat transfer co-efficient. It was found that the heat transfer coefficienct of pure material was 40% more than the mixture. Caldwell and Chan [96] compared two different numerical methods, the enthalpy method and the heat balance integral method for solidification in the spherical containment; they found that both methods showed good agreement for higher Stefan numbers. Ismail and Henriquez [97] also reported a numerical solidification based model

18

of a spherical vessel with PCM. The model was validated with available experimental results and found good agreement. Khodadadi and Zhang [98] developed a buoyancy driven convection model for constrained melting of PCM in a spherical capsule. Eames and Adref [99] conducted a solidification experiment with water in spherical capsules and developed an empirical relation to predict the solid fraction inside the capsule. Barba and Spiga [100] compared three different geometries and demonstrated that solidification took the shortest time in small spherical capsules. Later, Ismail and Henriquez [101] conducted a parametric study on ice formation inside a spherical capsule to find the effects of capsule size, inlet temperature on solidification. Wei et al. [102] performed an experimental and numerical investigation with PCM to observe the solidification phenomena of various geometries. Spherical geometry shows the best performance with the numerical and experimental data agreeing to within 10%. Chan and Tan [103] conducted a solidification experiment in spherical capsules where n-hexadecane was employed as PCM. The observation was made for constant temperature of the surface and concluded that initially the solidification rate is high and uniformly concentric. With time, the solidification rate decreases and forms a void inside the sphere. Tan [104] reported the visual observation of fixed and unfixed melting inside a spherical capsule using organic PCM for different wall temperatures. Later, Tan et al. [105] compared the experimental findings with numerical simulation for fixed melting of PCM inside a sphere. It was observed that the melting time in experimental finding was faster than in numerical studies, which was due to thermal stratification of the enclosure bath water. Rizan et al. [106] conducted an experimental investigation of melting in a spherical container. They also employed organic PCM, and uniform heat flux condition was maintained on the wall boundary. The highlight of the study was the effect of Stefan number on the melt fraction rate. Recently, Archibold et al. [107] numerically

19

investigated the heat transfer rate during the melting of NaNO$_3$ PCM inside a spherical capsule. They validated their numerical model with Tan's [104] experimental model and found good agreement. Also, calculated the liquid mass fraction of NaNO$_3$ and finally proposed a correlation for the liquid mass fraction, which will be helpful for designing thermal energy storage systems. Later, the same group proposed another numerical model for freezing in a spherical shell with NaNO$_3$ as PCM; this time they included the effect of simultaneous conduction, convection and thermal radiation during solidification [108].

2.8 Scope of Research

In this study, molten alkali metal nitrate based salts and their eutectics are selected as the PCM. The challenge is to fabricate encapsulated PCMs that can withstand the highly corrosive environment and the volumetric expansion of the PCMs on melting. The present work is concerned with the stability of the encapsulation material and thermophysical properties of the PCM before and after thermal cycling in various environments like air, thermal oil and molten salt.

As is evident from the literature survey, most of the LHTES studies have either been carried out for low temperature encapsulated PCMs ($<100^{o}$C) [81-82] or high temperature PCMs (m.p. $>300^{o}$C) encapsulated in large metallic cylindrical containers [83]. There are a few reports on the numerical analysis of high temperature LHTES based on macro or microencapsulated spherical PCMs capsules[84-86]; however, there is no report on the experimental demonstration of the packed-bed LHTES system that contains high temperature encapsulated spherical PCM capsules (m.p. $>300^{o}$C). As a result, this investigation focuses on constructing a packed-bed LHTES system with fabricated spherical capsules, and also, on evaluating the thermal performance of the system by measuring the temperature profile for different flow rates.

20

Lack of reports on melting and solidification of different-sized spherical capsules filled with high temperature PCM, points of the need for the study in this direction. In this investigation, different-sized complete capsules will be tested to observe the temperature profile and their charging discharging time. As graphene has lower density than $NaNO_3$ PCM and has higher thermal conductivity, various wt% of graphene are used as the dispersion particle to improve the heat transfer rate and compared with pure $NaNO_3$ capsules.

21

CHAPTER 3[1]:

MACROENCAPSULATION OF PHASE CHANGE MATERIAL FOR LATENT HEAT THERMAL ENERGY STORAGE

The present study was undertaken to fabricate encapsulated PCMs that can withstand the highly corrosive environment of molten alkali metal nitrate based salts and their eutectic. We report herein, an innovative approach to encapsulate salts and eutectics in the temperature range of 100-350°C [15,16]. The developed encapsulation technique does not require a sacrificial layer to accommodate the volumetric expansion of the PCMs on melting and reduces the chance of metal corrosion inside the capsule.

3.1 Encapsulation of PCM

There are three major concerns in the encapsulation of PCMs:

a) The first concern is to accommodate a large volumetric expansion of the PCM on melting.

b) The second concern is the pressure build-up due to the expansion of air as the temperature goes up during charging, if air is present in the capsule.

c) The third concern is the reactivity of the molten PCM with the encapsulant materials. The salts used in the present study are alkali metal nitrates, which are powerful oxidizers, especially in the molten state. These salts are highly reactive with a variety of metal, organic and inorganic materials [109-113].

---

[1]The content of 3.1 to 3.2 was published in T.E. Alam, J. Dhau, D.Y. Goswami,, E. Stefanakos, "Macroencapsulation and characterization of phase change materials for latent heat thermal energy storage systems," Applied Energy. 2015, 154, 92-101. DOI: 10.1016/j.apenergy.2015.04.086. Permission is included in Appendix C.
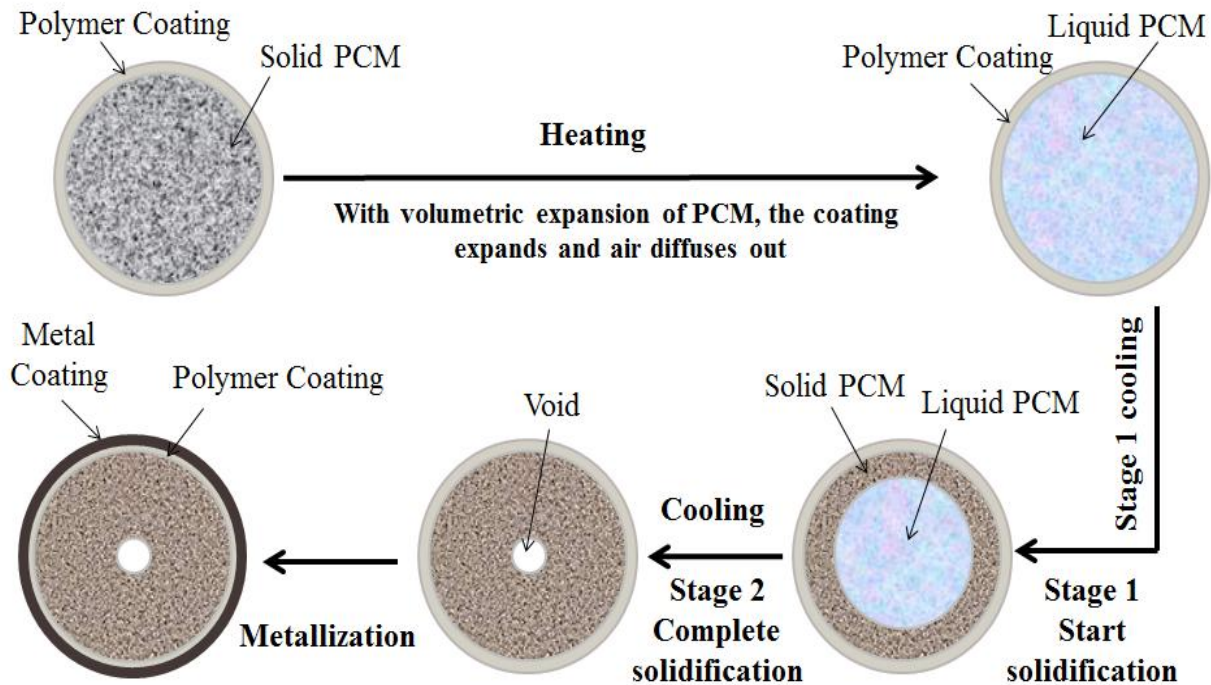
Figure 3-1: PCM encapsulation model
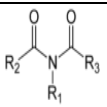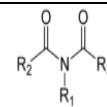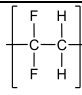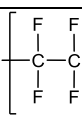
A selectively permeable coating that lets the hot air diffuse out but not the molten PCM will overcome the problem of pressure buildup due to the expansion of air on heating. Since the PCM solidifies from the outside-in (during the cooling process), it is postulated that an impervious solid layer will be formed that would prevent the air to diffuse back-in (Fig. 3-1). A flexible coating that can expand and contract would accommodate the large volumetric expansion of the PCM on melting. Therefore, a polymer coating that is both flexible and selectively permeable in nature was conceived to address the first concern.

3.1.1 Material Compatibility Study

In order to study the compatibility of the PCMs with the encapsulating material (third concern), a systematic study on the thermal and chemical behavior of the selected polymers with molten PCMs was conducted by thermal gravimetric analysis (TGA). The PCMs selected for the present study include sodium-, potassium- and lithium nitrate, and their eutectics. Three sets of

www.manaraa.com

polymers; non-fluorinated, partly-fluorinated and fully-fluorinated, were selected for the present study (Table 3-1).

Table 3-1: Effect of alkali metal nitrates on the thermal and chemical stability of the selected polymers

Polymer	Monomer Unit	Onset decomp. temp.	Onset decomp.[b] temp. with NaNO$_3$	Latent Heat (kJ/kg)			Molten nitrate salts (Testing temperature)		
				KNO$_3$ (92)[a]	NaNO$_3$ (172)[a]	LiNO$_3$ (362)[a]	KNO$_3$ (354°C)	NaNO$_3$ (326°C)	LiNO$_3$ (275°C)
PIF		569°C	467°C	91	157	343	Reactive	Reactive	Reactive
PI-84 (Resin)		-	-	86	146	341	Reactive	Reactive	Reactive
PVDF		441°C	436°C	86	173	363	Reactive	Reactive	Non-reactive
FEP		470°C	470°C	93	174	375	Non-reactive	Non-reactive	Non-reactive
PTFE		534°C	534°C	92	174	368	Non-reactive	Non-reactive	Non-reactive

[a]Values in the parentheses represent the latent heat of the as-received salts. [b]Decomp. = Decomposition

The TG analysis was performed at a ramp rate of 10°C/min under an inert (Argon) atmosphere. As evident from Fig.3-2, polyimide-film (PIF) has the highest, and PVDF the lowest thermal stability among the as-received polymers. However, their thermal behavior changed in the presence of molten sodium nitrate (NaNO$_3$). The decomposition onset temperature of the PIF decreased by more than 100°C (Table 3-1, Fig. 3-3).
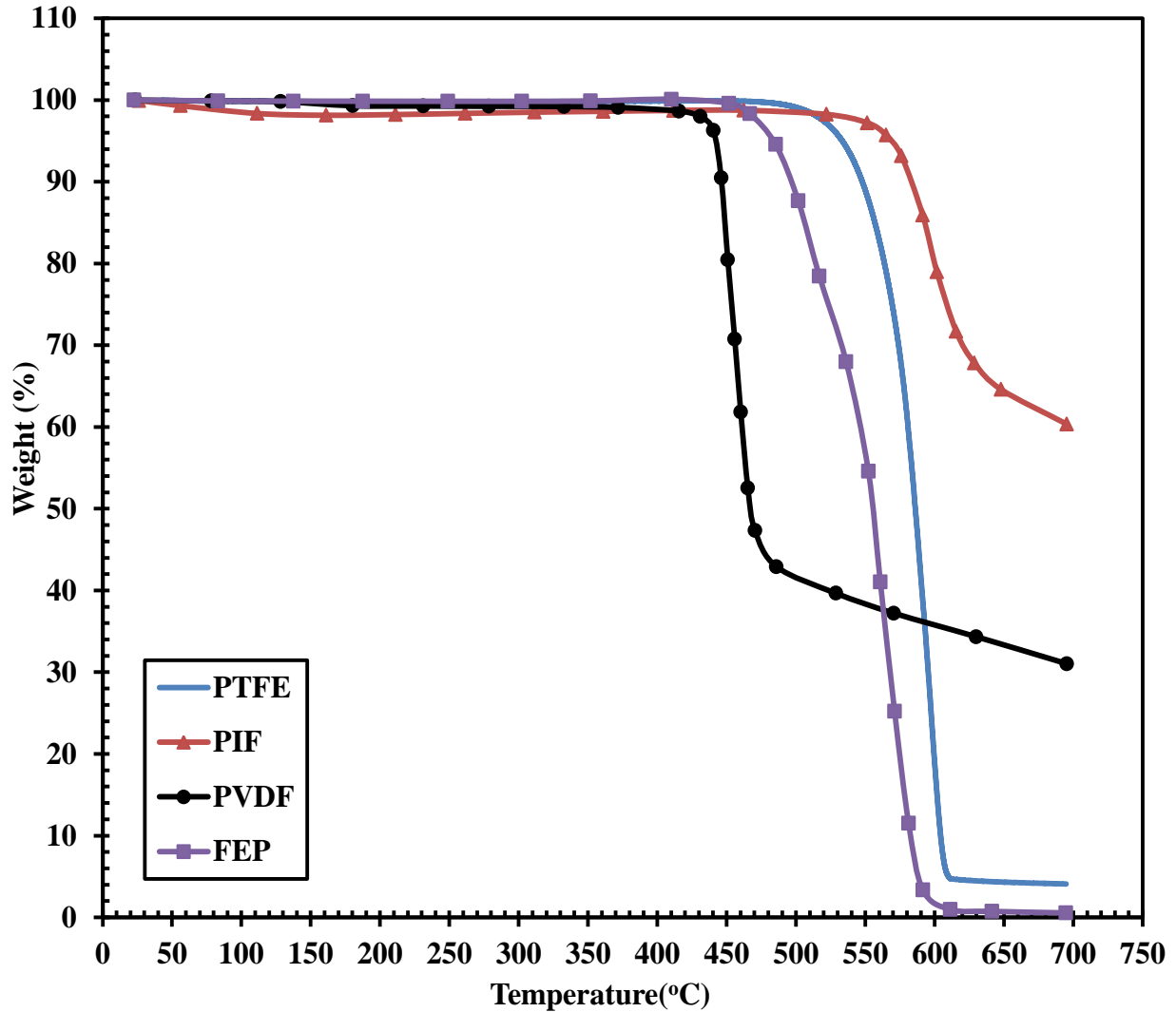
Figure 3-2: TGA of the selected polymers alone

In addition, an abrupt weight change was noticed at 466°C that signals the decomposition of NaNO$_3$ (onset of decomposition for the as-received NaNO$_3$ starts at 626°C). There is practically no change in the onset decomposition temperature of PTFE and FEP. PVDF shows a small decrease in the onset decomposition temperature and an additional step corresponding to the decomposition of NaNO$_3$ at 470°C. Based on these results, the thermal and chemical stability of the studied polymers is found to be as follows:

PIF > PTFE > FEP > PVDF   As-received

PTFE > FEP > PIF> PVDF   In the presence of molten NaNO$_3$

25
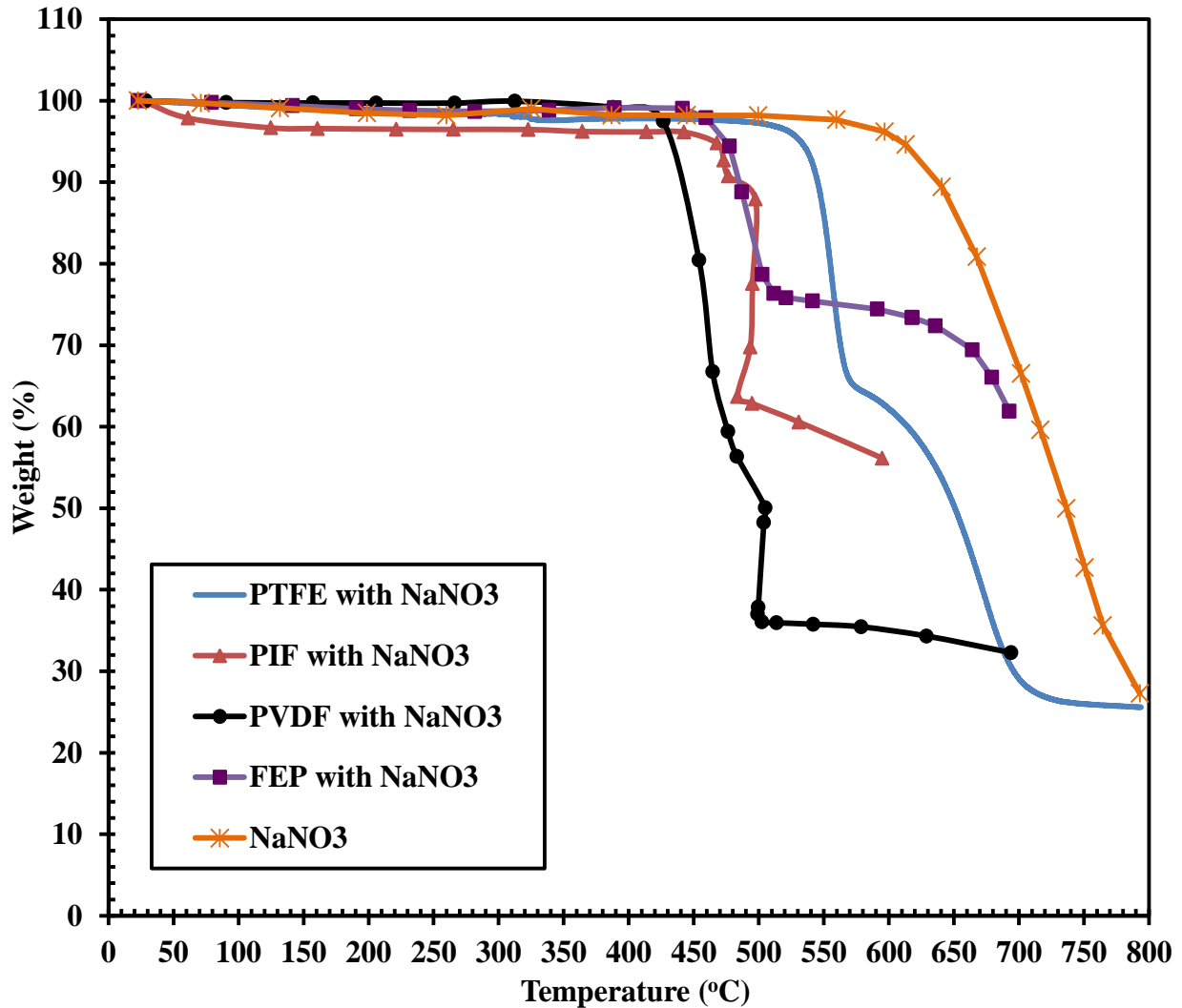
Figure 3-3: TGA of the selected polymers with NaNO$_3$

The selected polymers were also subjected to the isothermal Thermogravimetric analysis(TGA) in order to examine the suitability of these polymers over a long duration of usage at a temperature of 20°C above the melting point of the nitrate salts (326°C in the case of NaNO$_3$). No significant weight change was noticed for PTFE and FEP, whereas PI-84 and PVDF showed substantial weight loss (Figs. 3-4 and 3-5). Although no significant weight change was noticed in the PI-film there was substantial reduction in the latent heat value of NaNO$_3$ (152 kJ/g). The TGA of the polymers with KNO$_3$ gave results similar to those polymers with NaNO$_3$ (Fig.3-6).

26
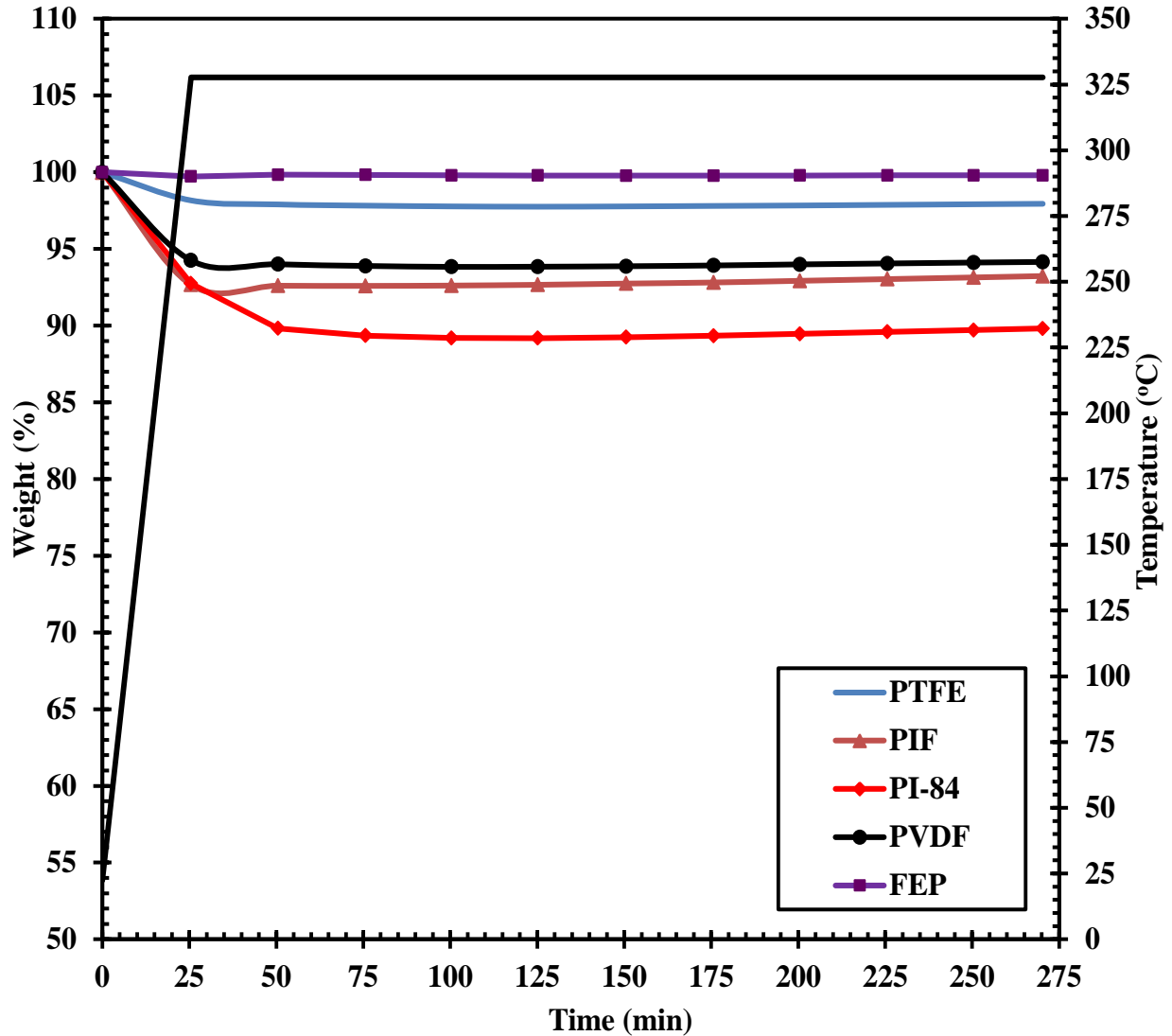
Figure 3-4: Isothermal TGA (4 h at 326°C) of as-received polymers

Unlike $NaNO_3$ and KNO_3, the PI-film showed substantial weight loss in the presence of molten $LiNO_3$. PI-84 showed an even more severe reaction, whereas PTFE, FEP and PVDF practically remained unreactive with the molten $LiNO_3$ (Fig. 3-7). It is evident from the later discussion that PIF, PI-84 and PVDF are not suitable for encapsulation of the nitrate based PCMs. The fully fluorinated polymers, PTFE and FEP, are the best materials to encapsulate PCMs as they showed no sign of reaction with the molten salts. PTFE was further tested for long hours(1000 thermal cycles) under high temperature and found stable with 0.2% of weight loss.

27
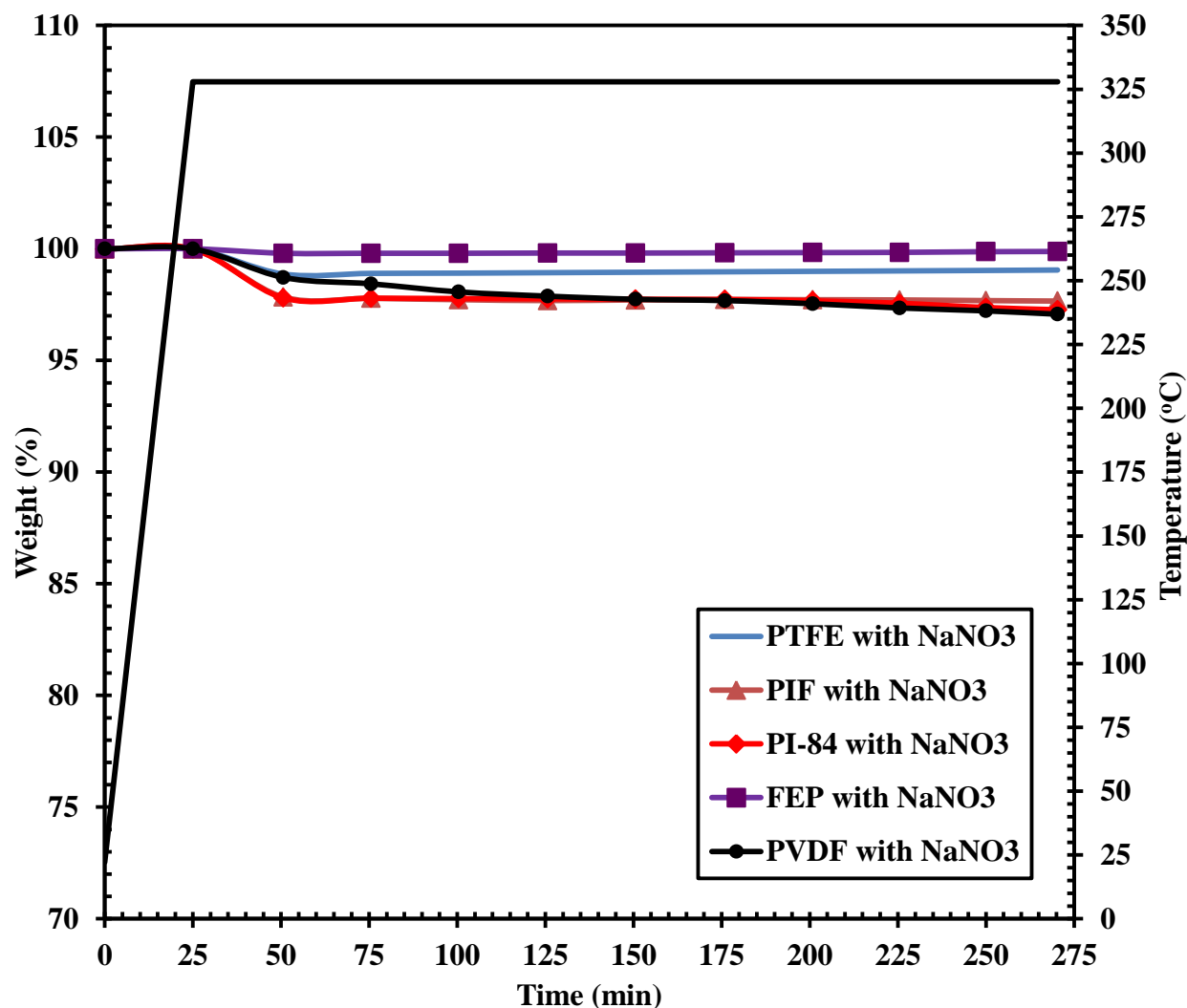
Figure 3-5: Isothermal TGA (4 h at 326°C) of polymers in the presence of NaNO$_3$

3.1.2 Encapsulation Procedure

3.1.2.1 Polymer Coating

NaNO$_3$ powder was pressed in a hydraulic press at 980 N of force to form hemispherical pellets of 12.5 to 25.5 mm diameter. This size range was chosen as optimum based on earlier theoretical modeling studies by Ramos-Archibold *et. al.* [107, 114]. The pressed pellets were then coated with a layer of polymer by using the jar-milling technique. The loosely held polymer particles were pressed in a hydraulic press at 980 N of force to form a thin polymeric film over the pellet. In another variation, a PTFE film was wrapped around the pellet and the whole pellet

28

was pressed in the hydraulic press to form a PTFE layer. It is desirable to have the PCM to polymer shell mass ratio as large as possible. However, practical fabrication of a uniform layer of polymer that would hold intact during cycling limited the thickness to $0.5 - 0.7$ mm (Fig. 3-8a) that gave the PCM-to-polymer mass ratio below 12:1. The coated capsules were heated to a temperature beyond the melting point of the PCM and then cooled to below the melting point to solidify the PCM.
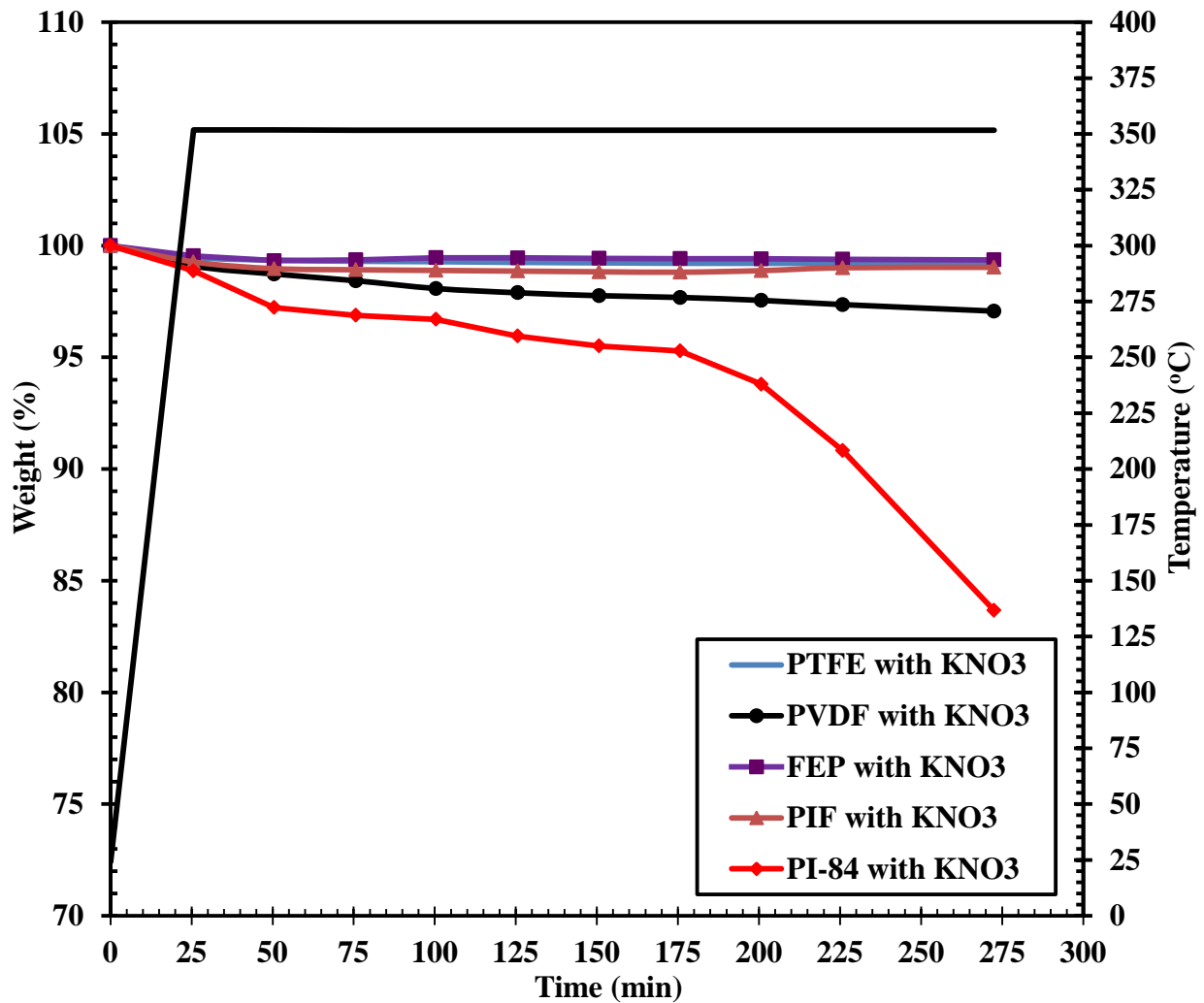
Figure 3-6: Isothermal TGA (4 h at $350\,^{\circ}C$) of polymers in the presence of KNO_3

As postulated (Fig. 3-1), the PCM solidifies from outside-in, therefore, the increased size of the capsule was maintained. As evident from Fig. 3-8b, a void zone is naturally formed within

29

the capsule when the remainder of the PCM solidifies. This void provides space for the expansion of the PCM when it melts again in the capsule. Two inch diameter $NaNO_3$ capsules were made with 18:1 core to shell ratio using the same technique. These capsules passed 1000 thermal cycle without failure (table 3-2). In another variation, PTFE-FEP composite material was used to encapsulate the $NaNO_3$-KNO_3 eutectic, whereas FEP alone was used to encapsulate the eutectic salts that melt below 200°C (Table 3-2). Thermophysical properties of the PCMs were measured after certain number of thermal cycles and it was found that there were no degradations of the properties in the PCMs.
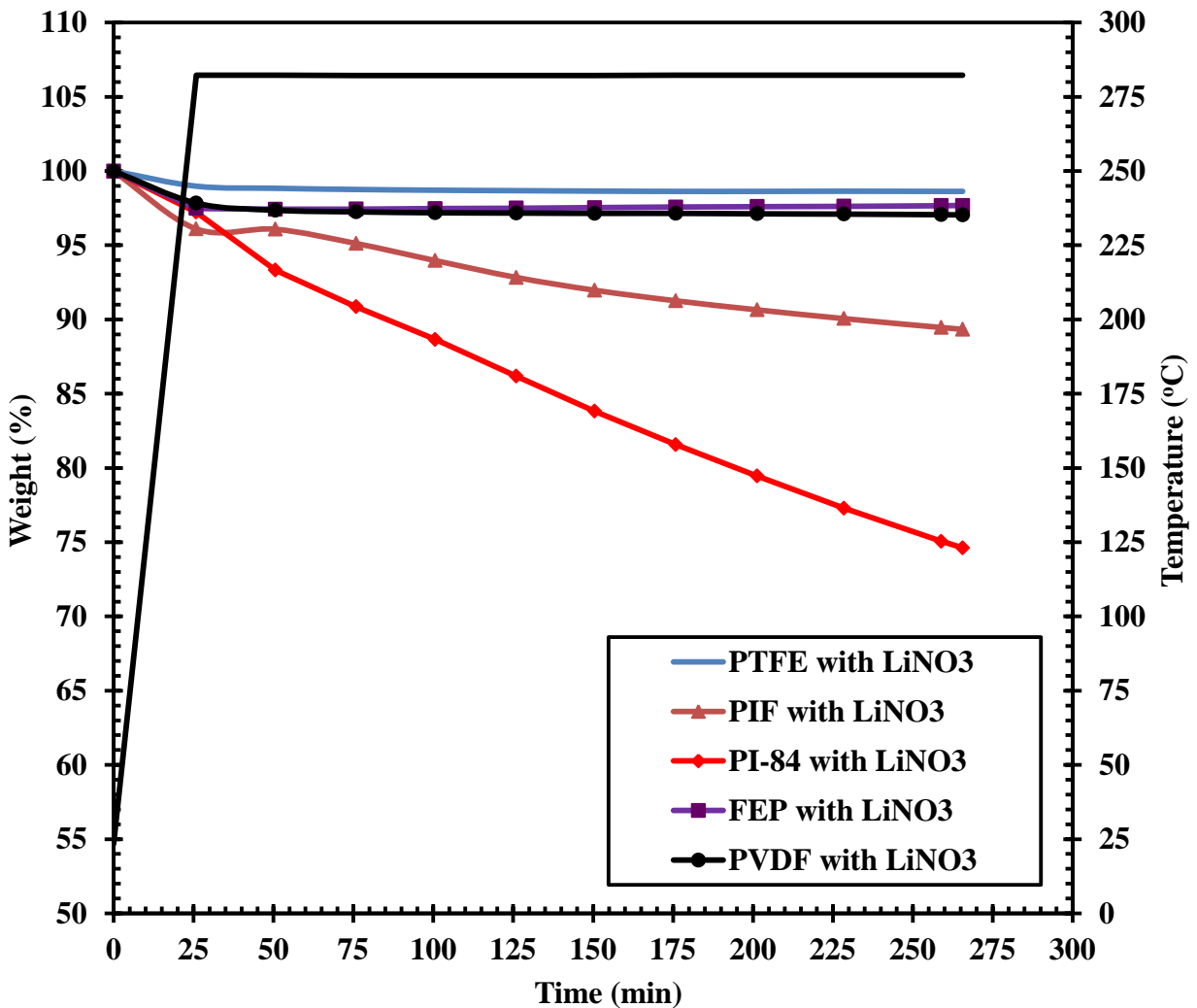
Figure 3-7: Isothermal TGA (4 h at 280°C) of polymers in the presence of $LiNO_3$

30
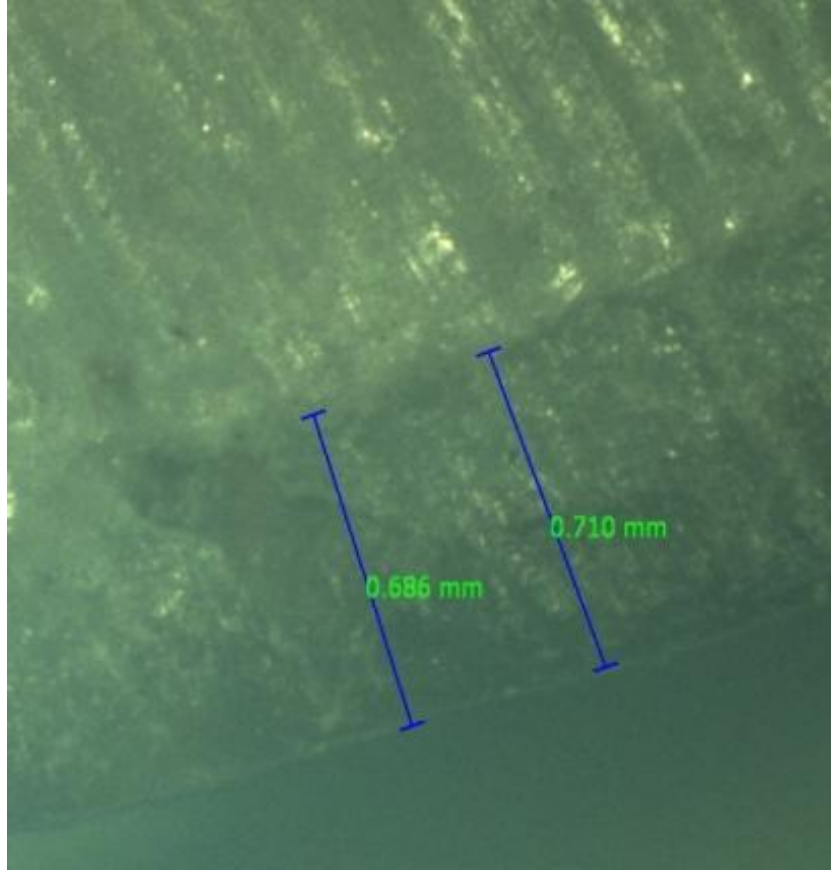
(a)

(b)

Figure 3-8: Bisected PCM capsule; a) optical microscope picture, b) showing voids created after thermal cycling

Table 3-2: Performance evaluation of encapsulated capsules

S. No.	PCM (M.p.)	Polymer	Metal coating	PCM-to-coating mass ratio	Max. Temp. (Charging temp.)	Min. Temp. (Discharging temp.)	No. of cycles passed	ΔH_f after thermal cycling (kJ/kg)
1.	NaNO$_3$ (306°C)	PTFE	Nickel (10-80 μm)	8:1 and 12:1	326 ^{o}C	250°C	2200 *	170 (172) **
2	NaNO$_3$	PTFE	–	12:1	326°C	250°C	1000 *	170
3	NaNO$_3$	PTFE	–	8:1	326°C	250°C	1000 *	170
4	NaNO$_3$	PTFE	–	20:1	326°C	250°C	5	170
5.	KNO$_3$ (334°C)	PTFE	Nickel (50-80 μm)	8:1	350°C	280°C	110*	92 (92) **
6.	50NaNO$_3$-50KNO$_3$ (222°C)	PTFE-FEP	–	12:1	242°C	180°C	1000 *	117 (120) **
7.	NaNO$_3$-KNO$_3$-LiNO$_3$ (122°C)	FEP	–	10:1	144°C	100°C	440*	140 (140) **
8	NaNO$_3$	PTFE	–	18:1***	326°C	250°C	1000 *	170

*Continuing; **As-received,*** Two inch diameter capsule

3.1.2.2 Metal Coating

A thin layer of metal may be needed over the PTFE layer to maintain its structural integrity in a packed bed environment. For this, it is desirable to develop a process which could be used to metalize polymer coated capsules on a commercial scale. The use of a vacuum based metallization technique is practically and economically not feasible for this application. We have developed a fully manufacturable proprietary method to metalize polymer coated capsules by utilizing commercially available electroless and electroplating chemistry. The method involves

32

Left hand side angle=108.040°

Left hand side angle =95.977°
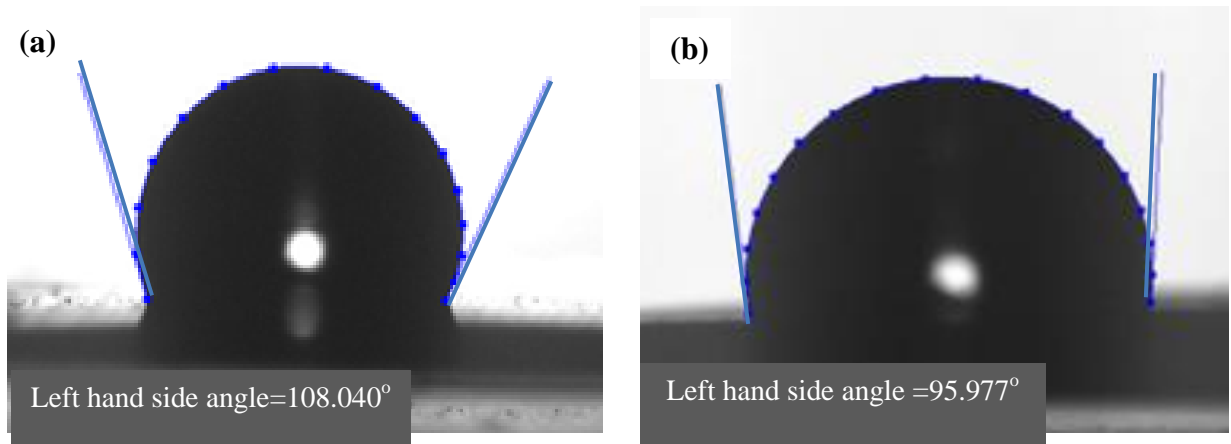
Figure 3-9: Contact angle measurement with DI water on a) as-received PTFE, b) Coated PTFE

Powder PCM

Hydraulic Press

Pressed PCM Pellets

Polymer Coating

Polymer Coated Capsule

i. **Electroless Deposition**
ii. **Electrolytic Plating**

Metal Coated Capsule
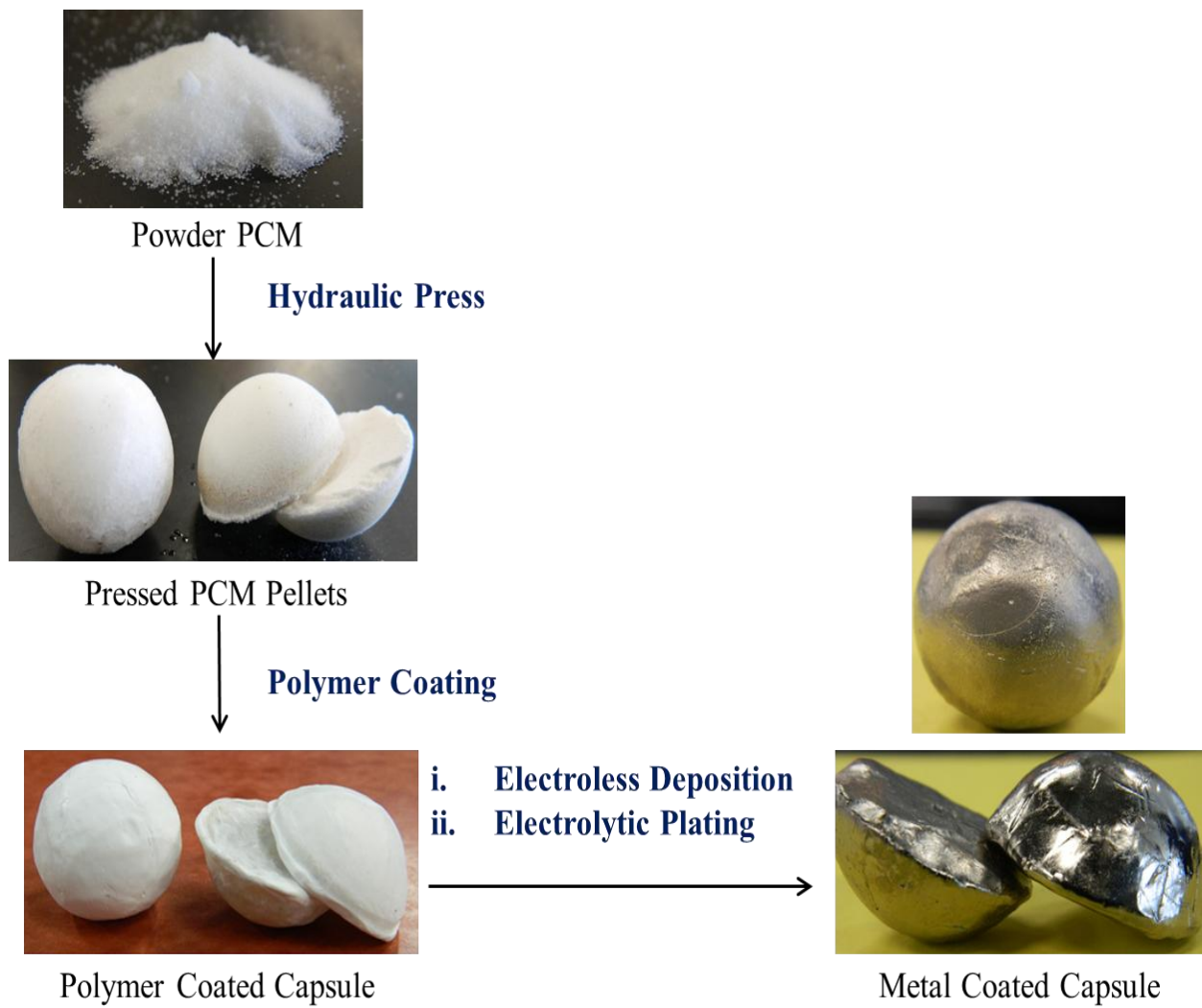
Figure 3-10: Procedure for the encapsulation of PCMs

33

coating of a PTFE layer with proprietary particles that make it hydrophilic and solvophilic in nature (Fig. 3-9). This is followed by deposition of a palladium catalyst that catalyzes the deposition of nickel. The initial electroless deposition is 1-4 micro inch, which is enough to make the PTFE layer conductive for the subsequent electrolytic deposition of nickel or other metals and metal alloys. The capsules have been electroplated with nickel, zinc, tin or zinc-nickel/iron alloy by the rack and barrel plating technique. The barrel plating technique was developed for plating a large number of capsules in a single step. The average thickness of the plated metal was measured to be in the 10 μm to 80 μm range. Figure 3-10 depicts all the steps involved in the encapsulation of the PCMs. Schematic of the electroless metal deposition and electroplating techniques are presented in Appendix B.

3.2 Experimental Measurements

3.2.1 Materials

Polytetrafluoroethylene (PTFE) films and fluorinated ethylene propylene (FEP) were obtained from McMASTER-CARR, USA. Sodium nitrate ($NaNO_3$), polyvinylidene fluoride (PVDF) and polytetrafluoroethylene (PTFE) powder were purchased from Sigma-Aldrich, USA. Lithium nitrate ($LiNO_3$) and potassium nitrate (KNO_3) were obtained from Alfa Aesar, USA. Polyimide sheets were purchased from HD Microsystems, USA. PI-84 sample was provided by EVONIK, Austria. Electroless nickel solution (Mid-phosphorus, 6-10 % by weight) and Nickel sulfamate electroplating solution (Macdermid Inc., USA) were procured from Transene Company Inc.,USA, and Allied Plating, USA, respectively.

3.2.2 Characterization

The DSC/DTA/TGA analyses were carried out using the SDT-Q 600 by TA instrument. This machine can simultaneously perform differential scanning calorimetry and

34

thermogravimetric analysis. Heat flow, temperature and weight accuracy of this device are ±2% (based on metal melting standards), ±1°C (based on metal melting standards) and ±1%, respectively. All the TG analyzes were performed at a ramp rate of 10°C/min under an inert (Argon) atmosphere The FTIR spectra were taken by using a JASCO 6300 Fourier transform infrared spectroscopy (FTIR) instrument. The thickness of the dissected capsules was measured with a Leitz Optical Microscope (5x to 100x). Contact angles on the polymer surface were measured by a Ramé-hart Contact Angle Goniometer, retrofitted with a digital camera. A K-type thermocouple was used to measure the temperature profile at the center of the capsule and the temperature was recorded with the aid of Labview.

3.2.3 Uncertainty Analysis

TGA, weight and temperature measurements were conducted several times to observe the repeatability of the measured data. The Root-sum-square method was employed to evaluate the uncertainty of the measurements [115, 116] with a 95% confidence level.

$$U_c = \sqrt{\sigma_{random}^2 + \sigma_{systemtic}^2} \tag{3-1}$$

Where, U_c, σ_{random} and $\sigma_{systematic}$ are the combined standard uncertainties for the measurements, random error, and systematic error, respectively.

3.2.4 Determination of the Temperature Profile Inside the Capsule

Before thermal cycling, we investigated the temperature distribution inside a single NaNO$_3$ capsule during the charging and discharging processes. A K-type thermocouple was implanted at the center of the capsule (Fig. 3-11). The capsule was placed in a furnace for thermal cycling from 280°C to 326°C. During this procedure, the temperature inside the capsule was monitored with the help of LabVIEW. From Fig. 3-12, it is clear that the melting took about 22 minnutes to complete. Further, it took about 70 minutes for the whole capsule to reach the

35

temperature of the furnace (326°C). Expectedly, the solidification took longer time (29 min) than

melting as it is conduction dominant process whereas melting is convection dominant process.
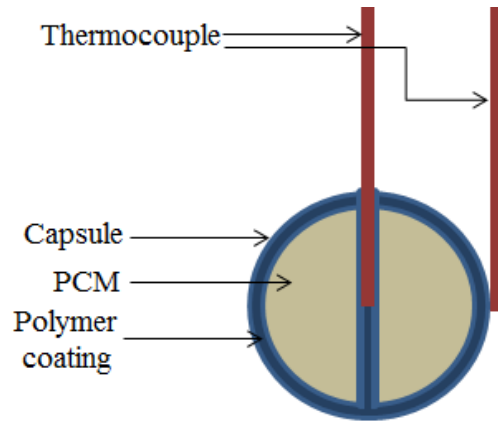
Figure 3-11: Schematic of the thermocouple setup inside the capsule
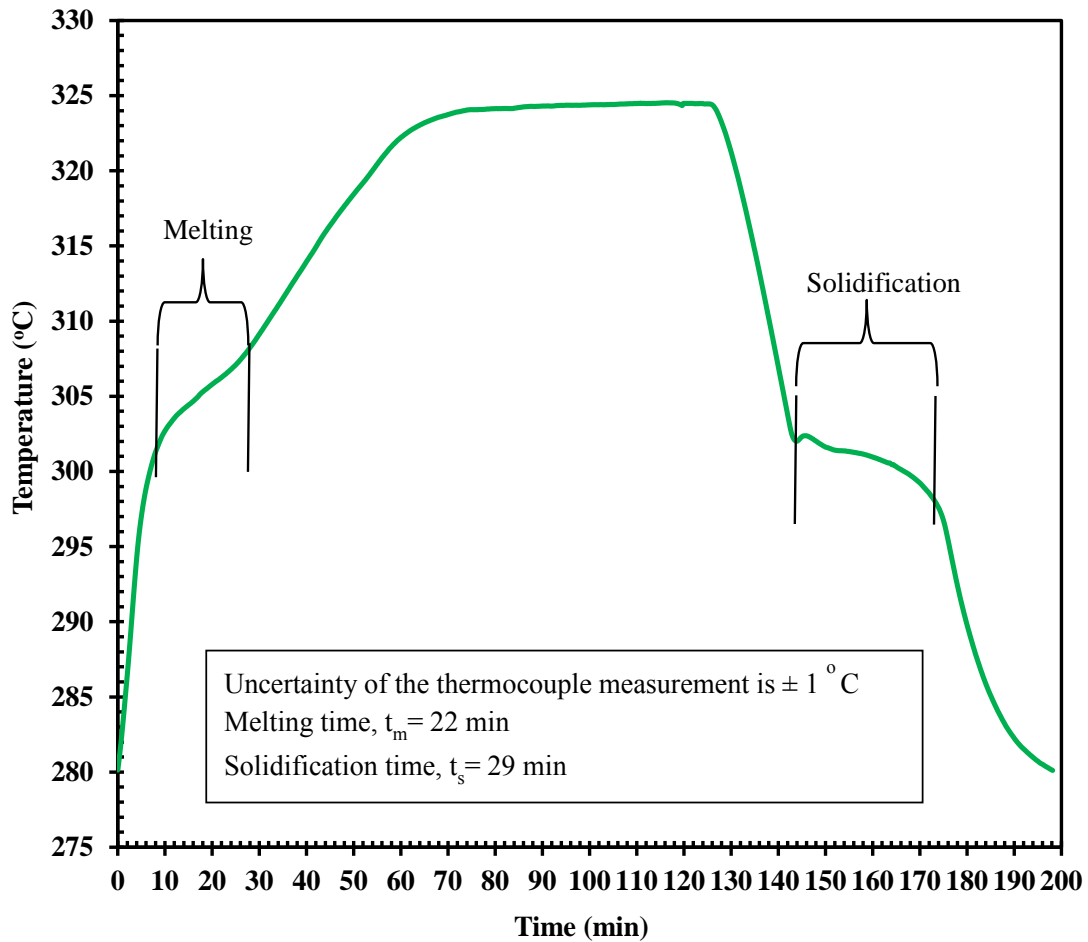
Figure 3-12: Average temperature profile inside NaNO$_3$ capsule thermal cycled between 280-326 ^{o}C
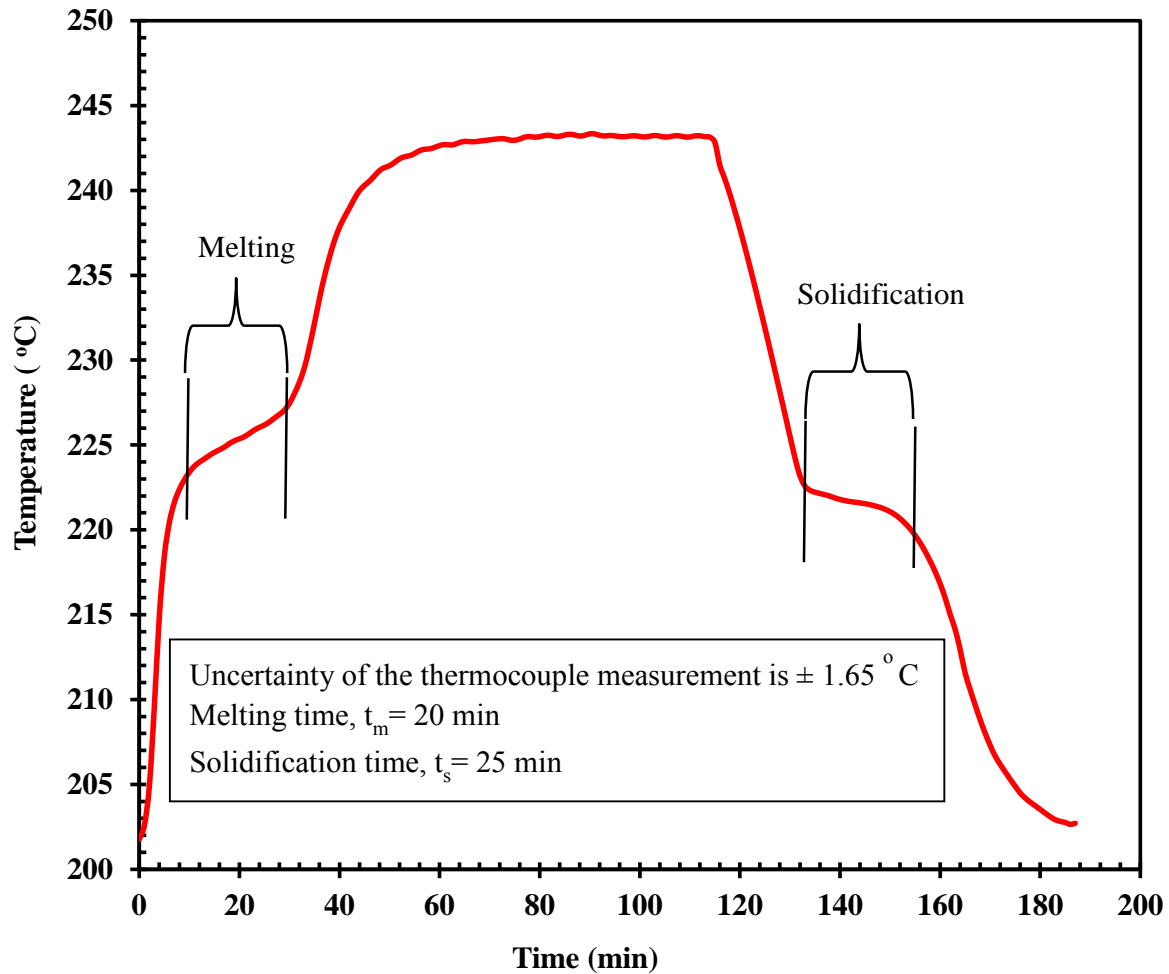
Figure 3-13: Average temperature profile inside KNO_3-$NaNO_3$ capsule thermal cycled between 202-242 ^{o}C

The experiment was performed six times to observe its repeatability. Similarly, the temperature distribution inside a KNO_3-$NaNO_3$ capsule was investigated between 202°C to 242°C. Melting took 20 min, whereas solidification took 25 min for completion (Fig. 3-13). The uncertainties in the measurement of temperature in $NaNO_3$ and KNO_3-$NaNO_3$ capsules are ±1.0^{o}C and ±1.65^{o}C, respectively. It is pertinent to mention that the numerical analysis of the heat transfer process during the melting of $NaNO_3$ in an encapsuleted spherical shell was done by other researchers in our group [107,114]. A mathematical correlation of the heat transfer rate and meltintg was developed from the numerical results [107,114].

37

3.2.5 Thermal Performance Evaluation of PCM Capsules in Air

Performance of the NaNO$_3$ capsules was evaluated by thermal cycling according to the profile shown in Fig. 3-14. The capsules were dwelled at 326°C for 80 min and then cooled to 280°C and then dwelled for 1 h in air inside a furnace.
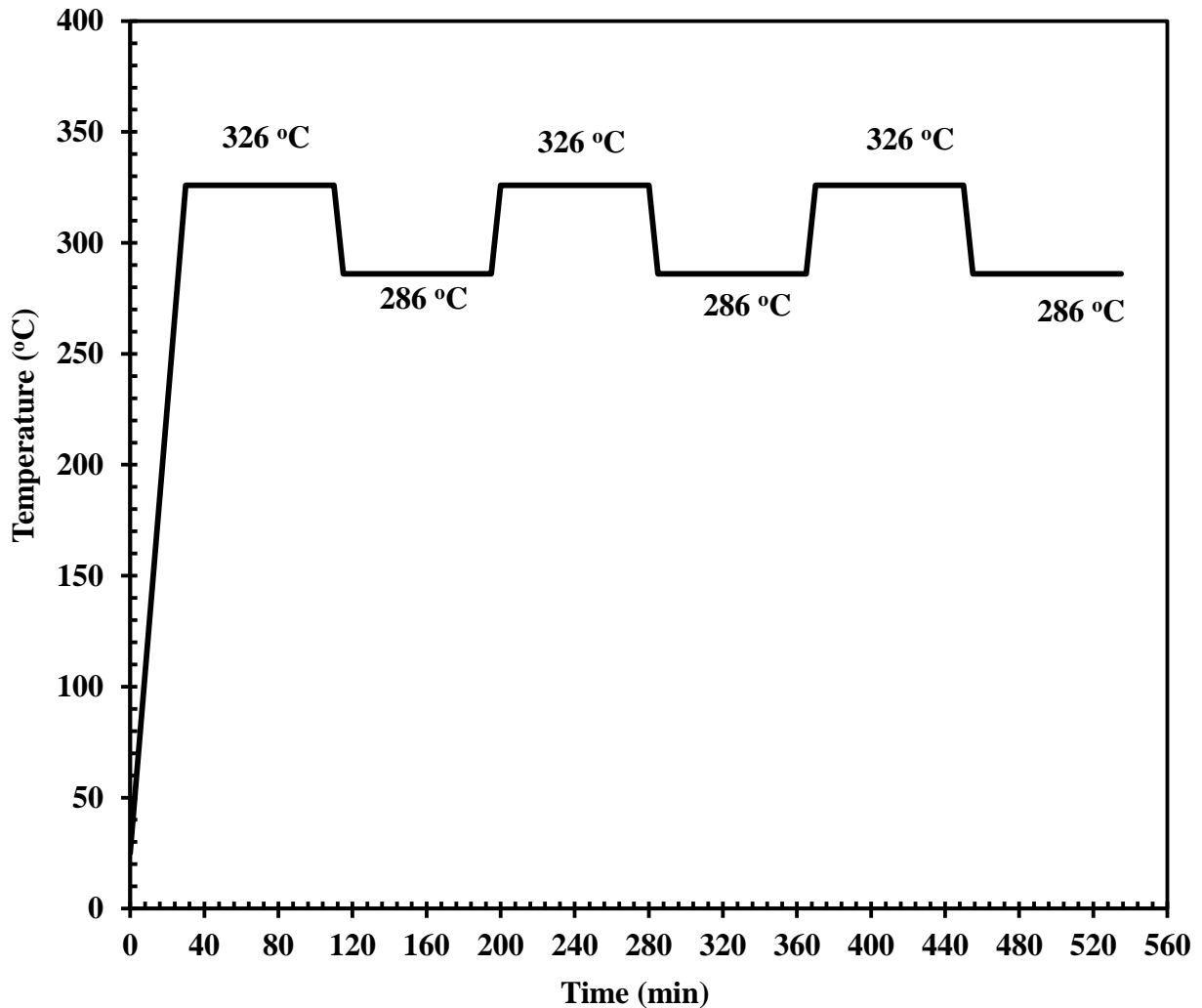
Figure 3-14: Thermal cycling profile

Figures 15a and 15b show two sets of capsules after 50 cycles, one set is polymer coated and the other is metal coated on polymer. Figure 15c shows a set of capsules, which have successfully passed 2200 thermal cycles and still continuing. The discoloration of the metal coat is due to the oxidation of the outer metal layer into metal oxide. Capsules with different polymer

38

thicknesses were fabricated to determine the minimum polymer thickness needed to maintain the integrity of the film and achieve a PCM to coating ratio as high as possible. The PCM-to-coating mass ratio was varied from 8:1 to 20:1 (Table 3-2). The capsules with 8:1 and 12:1 PCM-to-coating mass ratio have not shown any visible degradation in 1000 thermal cycles completed so far. Cycling of these capsules is continuing. The capsule with 20:1 mass ratio failed after only few cycles. The performance of the fabricated capsules has been tabulated in Table 3-2.

(a)   **(b)**

(c)
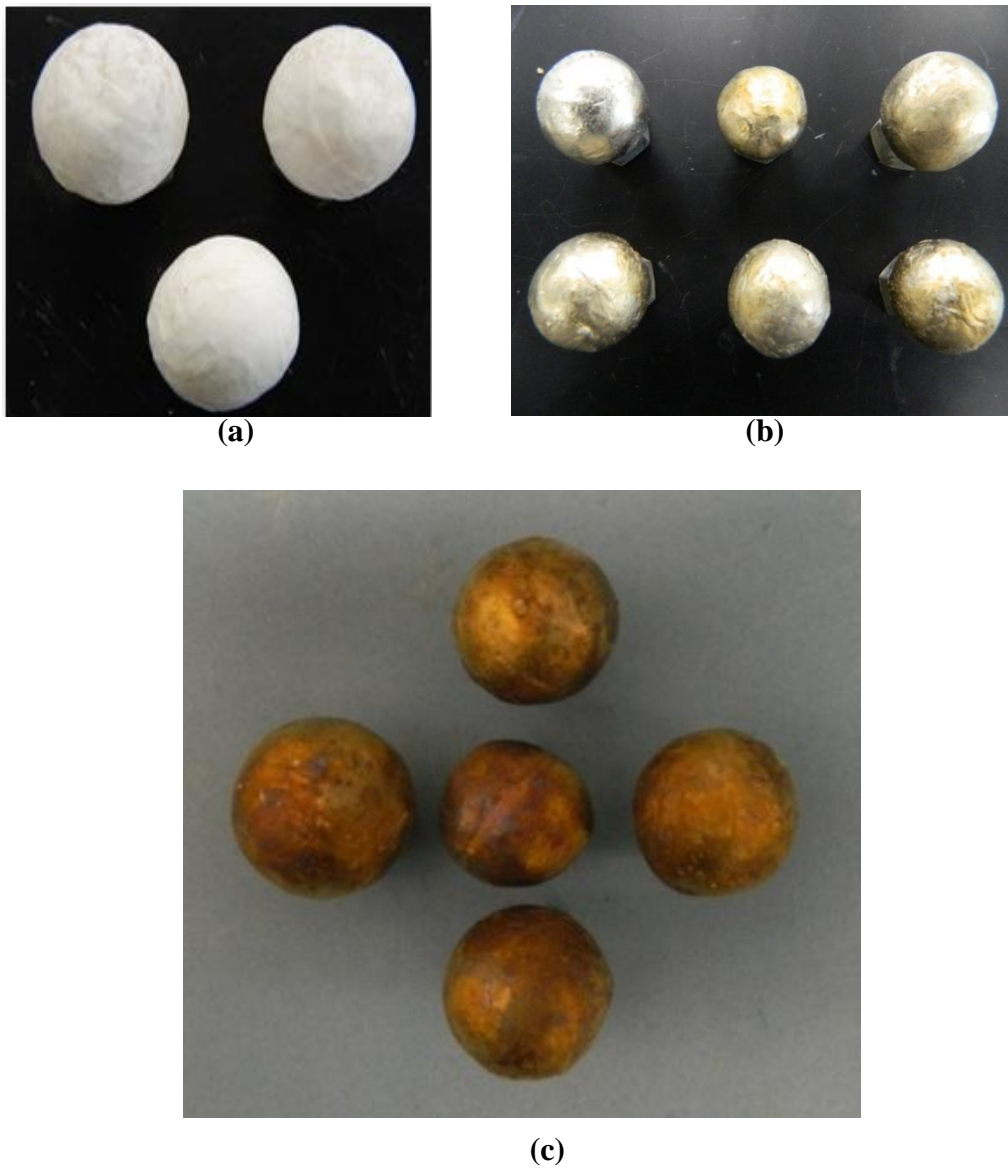
Figure 3-15: a) Only polymer coated capsules b) Metal coated capsules tested at 326°C after 50 cycles, b) Capsules tested at 326°C for 2200 thermal cycles

المنارة للاستشارات

www.manaraa.com
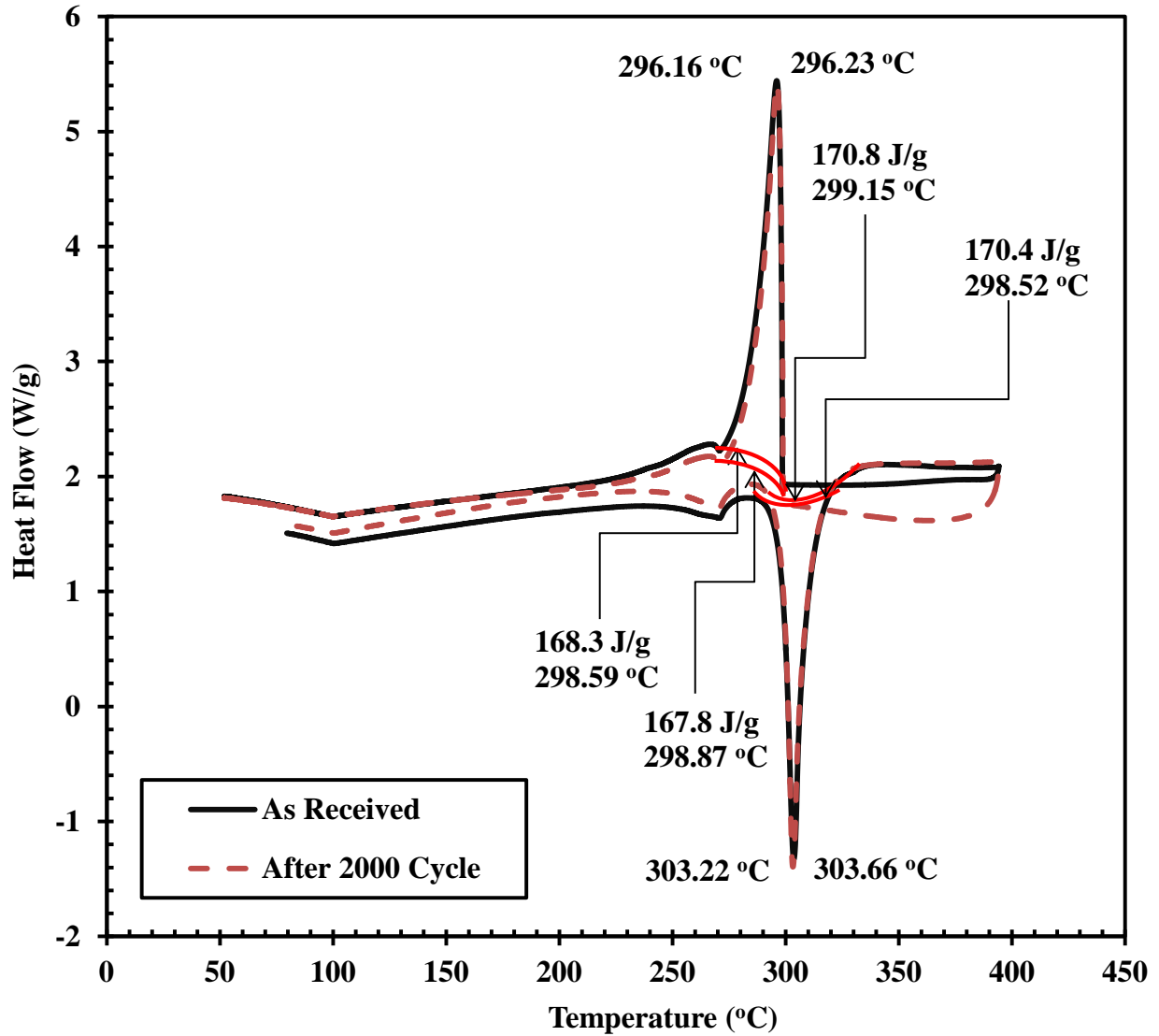
Figure 3-16: DSC of NaNO$_3$ before and after thermal cycling (>2200 cycles)

At various stages of thermal cycling, capsules were dissected to analyze their thermophysical properties. DSC analysis of the thermal cycled capsules of NaNO$_3$, KNO$_3$ and their eutectic showed no significant change in their thermophysical properties (Fig. 3-16 and Table 3-2). In addition, the weight change analysis showed no substantial weight change after thermal cycling (Fig. 3-17). FTIR was also used to characterize the NaNO$_3$ in the capsule before and after thermal cycling. The IR spectra of "as-received" and thermal cycled (after 2000 thermal cycles, Fig. 3-18) perfectly matched with each other.

All these tests indicate a compatibility of the coating material with the nitrate based salts over an extended period of usage. Polymer coated capsules and metal and polymer coated capsules were further tested in oil and molten salt environment as some of the CSP plants use oil or molten salt (KNO_3-$NaNO_3$). Weight change analysis, FTIR and thermophysical properties of the samples before and after various cycles were measured and compared with the as-received PCMs. To do the test in different environment two different set of capsules were made and further analyzed.
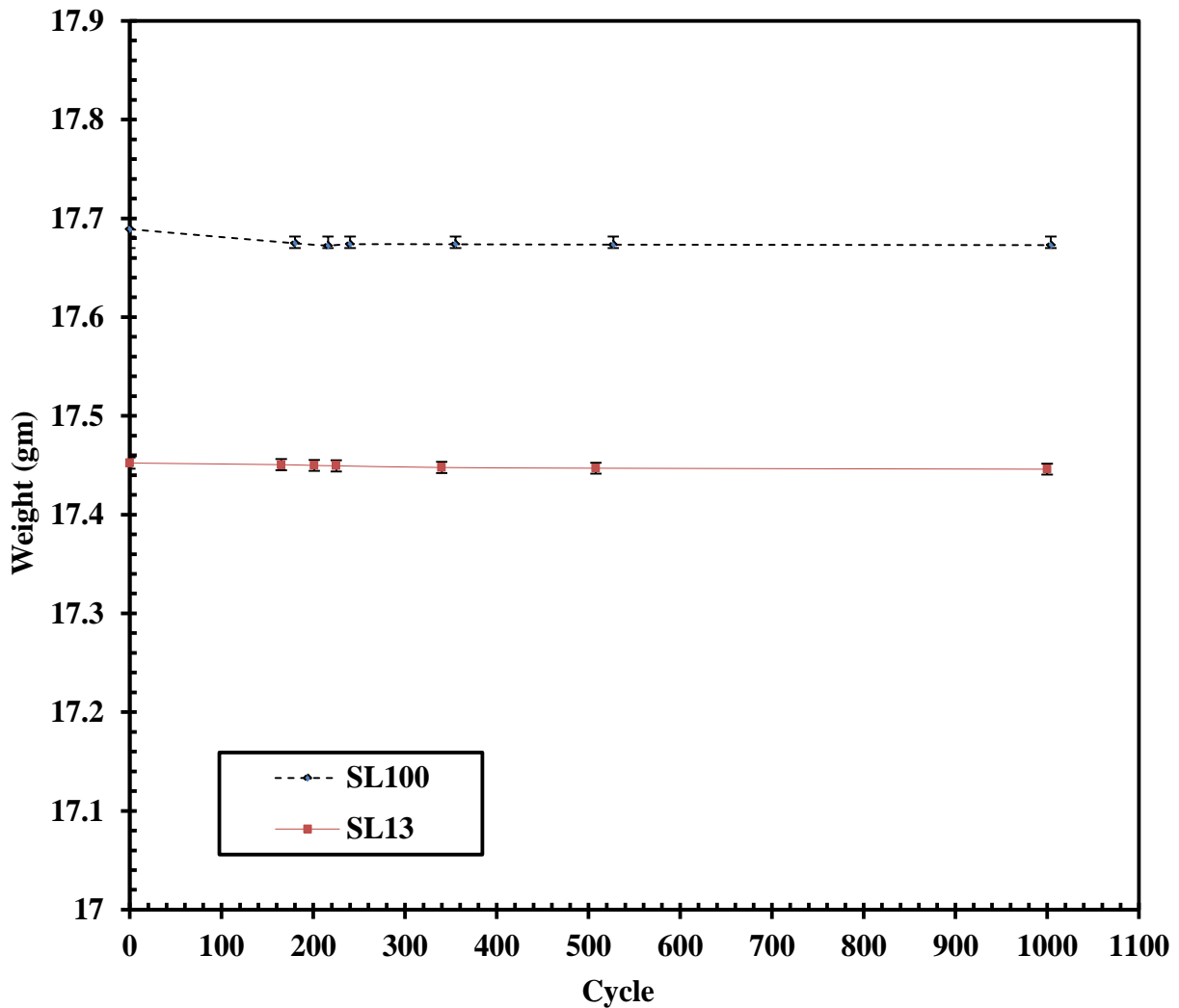
Figure 3-17: Weight of the PCM capsules after thermal cycling (uncertainty in the weight measurement is ±0.006 g)
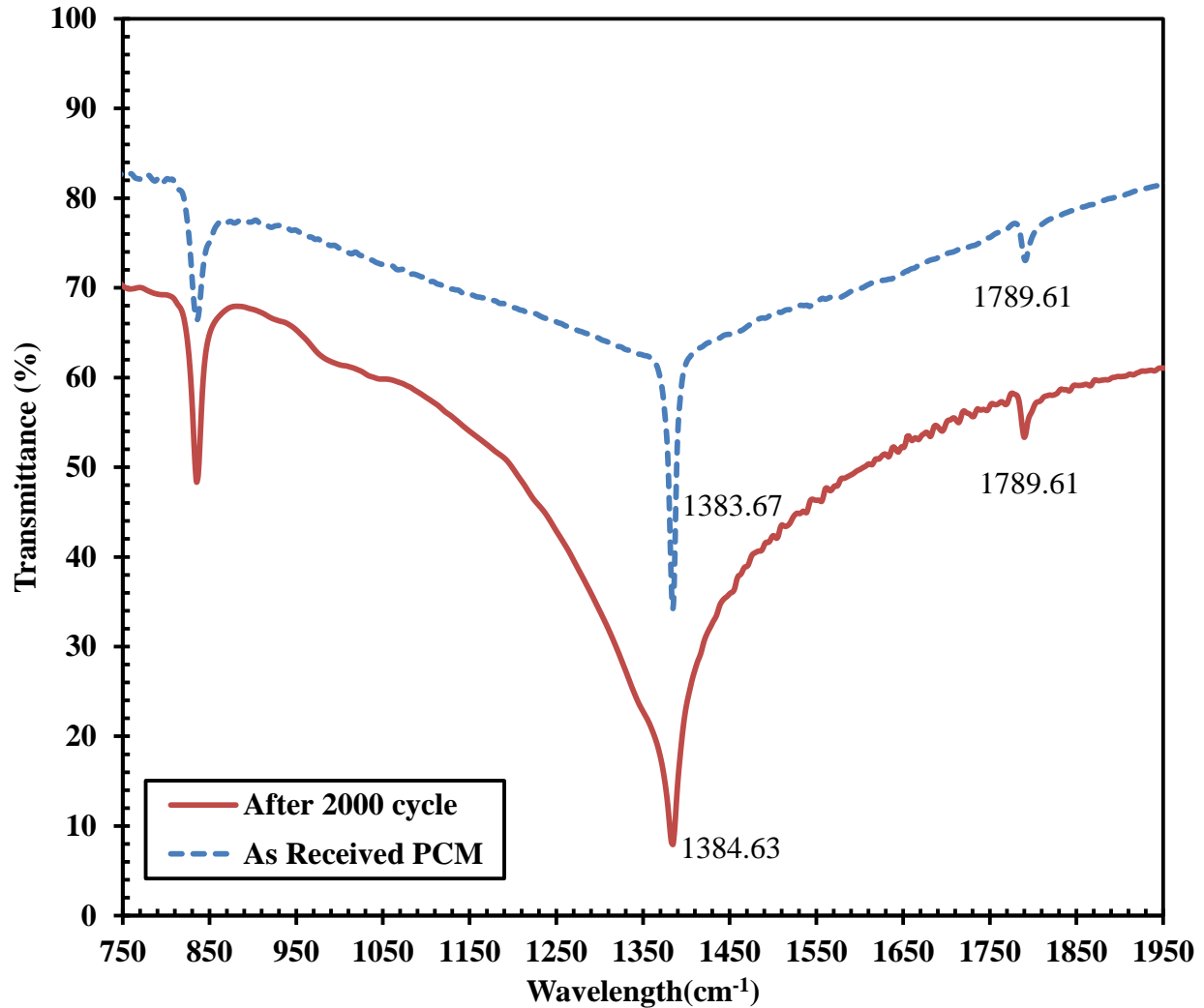
Figure 3-18: FTIR of as-received and thermal cycled $NaNO_3$

3.2.6 Energy Stored in A Single Capsule

The average theoretical energy stored in a single one inch diameter capsule over the temperature range of 286-326°C was estimated as 4.27±0.34 kJ. The following equation was used:

$$Q = m_{pcm} [C_{sp, pcm} (T_{m,pcm} - T_{i, pcm}) + L_{pcm} + C_{lp, pcm} (T_{f, pcm} - T_{m, pcm})]$$

$$+ m_{poly} [C_{ps, poly} (T_{f, poly} - T_{i, poly})] \tag{3-2}$$

The data used for calculating amount of energy stored in a single capsule is given in Table 3-3.

Table 3-3: Physical properties of NaNO$_3$ and PTFE used for the calculation of energy stored in a single capsule of one-inch diameter

NaNO$_3$ (PCM)		PTFE (Coating)	
m_{pcm}	17.4 g	m_{poly}	1.70 g
$C_{sp,pcm}$	1.655 kJ/kg.K[117]	$C_{sp,poly}$	1.500 kJ/kg.K [118]
$T_{m,pcm}$	306°C	$T_{f,poly}$	326 ^{o}C
$T_{i,pcm}$	286°C	$T_{i,poly}$	286°C
L_{pcm}	172 kJ/kg		
$T_{f,pcm}$	326°C		
$C_{lp,pcm}$	1.655 kJ/kg.K [117]		

3.2.7 Testing of a Packed-Bed System with PCM Capsules

These capsules were also tested in a packed-bed environment for more than 50 cycles [118]. The packed-bed thermal storage tank contained randomly packed 770 encapsulated spherical NaNO$_3$ capsules stacked one over the other. The average diameter of each capsule was 2.743±0.038 cm. The capsule contained an average of 17.4±1.6 g of PCM [118]. The capsules inside the packed-bed were observed after 50 cycles. All of the capsules survived thermal cycling without any leakage. There were nine layers of capsules lying on the top of the bottom layer capsules that are approximately 12 kg of weight on the capsules at the bottom layer. This demonstrates the mechanical stability of the capsules both under charging and discharging conditions.

3.3 Thermal Performance Evaluation of PCM Capsules in Oil

The performance of the NaNO$_3$ capsules was evaluated by thermal cycling according to the profile shown in Fig. 3-14. The capsules were dwelled at 326°C for 80 min and then cooled to 280°C and then dwelled for 1 h in an oil environment. Metal-polymer coated and polymer coated capsules (figure 3-19) were kept in a steel cylinder filled with high temperature oil

43

(specification of the HTF used in oil experiment mentioned in Appendix B). After certain number of cycles steel cylinder was opened to test the weight change and thermophysical properties of the capsules.

Figure 3-19: a) Polymer-coated capsules at zero cycle b) Steel cylinder filled with oil for thermal cycling c) Metal and polymer coated capsules after 1000 cycle d) Polymer coated capsules after 1000 thermal cycle

At various stages of thermal cycling, capsules were dissected to analyze their thermophysical properties. Each time, capsules were throughly cleaned with xylene and acetone.

DSC analysis of the thermally cycled capsules of $NaNO_3$ showed no significant change in their thermophysical properties (Table 3-4).

Table 3-4: DSC analysis results of spherical capsules in oil environment

Thermal cycle	Melting point (^{o}C)	Latent heat of Fusion (kJ/kg)
0	303.22	170.8±1.4
500	303.88	169.3±1.3
1000	303.95	169.9±1.8

In addition, the weight change analysis showed no substantial weight change after thermal cycling (Fig. 3-20).
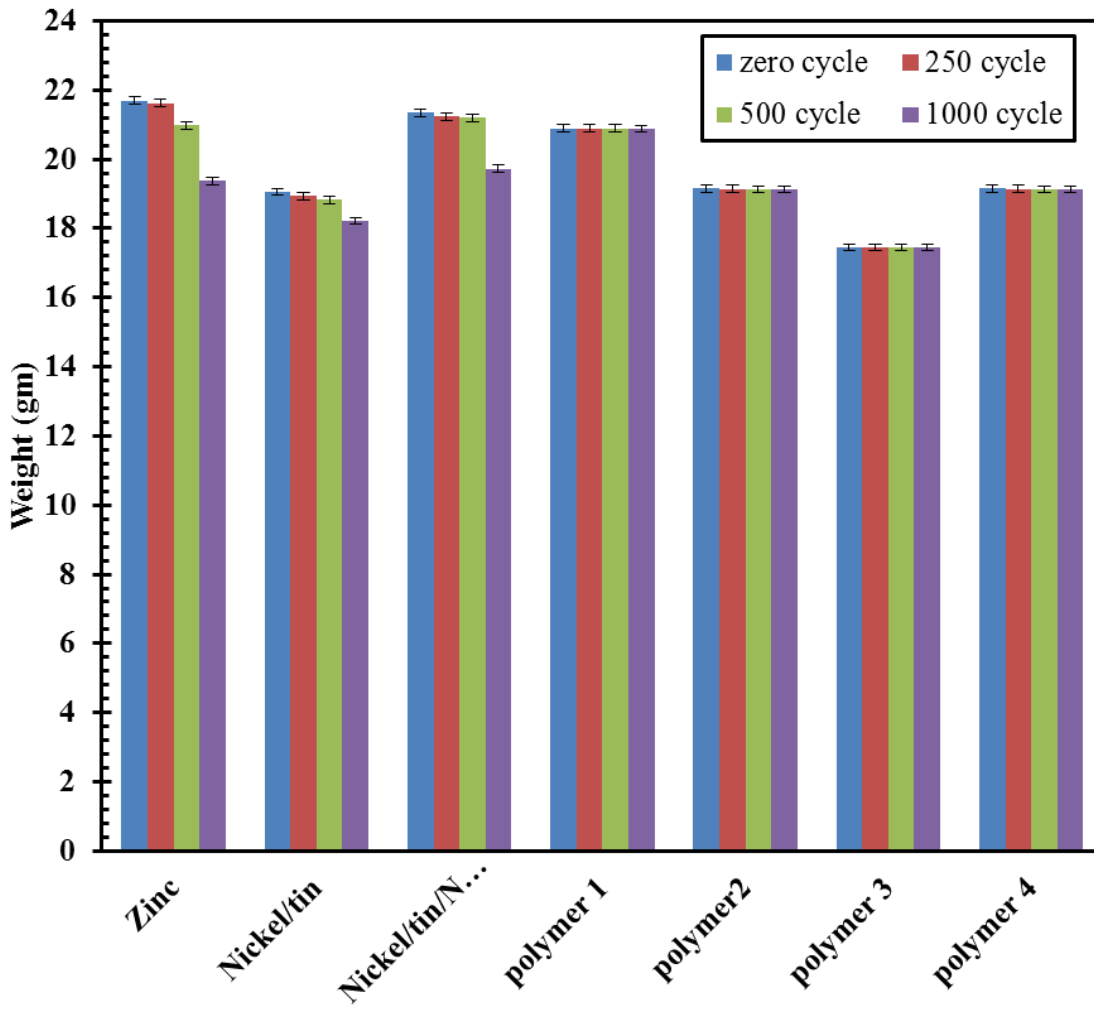
Figure 3-20: Weight measurement after various thermal cycles (in oil)

FTIR was also used to characterize $NaNO_3$ before and after thermal cycling. The IR spectra of "as-received" and thermal cycled (after 1000 thermal cycles, Fig. 3-21) perfectly matched with each other. All polymer coated capsules successfully passed 1000 thermal cycles with out any degradation in weight and thermophysical properties. The only problem was observed with zinc-polymer, nickel-tin alloy-polymer coated capsules. It showed some crack on the metal coating and some of the metal flakes come out of the capsule but polymer coating was intact. All these tests indicate a perfect compatibility of the coating material with the nitrate based salts over a long period of usage in oil environment.
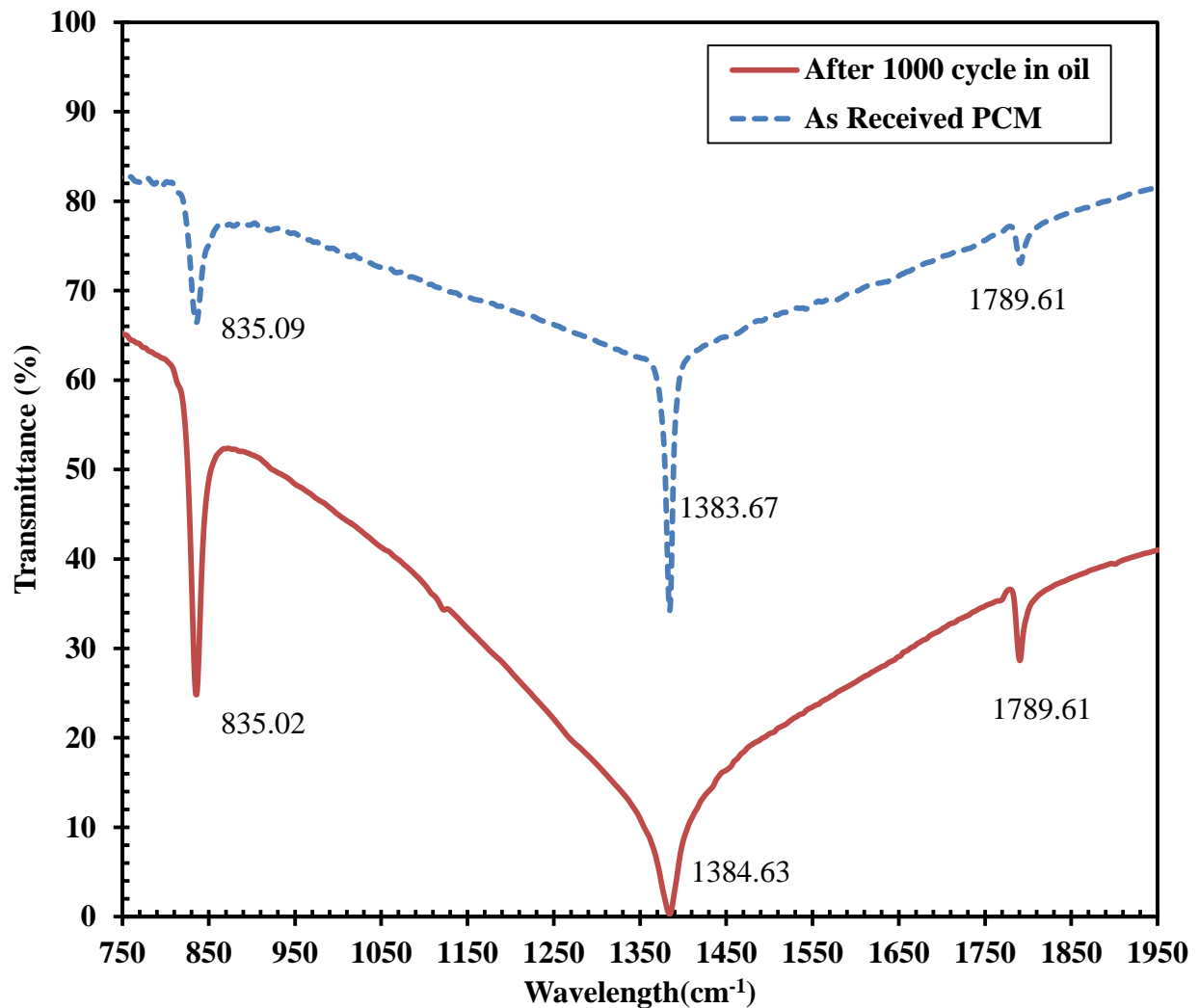
Figure 3-21: FTIR of as-received and thermal cycled $NaNO_3$ after 1000 thermal cycling in oil

46

3.4 Thermal Performance Evaluation of PCM Capsules in Molten Salt

The performance of the $NaNO_3$ capsules was evaluated by thermal cycling according to the profile shown in Fig. 3-14. The capsules were dwelled at $326^{o}C$ for 80 min and then cooled to $280^{o}C$ and then dwelled for 1 h in molten salt environment. Some polymer-coated capsules were immersed in $NaNO_3$- KNO_3 (melting point $222^{o}C$) molten salt bath (figure 3-22).
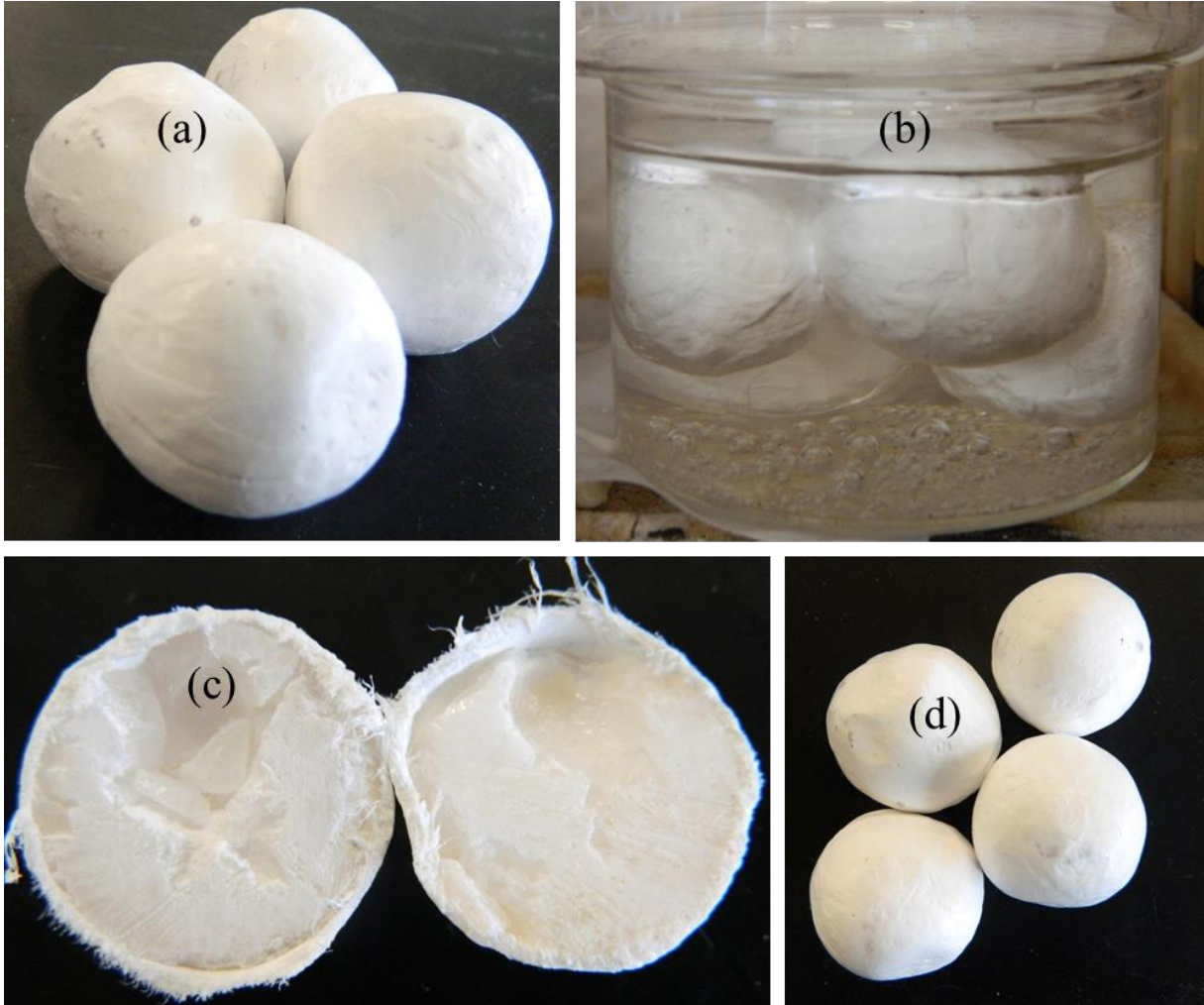
Figure 3-22: a) Polymer-coated capsules at zero cycle b) Beaker filled with molten salt and capsule for thermal cycling c) cross-section of polymer coated capsules after 1000 cycle d) Polymer coated capsules after 1000 thermal cycle

At various stages of thermal cycling, capsules were dissected to analyze their thermophysical properties. DSC analysis of the thermal cycled capsules of $NaNO_3$ showed no

significant change in their thermophysical properties (Table 3-5). In addition, the weight change

analysis showed no substantial weight change after thermal cycling (Fig. 3-23).

Table 3-5: DSC analysis results of spherical capsules in molten salt environment

Thermal cycle	Melting point (^{o}C)	Latent heat of Fusion (kJ/kg)
0	303.22	170.8±1.4
500	303.66	170.2±1.3
1000	303.35	170.3±1.5
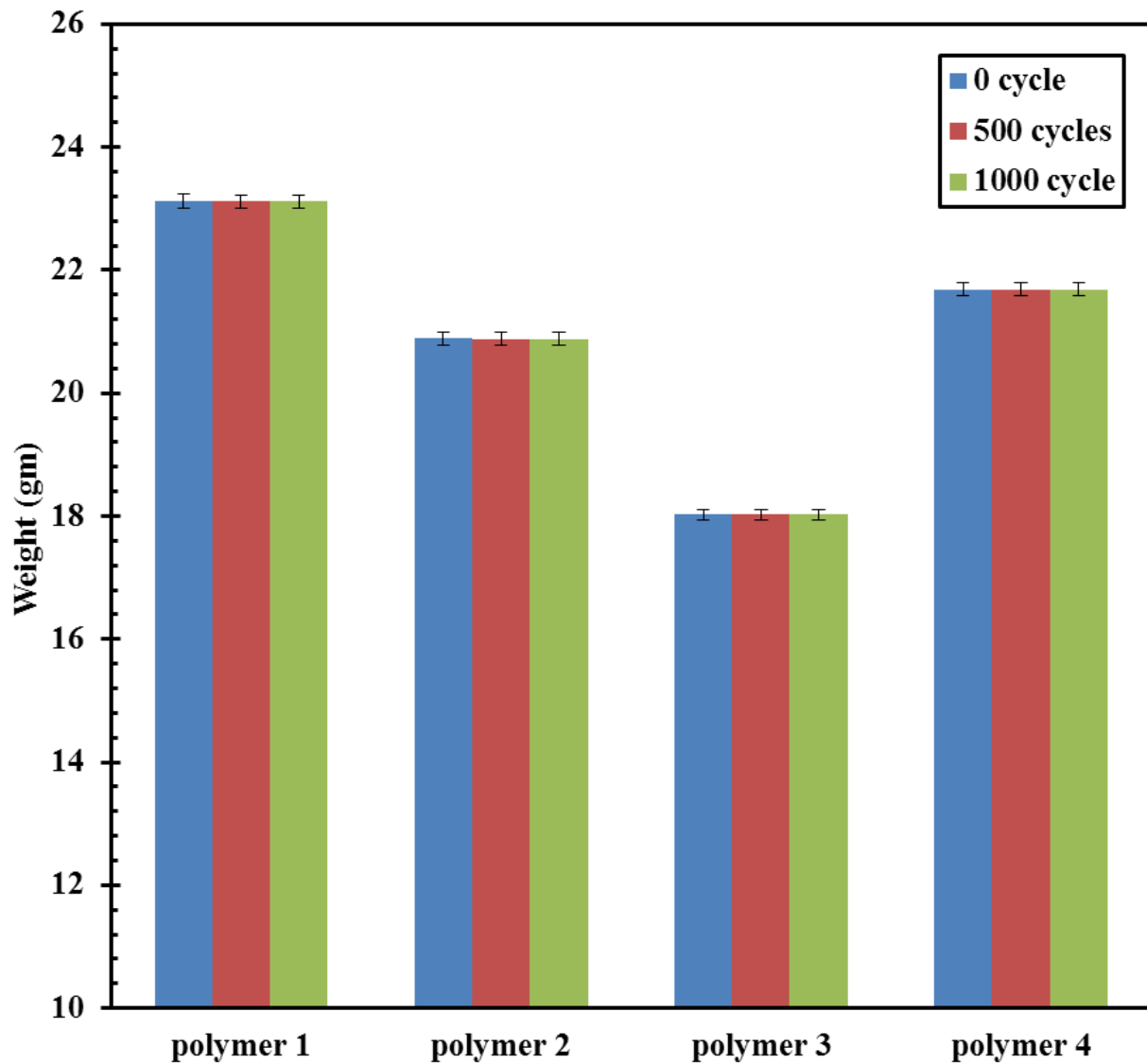
Figure 3-23: Weight measurement after various thermal cycles (in molten salt)

FTIR was also used to characterize the $NaNO_3$ in the capsule before and after thermal cycling. The IR spectra of "as-received" and thermal cycled (after 1000 thermal cycles, Fig. 3-24). These capsules successfully passed 1000 thermal cycles without any degradation in weight and thermophysical properties.
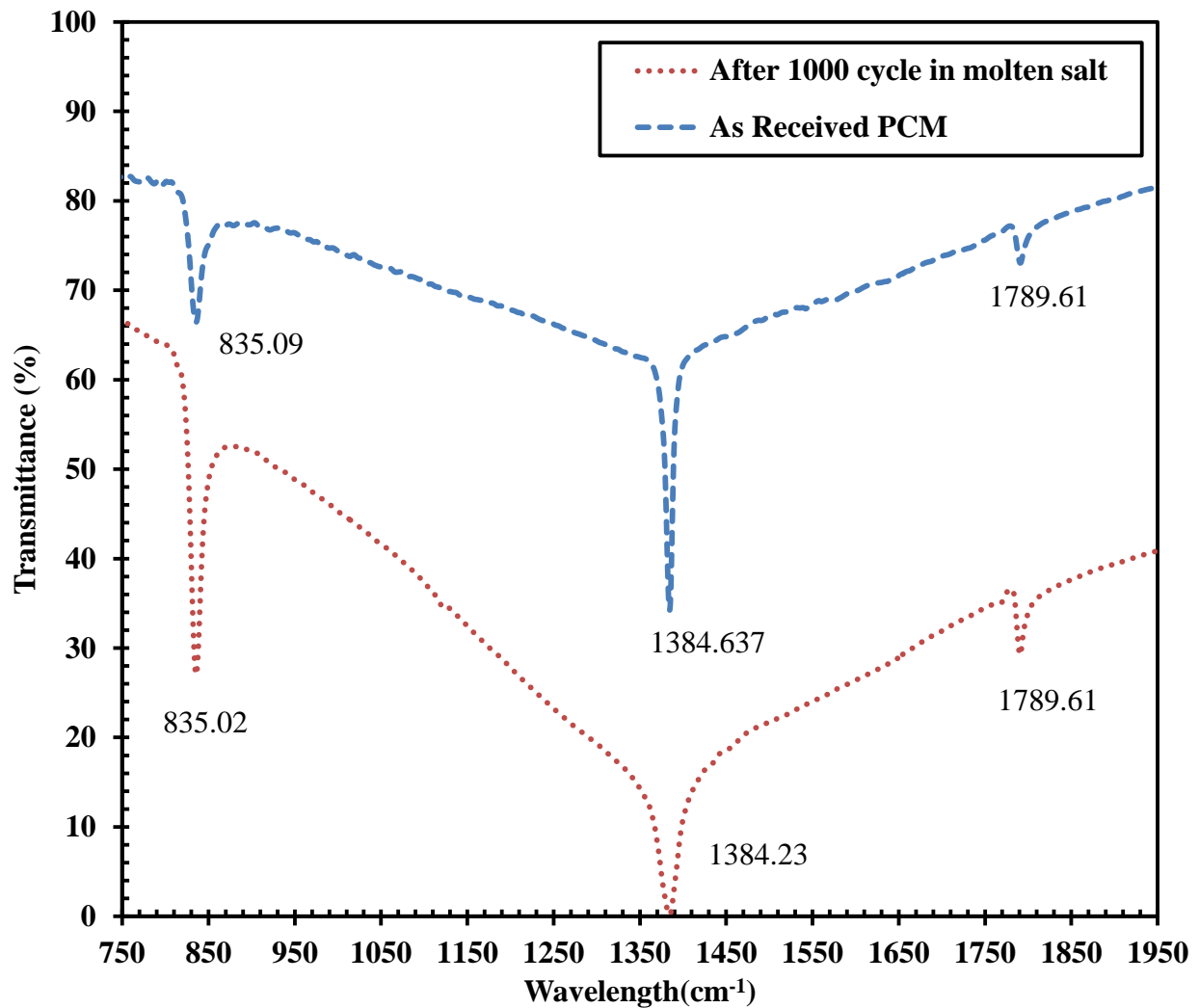
Figure 3-24: FTIR of as-received and thermal cycled $NaNO_3$ after 1000 thermal cycling in molten salt

EXPERIMENTAL INVESTIGATION OF A PACKED- BED LHTES WITH ENCAPSULATED PCM

The present work addresses the design and testing of laboratory-scale prototype packed-bed LHTES storage system that contains encapsulated PCMs. Since alkali metal-based nitrate salts and their eutectics have been widely studied as PCM candidates, in this study we used $NaNO_3$ as the PCM. $NaNO_3$ has a melting point of 306^oC and a heat of fusion of 176 kJ/kg [7]. Temperature profiles at various axial positions in the storage system were determined for three different flow rates using air as the HTF. Influence of the HTF flow rate on the system charging and discharging times as well as the pressure drop across the bed is discussed. Also the energy and exergy efficiencies of the system are calculated for three different flow rates.

4.1 Experimental Setup and Preparation of Spherical Capsules

4.1.1 Materials

The polytetrafluoroethylene (PTFE) films and sodium nitrate ($NaNO_3$) were purchased from McMaster-Carr, USA and Sigma-Aldrich,USA, respectively. The K-type thermocouples and temperature controller system were procured from Omega,USA. The cylindrical storage tank and diffuser cones were obtained from Florida Structural Steel, USA. Data acquisition system was procured from National Instrument, USA. The heating elements were purchased from Farnam custom products, USA.

The content of 4.1 to 4.5 was published in TE Alam, J Dhau, D.Y. Goswami, M.M. Rahman, and E.. Stefankos. "Experimental Investigation of a Packed-Bed Latent Heat Thermal Storage System With Encapsulated Phase Change Material,". In ASME 2014 International Mechanical Engineering Congress and Exposition. (2014, November). Permission is included in Appendix C.

4.1.2 Encapsulation of Sodium Nitrate Capsules

NaNO$_3$ powder (8-12 g) was pressed in a hydraulic press at 980 N of force to form hemispherical pellets of 12.5 to 25.5 mm diameter. The salt pellets were wrapped in a thin stretchable PTFE film. The PTFE coated pellets were again pressed in the hydraulic press at 980 N of force. These capsules were then heated to 326°C and annealed for an hour [15,16]. The PTFE coated capsules used in the packed bed are shown in Fig. 4-1.

Figure 4-1: PTFE coated capsules

4.1.3 Experimental Setup

In the present work, a latent heat storage packed-bed was constructed to experimentally determine the charging and discharging characteristics of the system. Figure 4-2 represents the schematic diagram of the setup. It consists of a blower, a cylindrical storage tank, electrical heaters and a flow-measuring device (Pitot tube). The operating temperature range of the system

51

was $286^{\circ}C$-$326^{\circ}C$ ($20^{\circ}C$ above and below the melting point of NaNO₃) and air was used as the HTF. During charging, air at the desired charging temperature ($326^{\circ}C$) was supplied at the top of the storage system and extracted from the bottom, with the flow direction of air (at $286^{\circ}C$) reversed during the discharging process. The storage tank is made up of carbon steel and is 25.4 cm in height and diameter.
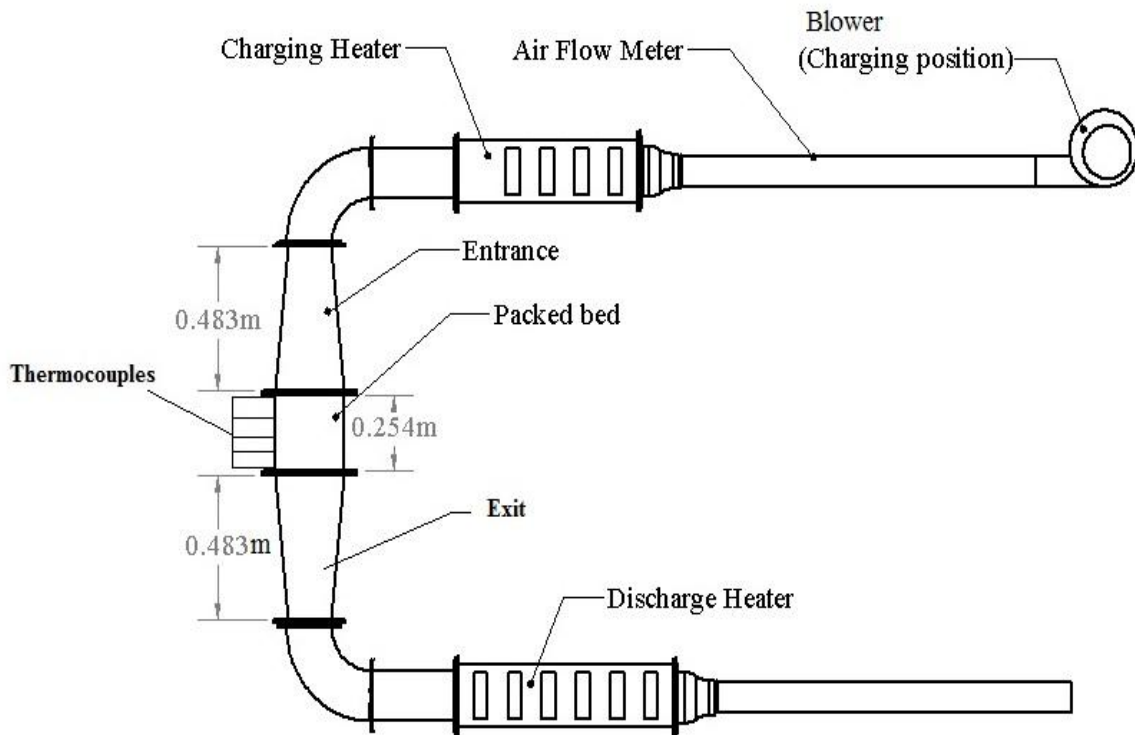
Figure 4-2: Schematic diagram of the experimental packed-bed storage system setup.

The whole structure is supported by a steel frame, and the system is well insulated with thermal insulation of 15.2 cm thickness. The packed-bed is randomly packed with 770 encapsulated spherical NaNO3 capsules, which were fabricated in the lab. The average diameter and volume of each capsule are 2.743±0.038 cm and 10.39±0.21 cm³, respectively. The capsule contained an average weight of 17.4±1.6 g PCM. Approximately 47% of the total volume of the tank is occupied by the PCM. The average porosity of the bed and bed-to-particle diameter was

fixed at 0.35 and 10, respectively. Table 4-1 represents the main characteristics and design parameters for the packed-bed thermal energy storage system.

Table 4-1: Characteristics of the packed-bed

Description	Nominal value
Bed height	0.254 meter
Bed diameter	0.254 meter
Tank material	Carbon steel
Total volume of packed bed	0.01287 m^3
Bed porosity	0.35
PCM($NaNO_3$) Melting point	306°C
PCM($NaNO_3$) density @below melting	2.26 gm/cm^3
PCM($NaNO_3$) density @above melting	1.90 gm/cm^3
PCM($NaNO_3$) heat capacity	1.655 kJ/kg.K
PCM($NaNO_3$) latent heat of fusion	170 kJ/kg
Wall insulation thickness	0.1524 m
Flexible insulation density	128.1 kg/m^3 (8 lb/ft^3)
Flexible insulation k-factor	0.10W/mK @ 427°C
Rigid insulation density	304.4 kg/m^3/(19 lb/ft^3)
Rigid insulation k-factor	0.1225W/mK @ 600 ^{o}C
Outer wall material	Aluminum sheet

The inlet and outlet temperatures of the HTF were measured by two thermocouples (K-type). One thermocouple was installed 2.54 cm above the top of the bed to measure the inlet (charging) temperature of the bed. Another thermocouple was installed at 2.54 cm below the bottom of the bed to measure the temperature of the air leaving the bed. A total of 24 K-type

53

thermocouples were used inside the bed and two thermocouples (K- type) were used at the exit point of each of the two heaters. Figure 4-3 shows the distribution of the thermocouples inside the bed. These thermocouples were installed along the axial and radial directions in the bed.
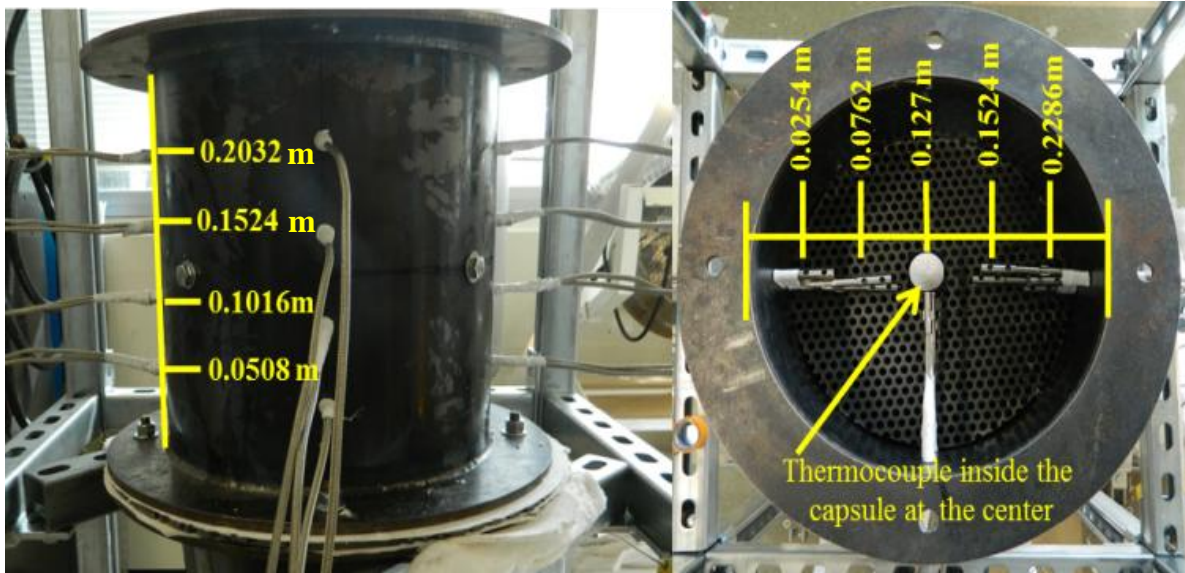
Figure 4-3: Positions of thermocouples inside the packed bed.

Axially, thermocouples were installed 5.08 cm apart from each other and were divided into four rows across the length of the bed starting from the top. In the radial direction, these thermocouples were placed at 2.54, 7.62, 12.7, 17.78, and 22.86 cm from the left side of the cylindrical wall. Thermocouples were also placed inside some of the centrally placed capsules 5.08 cm apart from each other. After insulating the bed, the exterior of the packed-bed was covered with aluminum sheets.

Figure 4-4 shows the complete experimental setup of the packed-bed. Table 4-2 specifies the packed-bed materials. A centrifugal blower was used to produce the air flow in the system and six heaters were used to maintain the desired temperature inside the bed. During charging, the blower was placed on the top section of the setup in front of the heater. Air heated to 326°C passes through the duct connecting the heater with the packed-bed and enters the bed at specific flow rates.

54
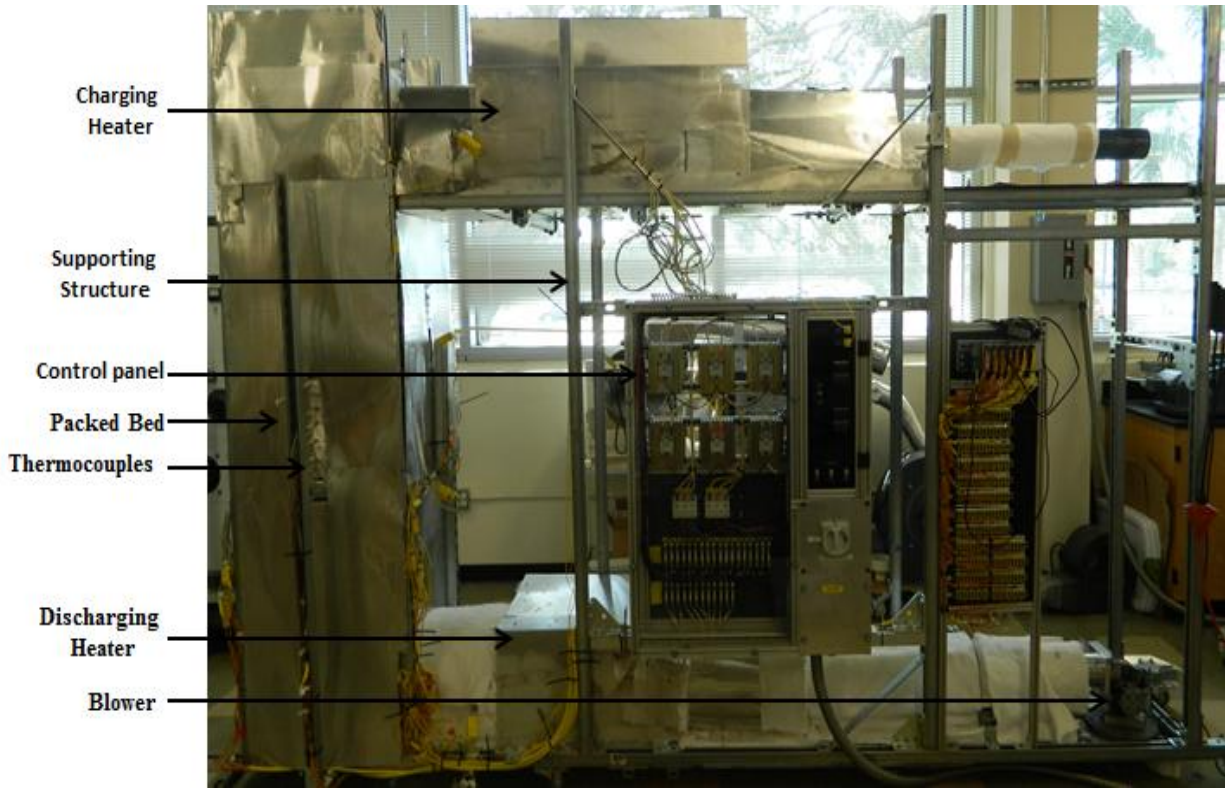
Figure 4-4: Complete experimental setup for testing of the packed bed

During the discharging period, the blower was placed at the bottom of the system in front of the discharging heater. In this position, air was heated to 286°C as it passed through the bottom heater. Air at 286°C enters the storage bed, absorbing thermal energy from the bed before leaving the system. The flow rate of the blower was controlled by a variable voltage supply controller. The output voltage of the inlet thermocouple was fed to the heater in order to maintain the desired temperature. Temperature data were collected by Labview Express at one minute intervals.

Table 4-2: Experimental components

Experiment	Items	Type
Heater element	6	Custom made heater. Product No-(DH6-6 KW-240-3 0112)
Data acquisition	1	National Instruments cDAQ 9178

55

Table 4-2: (Continued)

Experiment	Items	Type
Heater temperature controller	1	Omega series: CN9121A. 2 wire RTD input, relay output and pulse output. Accuracy- $\pm$ 0.25% FS $\pm 1 \, ^o$C. Auto calibration every five seconds. Control stability-$\pm$ 0.15% FS
Thermocouple (inside the PCM)	4	Omega, serial #KTSS-18E-12. K-Type. Accuracy is greater of 2.2 ^{o}C or 0.75% above 0 ^{o}C
Thermocouple	22	Omega, serial# XCIB-K-5-6-3. K-Type. Accuracy is greater of 2.2 ^{o}C or 0.75% above 0 ^{o}C
16-channel TC input module	2	National Instruments-9213
Data Acquisition software	1	LabView Express
Blower	1	Dayton Blower, Model-1TDP5 Horse Power: 1/30; volts: 115V Hz: 50/60, RMP: 2700/2880 CFM: 131 @free air 60 Hz
Pitot tube	1	Omega, High Accuracy Pitot Tubes FPT-6140 series. $\pm$2% rate of accuracy from 21 to 204°C and 0 to 150 psig
Digital Manometer	1	Dwyer, Series 475 Mark III Handheld Ranges from 1" w.c. to 150 psid, $\pm$0.5% F.S., 60 to 78°F; $\pm$1.5% F.S. from 32 to 60°F and 78 to 104°F Resolution of 0.001 inch w.c.

4.1.4 Experimental Procedure

Before charging, the air-blower was connected to the top side of the packed-bed system. The whole system was heated to 286°C and maintained at this temperature. During charging, the inlet temperature of the HTF was increased to 326°C. Charging was complete when the whole TES system reached 326°C. During discharging, the HTF entered the packed-bed at 286°C. The discharging period was considered complete when the system temperature decreased from 326°C

56

to 286°C. Testing of the system was carried out at three different flow rates (Table 4-3). The temperature distribution in the capsules and across the bed and the pressure drop across the system were measured at different flow rates.

Table 4-3: Different cases for charging and discharging

Case	Flow rate (m^3/h)	Charging temperature (°C) Bed initially at 286°C	Discharging temperature (°C) Bed initially at 326°C
1	110	326	286
2	131	326	286
3	151	326	286

4.1.5 Uncertainty Analysis

The Root-sum-square method was employed to evaluate the uncertainty of the measurements [115,116]. Experiments were carried out several times to observe the repeatability of the measured data and showed small deviation, the maximum uncertainty being 2.19%. The accuracy of the Pitot tube was ±2.0% of full scale. The digital manometer had an accuracy of ±0.5% of full scale with a resolution of 0.001 inch water column. Based on the equipment error and experimental values, the uncertainty in the flow rate was 5.78%. The maximum error associated with the pressure drop measurement across the bed was 1.14%. The thermophysical properties of $NaNO_3$ were measured using the SDT Q 600 by TA instrument which had an accuracy of 6.0%. The equation used to calculate the uncertainty is

$$U_c = \sqrt{(\sigma_{random})^2 + (\sigma_{systematic})^2} \tag{4-1}$$

where, U_c, σ_{random} and $\sigma_{systematic}$ are the combined standard uncertainties for the measurements, random error and systematic error, respectively.

4.2 Results and Discussion

4.2.1 Temperature Profile Inside the Capsules at Different Locations in the Packed-Bed

The temperature distribution of the PCM capsules during charging and discharging of the LHTS has three segments. Segment one is the sensible heat absorption zone by the solid PCMs from the hot HTF. Segment two is the latent heat absorption zone at constant temperature, and finally the third segment is the sensible heat absorption by the liquid PCM. Figures 4-5, 4-6 and 4-7 show the temperature profiles inside the capsules placed at different heights (5.8, 10.16, 15.24, and 20.32 cm) from the top at flow rates of 151, 131 and 110 m^3/h, respectively. It was observed that the top portion of the system charged up faster than the lower part. On the other hand, during discharging (flow from the bottom) the bottom part of the system released heat faster than the top section of the bed. The time required for charging the system was less than the time required for discharging. Melting of the PCM is faster because it is a natural convection dominated process. However, during solidification, the heat transfer rate between the capsule and the HTF is low as it forms a high resistance solid layer in the inside shell of the capsule. Solidification is conduction-dominated process, which is slower. Figures 4-8, 4-9 and 4-10 provide the average temperature profiles of the HTF at different positions in the storage system during charging and discharging cycles with flow rates of 151,131 and 110 m^3/h, respectively. It is evident that the top section of the capsules heats up quickly. During the discharging process, the reverse situation was observed. A typical phase change scenario is clearly evident in the figures. The temperature rise in each layer becomes very slow during the phase change process i.e. during melting of the PCM. After the completion of the melting/solidification process, the temperature of each row increases/decreases sharply.

58
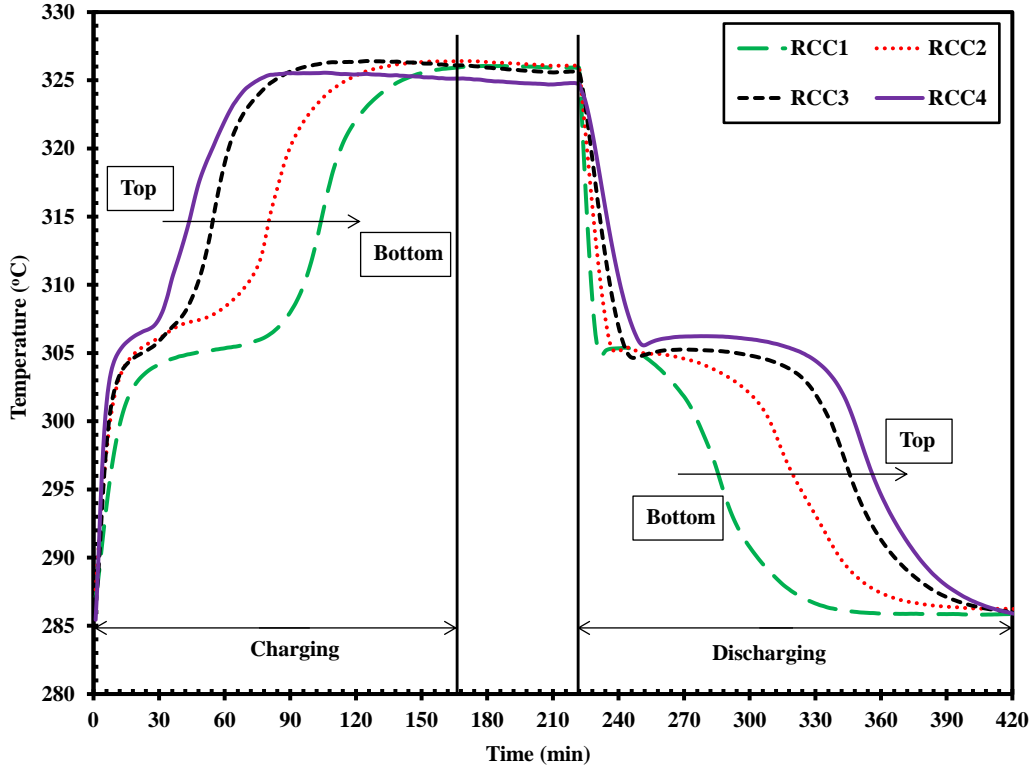
Figure 4-5: Temperature profile inside the capsule during the charging/discharging cycle (flow rate:151 m^3/h)
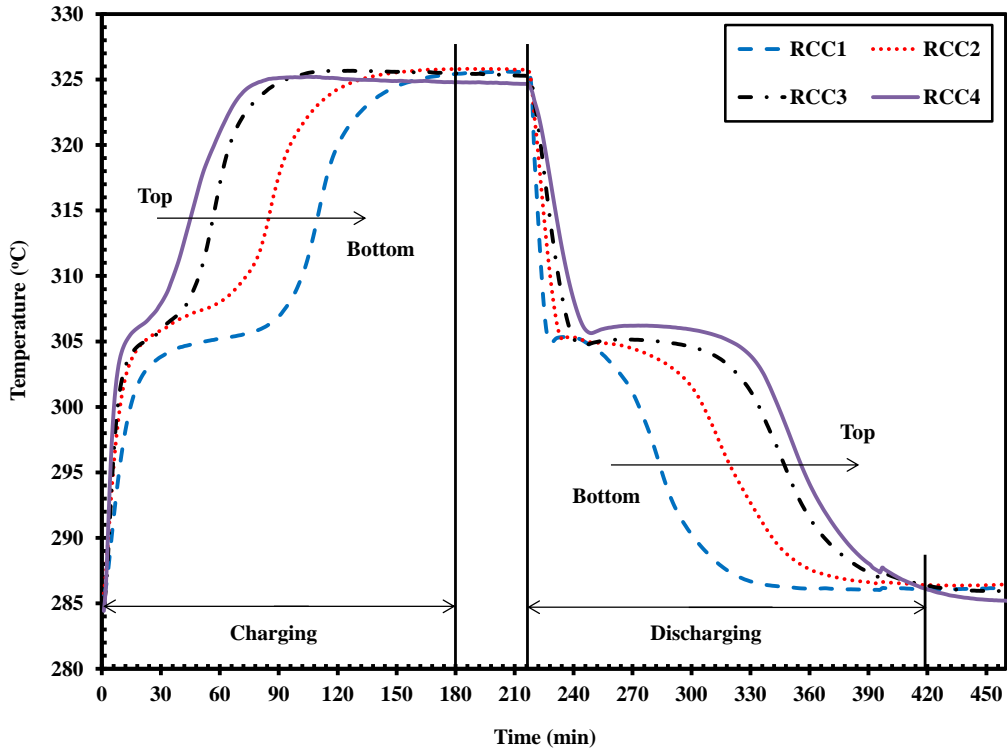
Figure 4-6: Temperature profile inside the capsule during the charging/discharging cycle (flow rate: 131 m^3/h)

59
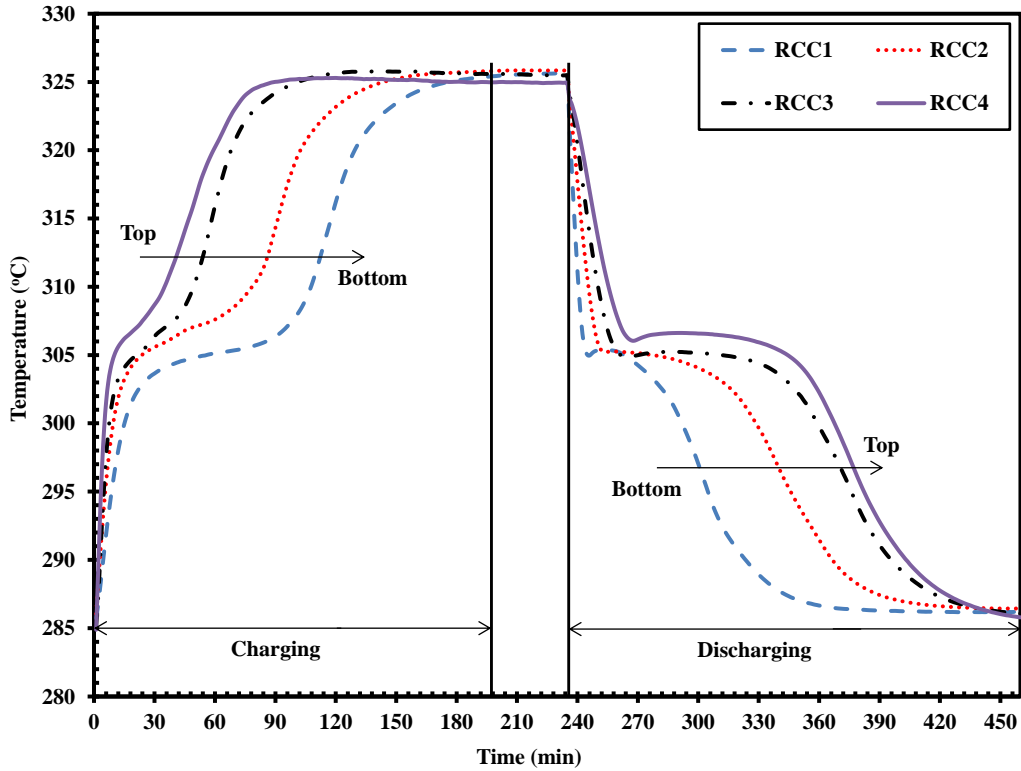
Figure 4-7: Temperature profile inside the capsule during the charging/discharging cycle (flow rate: 110 m^3/h)
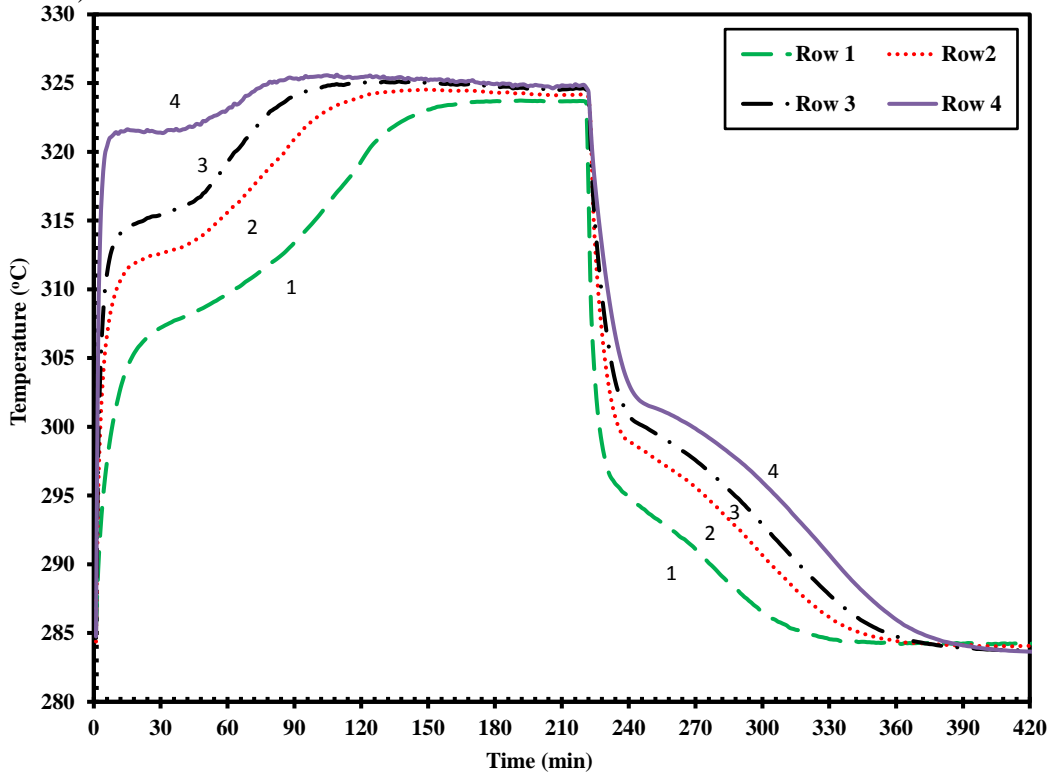
Figure 4-8: Average temperature profile for different rows during the charging/discharging cycle (flow rate: 151 m^3/h)

60
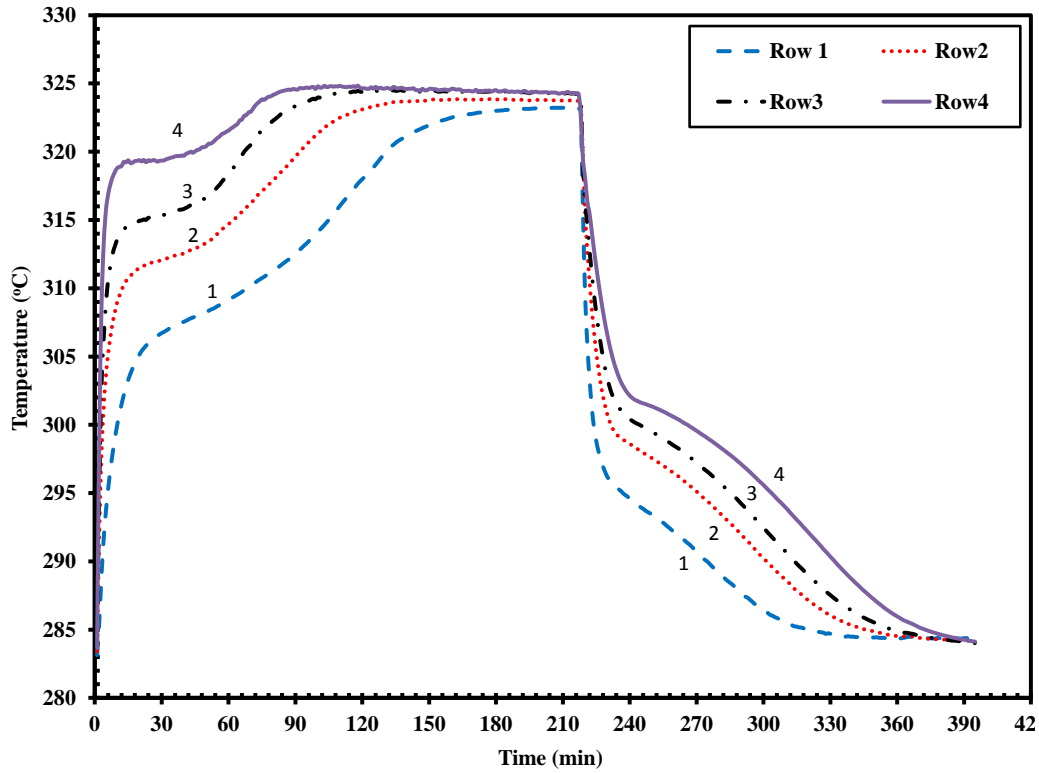
Figure 4-9: Average temperature profile for different rows during the charging/discharging cycle (flow rate: 131 m^3/h)
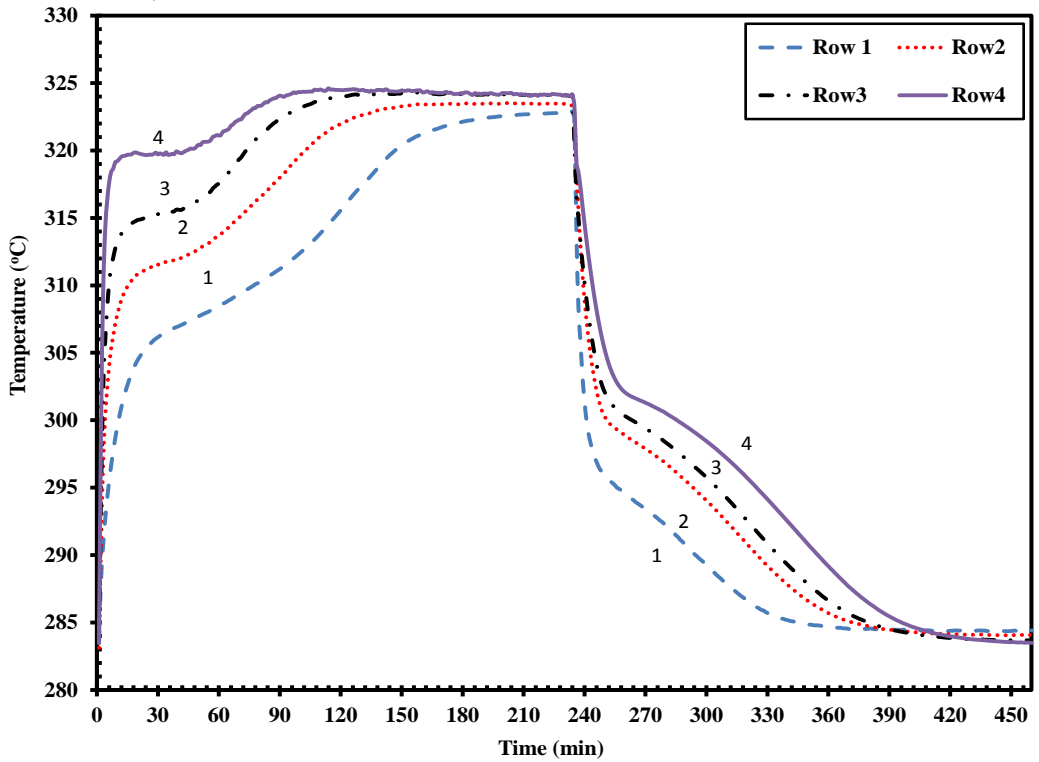
Figure 4-10: Average temperature profile for different rows during the charging/discharging cycle (flow rate: 110 m^3/h)

61

When the whole system is charged, the temperature gradient in each row diminishes. It was also observed from the experiment that when the volumetric flow rate increased from 110 to 131 m^3/h, the charging time reduced from 198 minutes to 180 minutes, which was approximately 9% improvement in the charging time. On the other hand, when the flow rate of HTF was changed from 131 to 151m^3/h, the charging time reduced from 180 to 169 minutes, approximately 6% improvement in the charging time. In the case of discharging, when the flow rate was changed from 110 to 131 m^3/h and 131 to 151 m^3/h, the discharge time reduce from 222 to 204 minutes and 204 to 198 minutes, respectively. The improvement of discharging time was approximately 8% and 3% for the aforementioned cases, respectively.

4.2.2 Influence of the HTF Flow Rate

The effect of the HTF flow rate on the thermal performance of the storage system was also investigated. Figure 4-11 shows a comparison of the temperature profiles of the capsules in rows 1 and 2 for three different flow rates during the charging process. It clearly shows that an increase in the flow rate of the HTF enhances the rate of the PCM melting process. This is because an increase in the flow rate allows the quick renewal of the HTF around the capsules resulting in the maintenance of a constant and enhanced temperature gradient between the HTF and the PCM. This leads to an increase in the overall heat transfer rate between the HTF and the PCM. Figure 4-12 shows the effect of the HTF flow rate on the charging time at various heights of the bed. The charging time is the time required for the PCM to reach the inlet HTF temperature at the considered height. It is evident from Figure 4-12 that the top of the bed charges faster than the bottom of the bed for all flow rates. Also, at a given bed height, the charging time decreases with an increase in the HTF flow rate. Higher mass flow rate leads to a shorter time interval for charging and discharging.

62
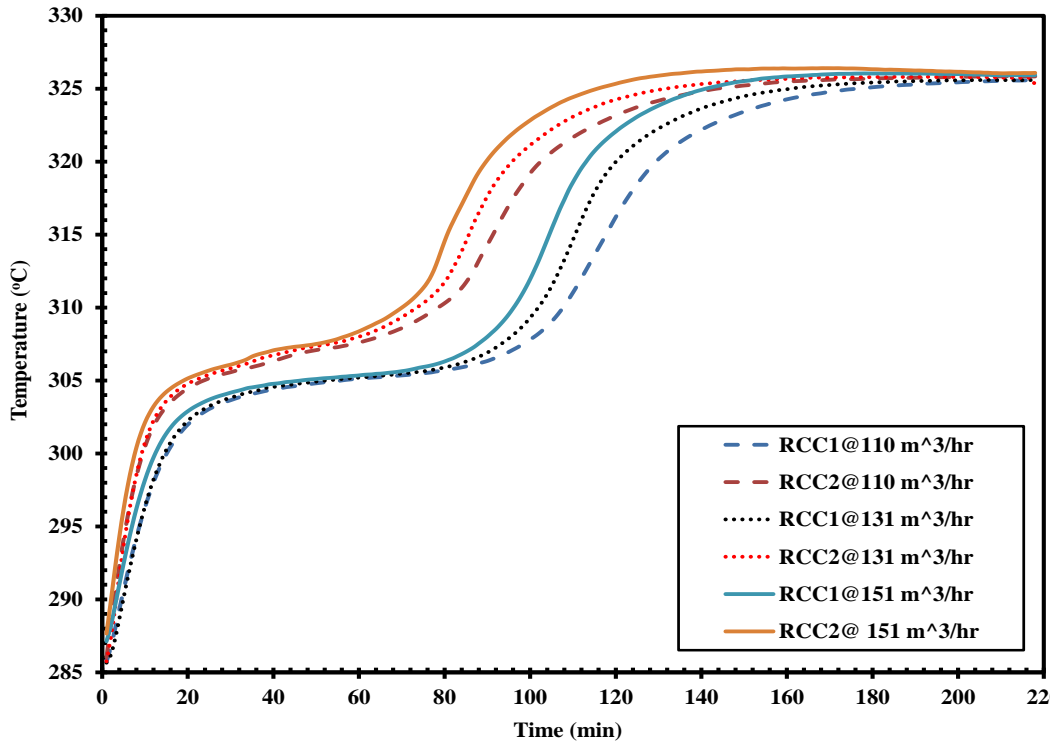
Figure 4-11: Comparison of the rows 1 and 2 temperature profiles for different flow rates during the charging process (inside the capsule)
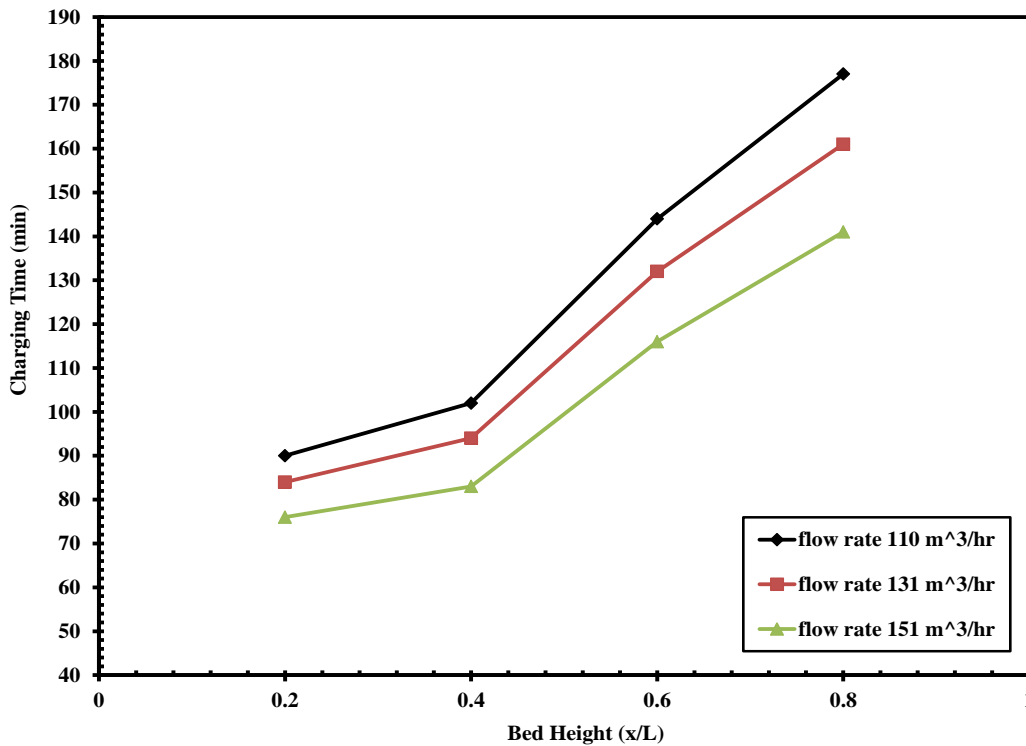
Figure 4-12: Charging time for the encapsulated LHTS system at different heights of the bed (uncertainty of the charging time is ±16.45 min).

4.2.3 Pressure Drop Across the Bed

The pressure drop across the bed is measured by a digital manometer. The pressure drop is measured and documented for three different flow rates (see Table 4-4). It is observed that the pressure drop increases with an increase in the mass flow rate. Experimental data in Table 4-4 indicates that the measured Reynolds numbers are greater than 1000. For Re_p >1,000, Burke-Plummer's equation predicts the pressure drop more accurately. According to Bird et al [120], the equation for determining the pressure drop is

$$\Delta P = \frac{1.75 \rho U^2 (1-\epsilon) l}{D_p \epsilon^3} \qquad (4\text{-}2)$$
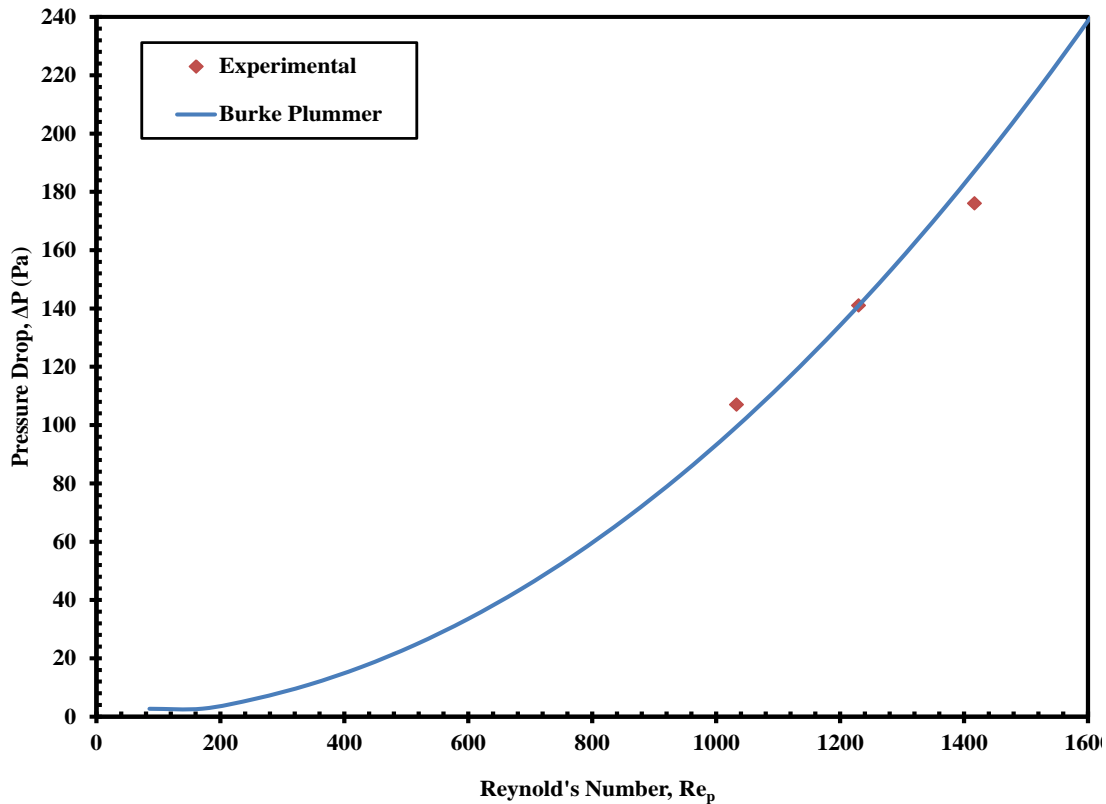
Figure 4-13: Comparison of experimental and predicted values of the pressure drop across the bed.

Figure 4-13 shows the experimentally measured pressure drop across the packed bed for three different flow rates and theoretically predicted values based on Equation (4-2). It is observed in Figure 4-13 that for low flow rates the experimental pressure drop is approximately

64

1-6% higher than the predicted value and for a higher flow rate, the pressure drop is approximately 6% lower than the predicted value. Higher flow rates produce larger overall pressure drops across the bed.

Table 4-4: Pressure drop across the bed for different flow rates

Flow rate (m³/h)	Superficial Velocity (m/s)	$Re_p = \frac{\rho U D p}{\mu}$	ΔP (Pa)
110	0.603	1033	107
131	0.718	1230	141
151	0.827	1417	176

4.2.4 Energy and Exergy Efficiencies

Performance of the LHTES can be analyzed by energy efficiency (first law of thermodynamics) and exergy efficiency (second law of thermodynamics). In this work, both of the parameters are calculated and presented in table 4-5 and figure 4-14. The physical properties of air are determined based on the bulk mean temperature [121].

$$T = \frac{T_f + T_i}{2} \tag{4-3}$$

Overall first law efficiency of the storage system is the ratio of net energy recovered during discharging over the net energy supplied during charging [121].

$$\eta = \frac{E_{Dch}}{E_{Ch}} \tag{4-4}$$

where, E_{Dch} and E_{Ch} are calculated from the following equations.

$$E_{Dch} = \dot{m}_{HTF} C_{p,HTF} \left(T_{HTF,out} - T_{HTF,in} \right) d\tau \tag{4-5}$$

$$E_{Ch} = \dot{m}_{HTF} C_{p,HTF} \left(T_{HTF,in} - T_{HTF,out} \right) d\tau \tag{4-6}$$

Exergy efficiency of the storage system for a complete charging and discharging cycle is the ratio of net exergy recovered to the net exergy supplied [121].

65

$$\eta_{II} = \frac{Ex_{recovered,HTF,net}}{Ex_{supplied,HTF,net}} \qquad (4\text{-}7)$$

where, $Ex_{recovered,HTF,net}$ and $Ex_{supplied,HTF,net}$ was calculated from the following equations.

$$Ex_{recovered,HTF,net} = \int_{t_{i,Dch}}^{t_{f,Dch}} \left[\dot{m}_{HTF} C_{p,HTF} \left(T_{HTF,out} - T_{HTF,in} - T_o \ln\left(\frac{T_{HTF,out}}{T_{HTF,in}}\right) \right) \right] dt \qquad (4\text{-}8)$$

$$Ex_{supplied,HTF,net} = \int_{t_{i,Ch}}^{t_{f,Ch}} \left[\dot{m}_{HTF} C_{p,HTF} \left(T_{HTF,in} - T_{HTF,out} - T_o \ln\left(\frac{T_{HTF,in}}{T_{HTF,out}}\right) \right) \right] dt \qquad (4\text{-}9)$$
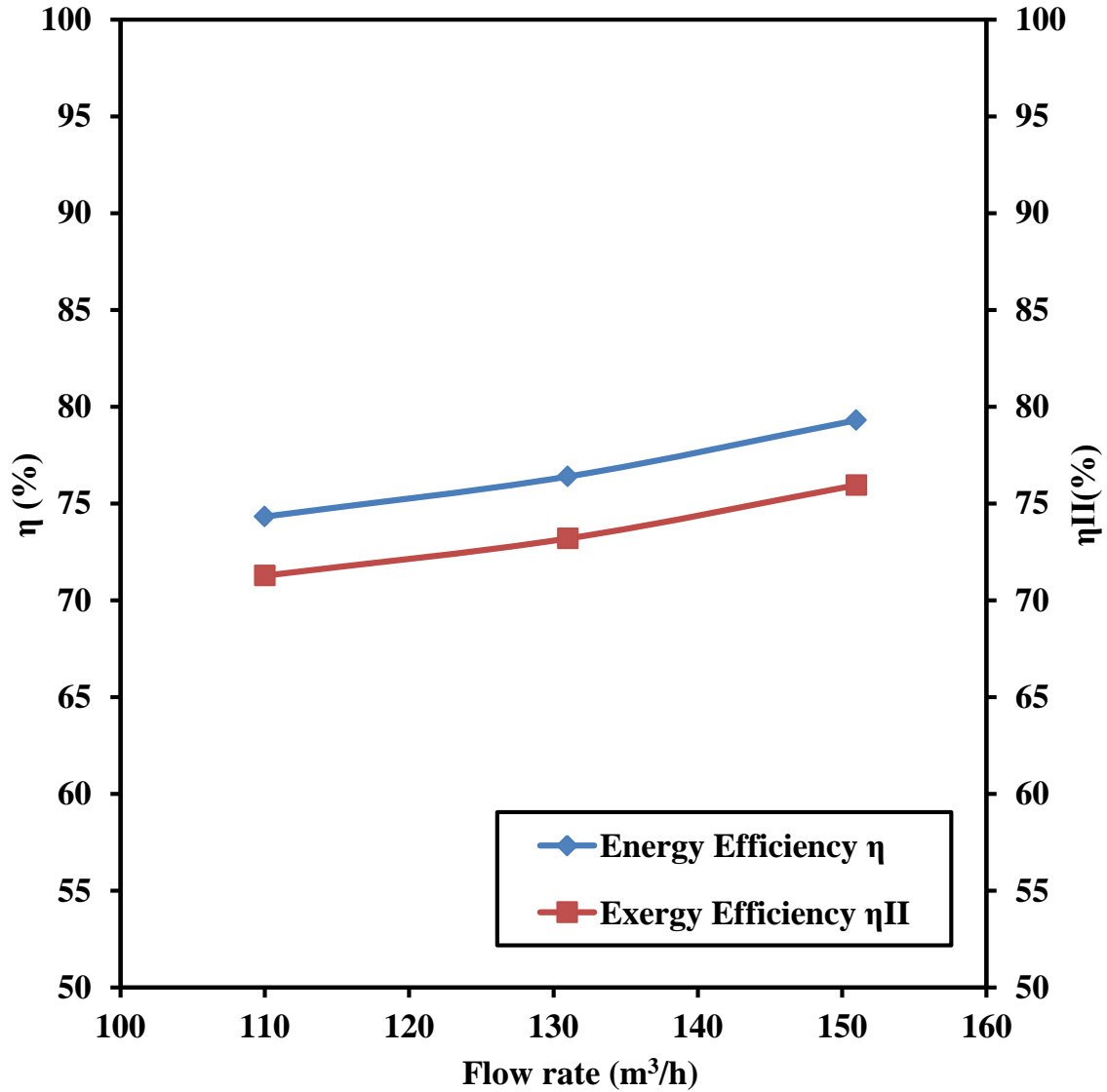
Figure 4-14: Energy and exergy efficiency for different flow rates

Table 4-5: Efficiencies at different flow rates

Flow rate (m³/h)	Energy Efficiency (η)	Exergy Efficiency (η$_{II}$)
110	74.33	71.28
131	76.40	73.20
151	79.31	75.96

Figure 4-14 shows the energy efficiency and exergy efficiency for three different flow rates. It is found that energy and exergy efficiencies vary between 74.33-79.31% and 71.28-75.96%, respectively, increases with the flow rate. Energy efficiency was found higher than the exergy efficiency for different flow rate. Energy efficiency was calculated based on the total quantity of energy transferred throughout the system and could be maximized by providing sufficient insulation, consequently minimizing the heat loss. On the other hand, the exergy efficiency quantified only useful amount of energy [121]. To increase the exergy efficiency, it is necessary to prevent the destruction of exergy during discharging. The way to accomplish this target is by decreasing the discharging time.

67

CHAPTER 5

EXPERIMENTAL INVESTIGATION OF DIFFERENT SIZE SPHERICAL CAPSULES

This chapter presents the investigation of constrained melting and solidification of sodium nitrate PCM inside spherical capsules. The effects of melting and solidification were observed for various diameter capsules (25.4, 50.8 and 76.2 mm) inside an electrically heated furnace. In each capsule, three thermocouples were installed vertically at three equidistant positions in the capsule. It is mentioned in chapter four that decreasing the discharging time is necessary to reduce the destruction of exergy. Shorter discharging time could be achieved by enhancing the heat transfer rate during solidification. In this investigation, 5 wt% and 7 wt% of graphene were used as the highly conductive dispersion particle (as graphene has higher specific surface area and less density than $NaNO_3$ in both solid and liquid state. See table 2-2) to enhance the heat transfer rate during solidification, and compared with pure PCM capsules. The main objectives of the experiment are as follows:

a) To observe the temperature profile of different size capsules during melting and solidification.

b) Measure the melting and solidification time for different size capsules

c) Determination of enhancement effect by adding 5 wt% and 7wt% of graphene.

5.1 Experimental Setup and Procedure

5.1.1 Materials

Polytetrafluproethylene (PTFE) films, graphene (60 nm) and sodium nitrate ($NaNO_3$) were purchased from McMaster-Carr,USA, Graphene Supermarket, USA, and Sigma Aldrich,

68

USA respectively. The K-type thermocouples and data acquisition system were obtained from Omega, CT, USA and National Instrument, Texas, USA respectively. To observe the melting and solidification of the spherical capsules, a multi-stage programmable Vulcan bench top furnace was procured from DENTSPLY, USA.

5.1.2 Characterization

The DSC/DTA/TGA analyses were carried out using the SDT-Q 600 by TA instrument. This machine can simultaneously perform differential scanning calorimetry and thermogravimetric analysis. Heat flow, temperature and weight accuracy of this device are $\pm 2\%$ (based on metal melting standards), $\pm 1^{o}C$ (based on metal melting standards) and $\pm 1\%$, respectively. All the TG analyses were performed at a ramp rate of $10^{o}C/min$ under an inert (Argon) atmosphere. The thermal diffusivity analysis was performed by XFA 300/600 Linseis diffusivity measurement apparatus and the accuracy of this device was $\pm 6\%$.

5.1.3 Encapsulation of NaNO$_3$ Capsules

Sodium nitrate salts were grounded very well to make fine power. This powder was then pressed in a hydraulic press (inside specific die) at 980 N of force to form hemispherical pellets of 25.4, 50.8, and 76.2 mm diameter. The salt pellets were coated with thin stretchable PTFE films . The coated pellets were again pressed in the hydraulic press at 980 N of force. The thickness of all the capsules was maintained 0.052 ± 0.005 cm. These capsules were then heated to $326^{o}C$ and annealed for one hour, two hours and three hours for 25.4, 50.8, and 76.2 mm diameter capsules respectively. Also, two capsules of 25.4 mm diameter were made with 5 wt% and 7 wt% of graphene with NaNO$_3$ by using cold compression method. In cold compression method, the salt and the dispersion particles were mixed and compressed at room temperature to form spherical capsules.

69

5.1.4 Experimental Setup

To observe the melting and solidification profile inside the capsule three thermocouples were installed. Initially, the capsules were drilled, and three thermocouples were placed vertically at three equidistant positions inside the capsules. Thermocouples were wrapped with PTFE tape to hold these in a steady position. Table 5-1 represents the positions of the thermocouples inside the capsule. Then the capsules were re-coated from the top to prevent the leakage of the PCM in molten state.

Table 5-1: Vertical position of the thermocouples inside the capsule

Case	Capsule size	Top position (P1) (cm)	Center position (P2) (cm)	Bottom position (P3) (cm)
Case 1	25.4 cm capsule	6.35	12.7	19.05
Case 2	50.8 cm capsule	12.6	25.2	37.8
Case 3	76.2 cm capsule	19.05	38.1	57.15

*All positions were measured from the top (after the shell material)

A schematic of the experimental setup is illustrated in figure 5-1. It contained a polymer capsule, a programmable furnace, five calibrated K-type thermocouples (nominal diameter 0.25 mm), data acquisition system, and a data logger system. The polymer-coated capsule was placed at the center of the furnace, three thermocouples were installed inside the capsule (figure 5-2, figure 5-3), one thermocouple was placed on the right side of the capsule and another at the top of the capsule. Thermocouples were allocated from the top of the furnace and properly insulated to reduce the heat losses. Error associated with these thermocouples was ± 2.2°C or 0.75% of the maximum temperature. The thermocouples were attached to a data acquisition system (by National Instrument, NI cDAQ-9178). Temperature data were collected and recorded by Labview Express at one-minute intervals. The furnace was cycled in the temperature range of 286°C to 326°C. In the cases 1, 2 and 3, capsules had 17.40±0.10 gm, 114.24±0.16 gm and

70

354.60±0.18 gm of $NaNO_3$ respectively. The coating material was flexible to accommodate the expansion of the PCM in the liquid state. The heat transfer from the furnace to the capsule was transferred via two parallel paths. One was convective heat transfer from the furnace air to the surface of the capsule. The second method was radiative heat transfer from the resistance heater to the capsule surface.
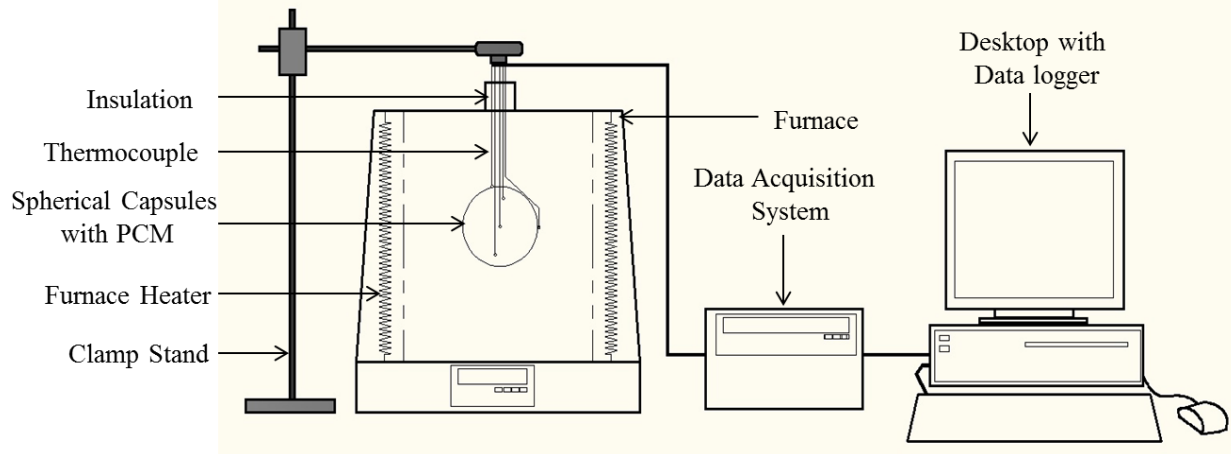
Figure 5-1: Experimental setup for different size capsules
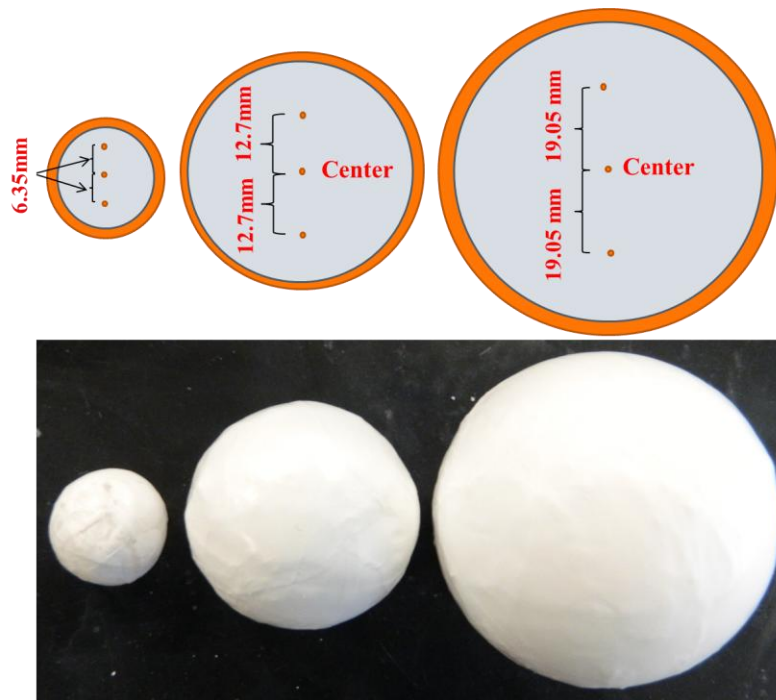
Figure 5-2: Position of the thermocouple in different size capsules (polymer coated)

71
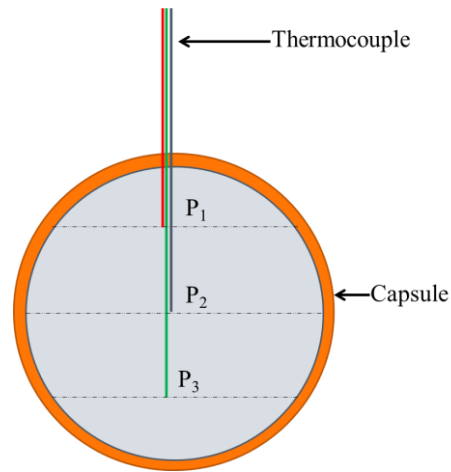
Figure 5-3: Three K-type thermocouples inside the capsule

5.1.5 Experimental Procedure

After placing the capsule inside the furnace and connecting the thermocouples with the data logger, the lab view program was started to collect the data at one-minute intervals. The furnace was programmed for two consecutive cycles. The steps of the two consecutive cycles for three cases are stated in table 5-2. At the 1st step, the furnace was set at 286 ^{o}C for two hours to stabilize the spherical capsule temperature at 286°C for all cases and ensured that all the thermocouples were at 286 ^{o}C. For the 2nd step (1st melting step) the furnace was ramped up to 326°C at a ramp rate of 40 ^{o}C/min and maintained at this temperature for two hours, four hours and six hours for cases 1,2 and 3 respectively, to ensure that all the thermocouples reach the desired temperature. On the 3rd step (1st solidification step), the furnace was programmed to cooled down to 286°C at the same ramp rate as before and maintained at this temperature for two, five and seven hours for the cases 1,2 and 3 respectively. Steps two and three were repeated one more time to complete two consecutive cycles. This two-cycle process was repeated three more times to confirm the uncertainty of the measured data. The uncertainty of the temperature

72

measurement experiment was approximately ±3.54%. For the 5 wt% and 7 wt% of graphene capsules, the same methodology was followed in case 1.

Table 5-2: Furnace time steps for different cases

Case	Melting Step (hr)	Solidification Step (hr)
Case 1	2	2
Case 2	4	5
Case 3	6	7

5.1.6 Uncertainty Analysis

TGA, diffusivity and temperature measurements were conducted several times to observe the repeatability of the measured data. The Root-sum-square method was employed to evaluate the uncertainty of the measurements [115, 116] with a 95% confidence level.

$$U_c = \sqrt{\sigma_{random}^2 + \sigma_{systemtic}^2} \tag{5-1}$$

where, U_c, σ_{random} and $\sigma_{systematic}$ are the combined standard uncertainties for the measurements, random error, and systematic error, respectively.

5.2 Results and Discussion

5.2.1 Temperature Profile of Different Size Capsules

In the presence of a thermocouple, the solid PCM clasps itself to the thermocouple preventing the solid PCM from sinking/rising to the bottom/top to the capsule due to density difference of two phases of the PCM. This approach is called constrained melting. Tan et al. [103] visually observed this phenomenon by melting of n- Octadecane in a spherical capsule presented in figure 5-4. It is observed that the melting of the PCM was concentric, and last point of melting was almost two thirds of the distance from the top. Initially, conduction was the dominant process. It created a constant liquid layer near the inner wall of the capsule. With the

73

time lapse, convective heat transfer became dominant and created an upward motion of the molten liquid along the capsule wall and downward motion of the colder liquid. Buoyancy-driven convection was the reason for faster melting in the top portion than the bottom [98, 104]. Similar phenomena were observed in the melting of different size capsules in this experiment.

(a) 10 minutes   (b) 20 minutes   (c) 30 minutes

(d) 50 minutes   (e) 70 minutes   (f) 90 minutes

(j) 110 minutes   (k) 130 minutes   (l) 150 minutes
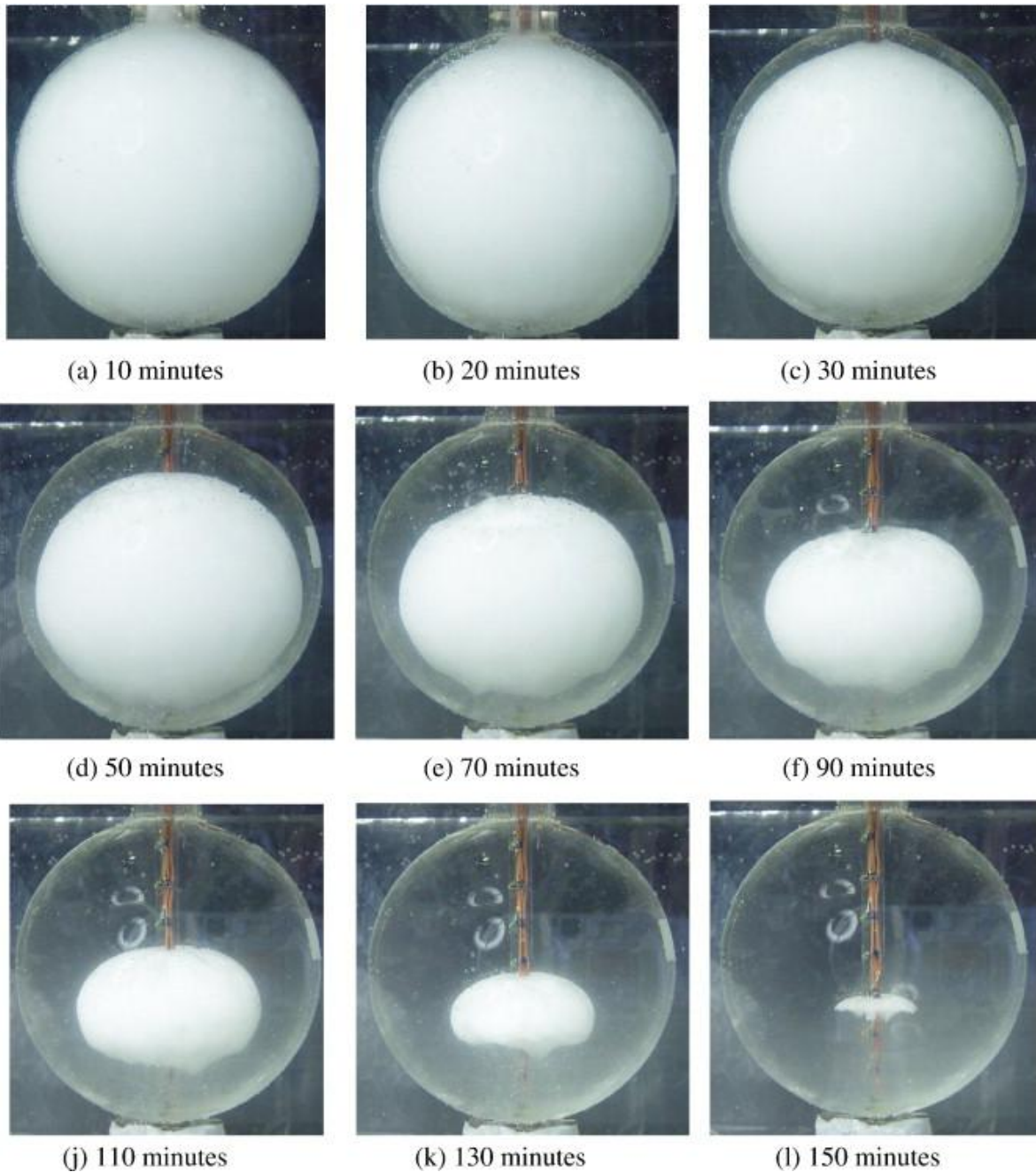
Figure 5-4: Constrained melting of n-Octadecane in spherical capsule [103](Permission is in Appendix C)
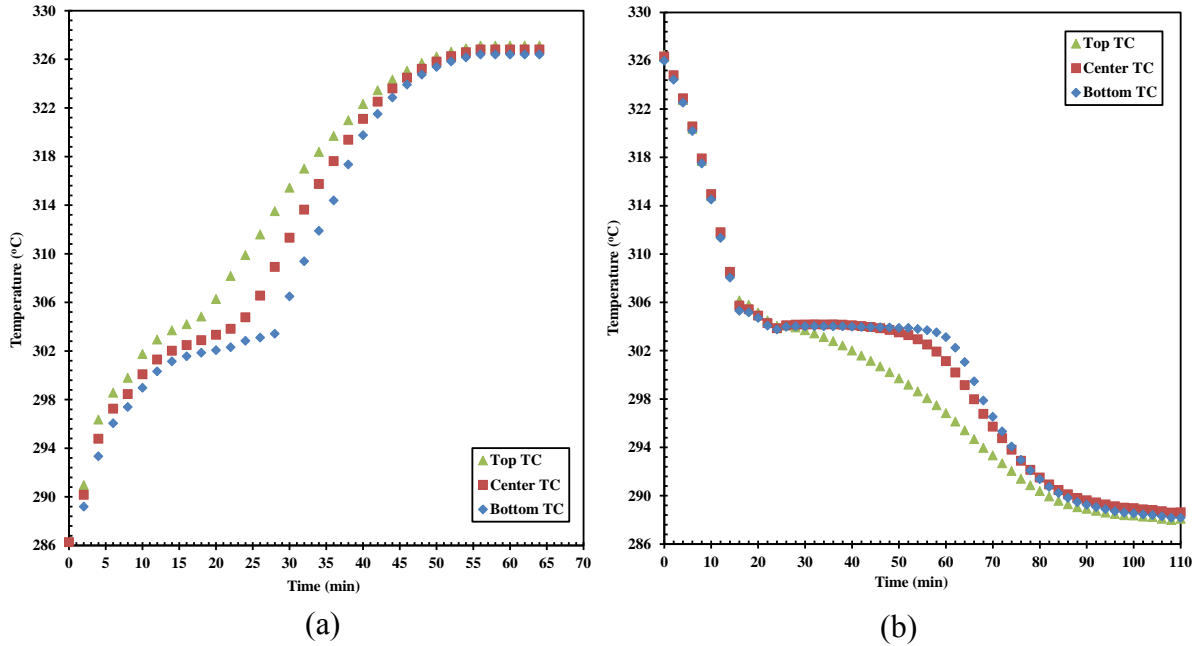
Figure 5-5: Melting (a) and solidification (b) profile of 25.4 mm capsule
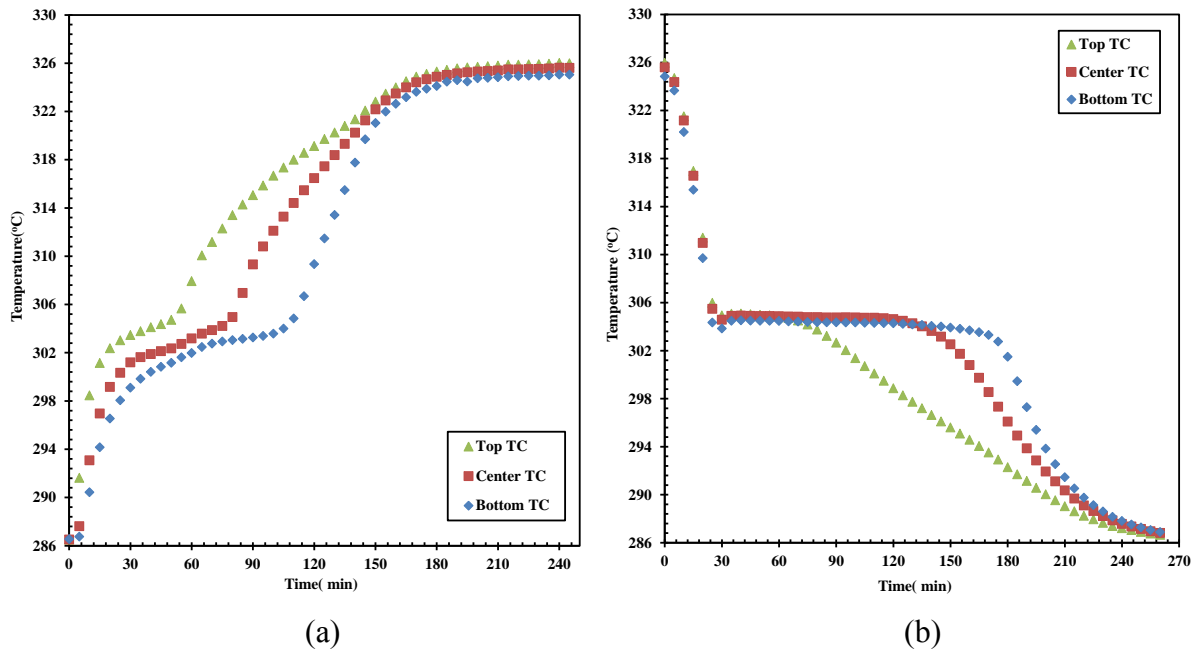
Figure 5-6: Melting (a) and solidification (b) profile of 50.8 mm capsule

The heating of the capsule was divided into three segments. Segment one is the sensible heat absorption zone by the solid PCMs. Segment two is the latent heat absorption zone at a constant temperature, and finally the segment three is the sensible heat absorption by the liquid

PCM. Figures 5-5(a), 5-6 (a), 5-7 (a) show that the top thermocouple at P1 position observed the quickest melting, after that P2 melted. The thermocouple at P3 position observed the last melting as it was positioned at two-thirds the distance from the top.

(a)

(b)
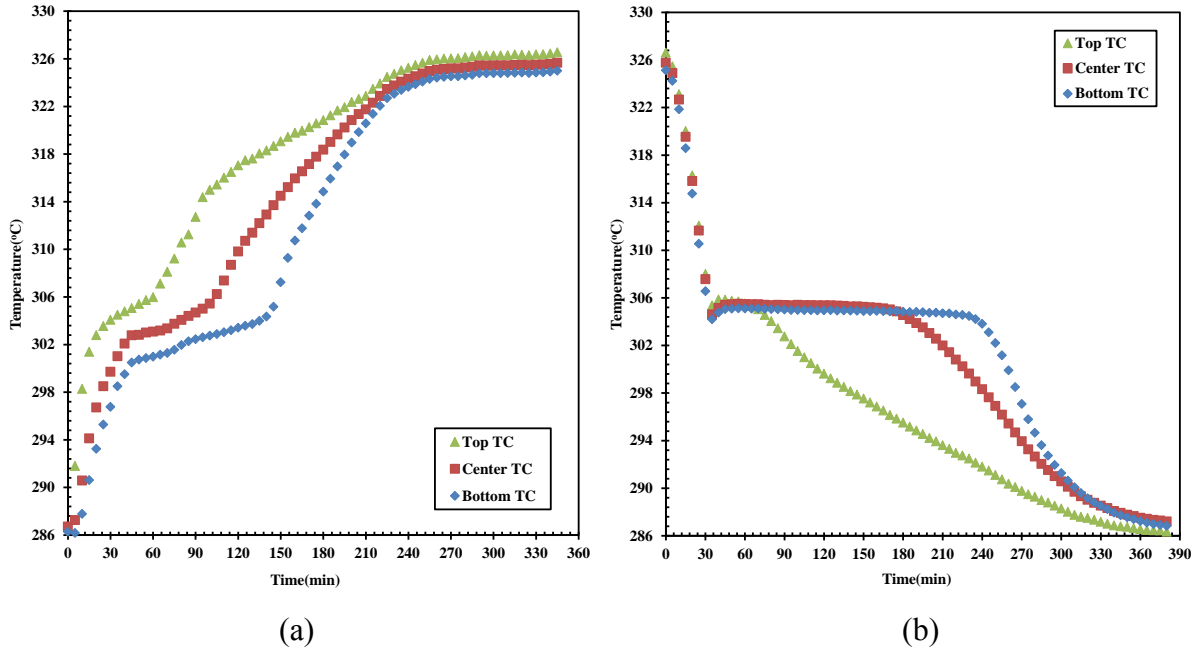
Figure 5-7: Melting (a) and solidification (b) profile of 76.2 mm capsule

(a)

(b)
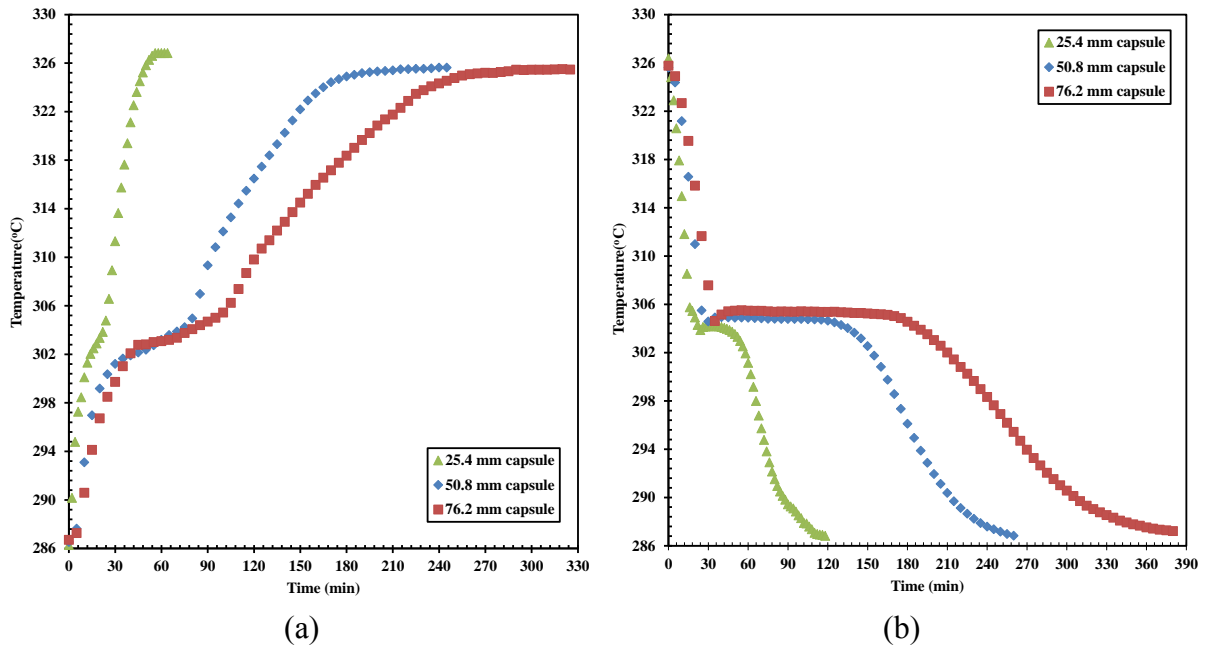
Figure 5-8: Comparison of the melting (a) and solidification (b) profile of different size capsules at center thermocouple

76

Solidification of the spherical capsule took place from the outside-in and it thus developed a high resistance solid layer at the inner wall of the capsule. Therefore, solidification is a conduction-dominated process, which is slower. Figures 5-5(b), 5-6 (b), 5-7 (b) show that the top thermocouple observed the solidification much more quicker than the center and the bottom thermocouples. Center and the bottom thermocouple observed solidification at a close-by interval. It is evident that because of the constrained solidification, the last point of solidification shifted below the center point. Figure 5-8 represents the melting and solidification profiles of different size capsules at the center thermocouple. It shows that cases 2 and 3 took 271% and 342% more time to melt than case 1, respectively. During solidification, cases 2 and 3 took 223% and 363% more time to solidify than case 1, respectively. Melting and solidification times for three different cases are tabulated in table 5-3.

Table 5-3: Melting and solidification time for three different size capsules

Case	Top position Melting/Solidification (Minutes)	Center position Melting/Solidification (Minutes)	Bottom position Melting/Solidification (Minutes)
Case 1(25.4 mm)	9/13	14/30	18/42
Case 2 (50.8 mm)	32/42	51/97	71/137
Case 3(76.2 mm)	38/45	62/139	94/194

* Uncertainty associated with this measurement is ±7%.

5.2.2 Heat Transfer Enhancement with Dispersed Graphene

Graphene has higher thermal conductivity and higher specific surface area with lower density than $NaNO_3$. Initially, capsules were made of low concentration graphene with $NaNO_3$ PCM. It was found that with low concentration, these particles tended to settle down on the periphery of the capsule wall rather than dispersing throughout the capsule. At the same time, melting time of the capsules was increased as these obstructed the natural convection of the PCM

77

at liquid state. Later, 5 wt% and 7 wt% of graphene was employed to complete the investigation. Figure 5-9 shows the distribution of the 5wt% of graphene in NaNO$_3$ capsule after 30 thermal cycles.

Figure 5-9: 5 wt% of graphene dispersed in NaNO$_3$ capsule

|(a)|(b)|
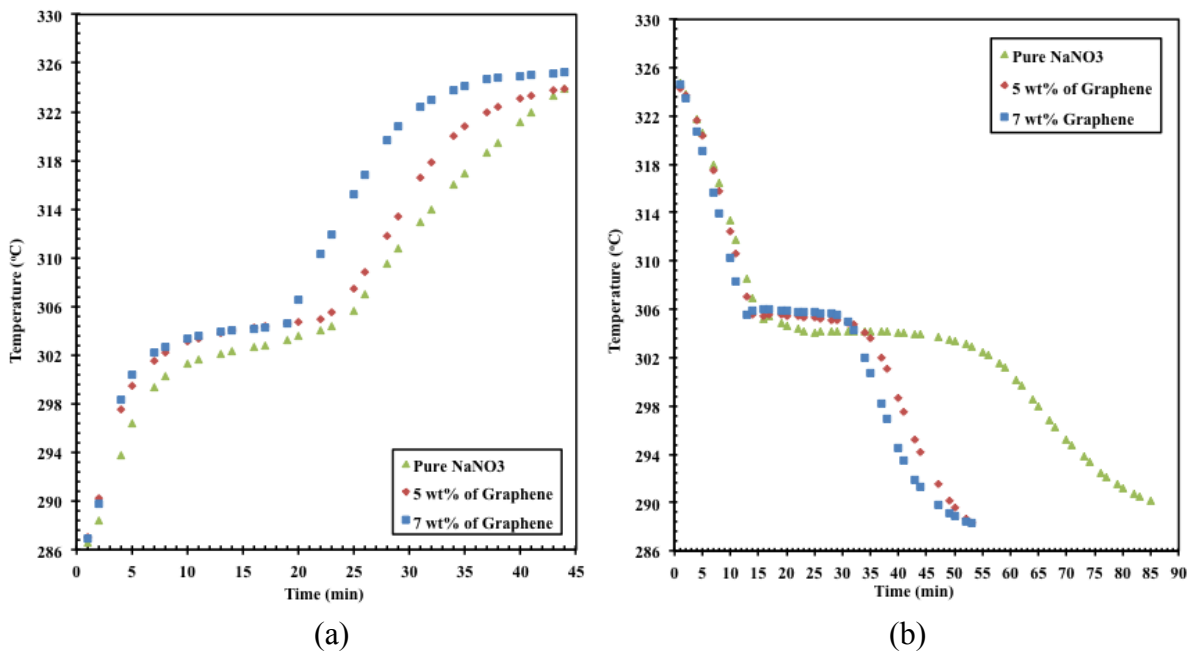
Figure 5-10: Comparison of the melting (a) and solidification (b) profile of 25.4 mm capsule filled with pure NaNO$_3$ / composites

Figure 5-10 shows the transient temperature profile of pure $NaNO_3$ and two other composites. In all cases, melting in the capsule was divided into three segments. Segment one is the sensible heat absorption zone by the solid PCMs. Segment two is the latent heat absorption zone at a constant temperature, and finally segment three is the sensible heat absorption by the liquid PCM. It is observed from the figure 5-10(a) that with both 5 wt% and 7 wt% of graphene, PCM completed the solid phase sensible heat absorption zone more sharply than the pure $NaNO_3$ and reached the phase change process earlier than the pure $NaNO_3$. 7 wt% of graphene finished the melting process 13% quicker than the pure $NaNO_3$ capsule. Even though, 5 wt% of graphene started melting early; it took almost the same time to melt as pure $NaNO_3$ capsule. This is probably because the 5 wt% of graphene was hindering the natural convection process inside the capsule, and the conductive heat transfer was not strong enough to reduce the melting time. Even though 7 wt% of graphene would also obstruct the convection process inside the capsule; the increased conductive heat transfer due to the highly conductive graphene was more than enough to overcome it. After finishing the melting zone, composites reached the final temperature more sharply than the pure PCM did.

Figure 5-10 (b) shows the solidification profile of the composites and the pure PCM. During solidification stage, both 5 wt% and 7 wt% of graphene composites exhibited better performance than melting process as solidification is a conduction dominated process. 5 wt% and 7 wt% of graphene composites reduced the solidification time by 41% and 50% respectively and completed the whole solidification cycle approximately 30 minutes before the pure $NaNO_3$.

With the increasing mass fraction of the graphene, the storage capacity of the capsules was decreased even though the heat transfer rate increased. Table 5-4 presents the thermophysical properties of pure $NaNO_3$ and different mass fraction of the composite. It is

79

observed that phase change temperature was slightly higher than that of pure $NaNO_3$ that was also observed in figure 5-10. With the increasing mass fraction of the graphene particles, the latent heat of fusion decreased.

Table 5-4: Thermophysical property of $NaNO_3$/composite

Material	Melting point (^oC)	Latent Heat of Fusion (kJ/kg)
$NaNO_3$	303.22	170.8±1.2
5 wt% of Graphene with $NaNO_3$	304.35	161.4±2.5
7 wt% of Graphene with $NaNO_3$	304.84	157.8±3.5

Figure 5-11 presents the thermal diffusivity of pure $NaNO_3$ and different mass fractions of the composite at different temperatures. Thermal diffusivity indicates the reaction time of a material with the change in temperature. As expected from the previous experiments, 7 wt% concentration has higher thermal diffusivity value than the 5 wt% concentration composite and the pure PCM. The uncertainty of this analysis was ± 6%.
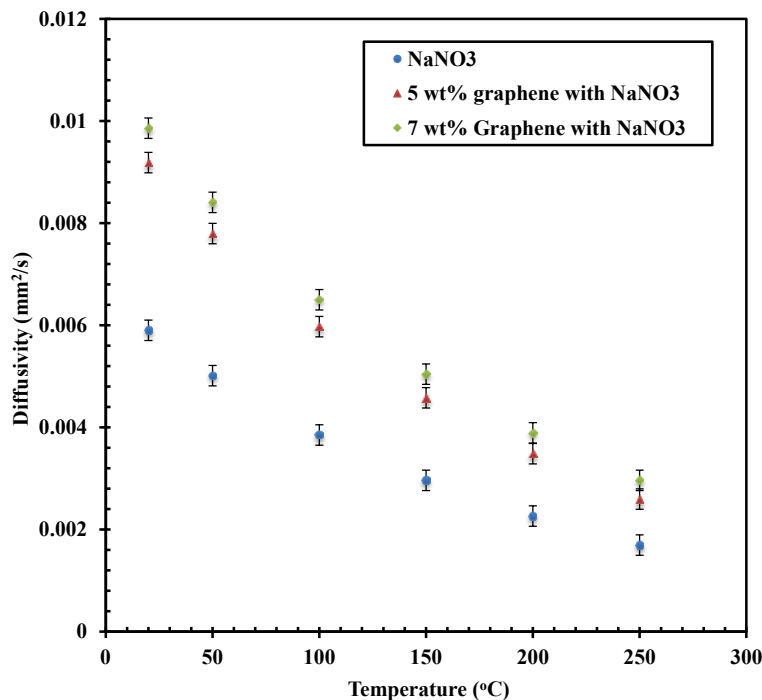
Figure 5-11: Thermal diffusivity of pure $NaNO_3$ and different mass fraction of the composite at different temperature.

CHAPTER 6:

PROPOSED MANUFACTURING STEPS

This Chapter discusses manufacturing process steps of the encapsulated capsules for the latent heat storage system.

6.1 Manufacturing Process

Manufacturing process is the conversion of raw material to finished products. Companies in the recent past have outsourced their production process to third parties and focused on product development [122]. However, having the manufacturing process in-house adds not only the physical value of the machinery, but also the intellectual capital. The knowledge of the production process is difficult to reproduce by competitors giving the company a distinct advantage.

The main benefits of manufacturing are given by Duarte [123]. Having manufacturing capability can significantly reduce the time required to get the final product to market. It can also hasten the ramp-up period so that full production capacity is reached faster. Manufacturing facility allows for customizations to the product without compromising on the quality. Finally, it leads to a stronger proprietary position as the production process can be kept a secret. All of these contribute to more profits for the firm and less reliance on third-party manufacturers.

Having improved production capability is a result of process development projects and production experience. Process development successfully identifies bottlenecks and difficult tasks in the production line. This is called learning before doing. Production experience refers to the time required for workers to get familiar with the process and get information on problems to

81

find opportunities to improve. This is called learning by doing. Thus, learning before doing and learning by doing together increase the knowledge base, which leads to improved production. This is how innovation takes place.

6.1.1 Steps Discussion

Manufacturing steps of the encapsulated capsules could be divided in four different sections: PCM preparation, polymer coating, metal coating and packaging. In the PCM preparation section, raw materials are collected from the vendor. After the raw materials pass the quality check, PCM powders are added to the Homogenizer with a constantly rotating screw and a mesh at the bottom to enable uniform sized particle distribution. The PCM particles fall through the bottom of the homogenizer to a conveyor belt that carries the PCM to the rotary press. There are pre-prepared dies to press the PCM into shape. Polymer coating is applied in the next stage, which can be done by hand-wrapping. The encapsulated PCM then goes through an IR heater for post-coating thermal treatment. A series of sub-steps follow to achieve electroless coating. In the subsequent sub-steps, electroplating of the encapsulated PCM pellets takes place. Finally, the finished product is obtained. Last step of the whole process is packaging and transportation of the capsules to the plants.
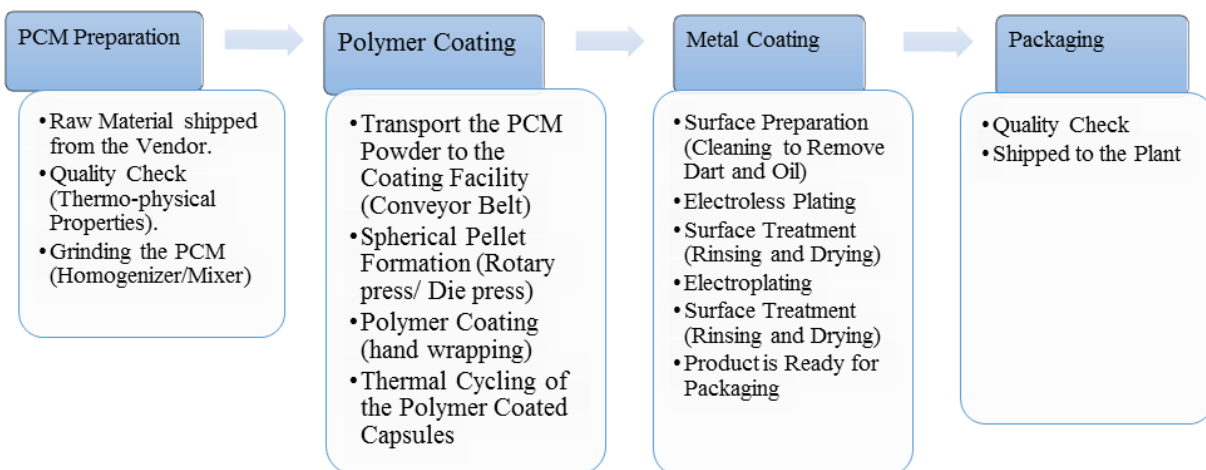
Figure 6-1: Production line of the encapsulated capsule

There are several important parameters to be maintained to ensure quality control. These

are:

a) monitoring the flow through the feeder,

b) particle size coming out of the homogenizer,

c) size, strength and weight loss of the pellets, and finally

d) thermal cycling of the PCM

List of some vendors are provided for some components:

a) Powder grinding machine: (Amisy Machinery, China; Kemutec, PA,USA)

b) Conveyor Belt: (ASGCO, PA, USA; Ace Belting company, NJ, USA)

c) Polymer: (Dupont, NJ, USA; Lin'an Linfeng Fluorine Plastics Co., Ltd., China)

d) Electroless solution: (Macdermid Inc., USA; Transene Company Inc.,USA)

e) Electroplating solution: (Allied Plating, USA)

CHAPTER 7:

CONCLUSIONS AND RECOMMENDATIONS FOR FUTURE WORK

7.1 Summary and Conclusion for Chapter 3

An innovative PCM encapsulation technique has been developed that does not require a sacrificial layer to accommodate the volumetric expansion of the PCM on melting. From this research and development, PTFE and FEP were found to be appropriate coating materials for encapsulating nitrate based PCMs for the temperature range of 120-350°C. A non-vacuum based technique was developed to coat a metal on the polymer layer that provides sufficient strength to stack the capsules in a thermal storage tank. The developed process reduces the chance of metal corrosion due to molten salts as there is a polymer layer in-between the PCM and the metal coating. The flexible coating over the capsule has allowed the use of a very thin coating layer that has significantly increased the PCM-to-coating ratio. In addition, the PCM in the macro-capsules melts and solidifies in a short period of time to satisfy the need for a quick response time for generating power on demand. Thermal cycling tests have shown that the encapsulated nitrate based materials have excellent thermal and chemical stability even after more than 2200 thermal cycles. Also, the capsules were tested in oil and molten salt environment and passed 1000 thermal cycles. Their thermophysical properties and weight change analysis suggested the stability of the capsules in three different environments. Based on these results, it can be concluded that the developed materials have good potential for use in LHS systems in renewable energy and conventional power plants.

84

7.2 Summary and Conclusion for Chapter 4

An experimental investigation on a high-temperature packed-bed LHTS system that contained macroencapsulated spherical capsules as the storage material was conducted. Sodium nitrate was used as the PCM and air as the heat transfer fluid. To understand the temperature profile and the pressure drop during charging and discharging of the system, cyclic experiments were conducted between 286°C and 326°C and at three different flow rates. It was observed from the experiment that when the volumetric flow rate increased from 110 to 131 m^3/h, the charging time reduced from 198 minutes to 180 minutes, which was approximately 9% improvement in the charging time. On the other hand, when the flow rate of HTF was changed from 131 to 151m^3/h, the charging time reduced from 180 to 169 minutes, approximately 6% improvement in the charging time. In the case of discharging, when the flow rate was changed from 110 to 131 m^3/h and 131 to 151 m^3/h, the discharge time reduced from 222 to 204 minutes and 204 to 198 minutes, respectively. The improvement of discharging time was approximately 8% and 3% for the aforementioned cases, respectively. Furthermore, energy efficiency and exergy efficiencies were calculated. It was found from the investigation that as the flow rate increased, the efficiencies increased. Increasing flow rate enhanced the heat transfer rate and shortened the charging and discharging time. In general, the experimental results did not show any surprises. However, because of a general lack of experimental studies of latent heat TES systems in the literature, these results will prove to be valuable for the system designers and the researchers conducting modeling simulation of the systems.

7.3 Summary and Conclusion for Chapter 5

In this investigation, the main objective was to observe the transient temperature response of NaNO$_3$ PCM inside various sizes of capsules during melting and solidification. A constrained

85

experimental setup was designed to fulfill the goal. It showed that during melting, cases two and three took 271% and 342% more time to melt than case one, respectively. During solidification, cases two and three took 223% and 363% more time to solidify than case one, respectively. It was also observed that both constrained melting and solidification process was concentrically inward and which was 25% below the center point. To improve the heat transfer rate in the encapsulated $NaNO_3$ PCM, various concentrations of graphene were dispersed. It was observed that low concentration of the graphene had a tendency to settle down on the periphery of the capsule. 5% and 7% of graphene exhibited good performance as these two concentrations dispersed throughout the capsule. Also, 5 wt% and 7 wt% of graphene composites reduced the solidification time by 41% and 50% respectively and completed the whole solidification cycle approximately 30 minutes before the pure $NaNO_3$. Thermophysical properties of different concentrations were measured and showed good stability after 30 thermal cycles.

7.4 Summary and Conclusion for Chapter 6

This chapter discussed probable steps involved with the production process of the capsules. It also discussed several important parameters to ensure quality control of the produced capsules and list of some vendors to buy different materials and machines.

7.5 Future Recommendations

a) Polymer and metal based encapsulation technique was developed for nitrate based PCMs and their eutectics. Several other combinations of PCM hydrates, chloride and nitrate based eutectics could be employed.

b) High temperature PCM encapsulation could be the next goal.

c) Mechanical strength of the capsule at molten state and solid state of PCM could be a great inclusion in the study.

86

d) Experimental latent heat packed-bed storage was constructed with single PCM capsules. This packed-bed storage could be implemented with various PCMs and different size of capsules.

e) Different HTF can be employed in the packed-bed thermal energy storage like oil and molten salt to test the encapsulated capsules.

REFERENCES

[1] Stekli, J.; Irwin, L.; Pitchumani, R. Technical Challenges And Opportunities For Concentrating Solar Power With Thermal Energy Storage. ASME Journal of Thermal Science and Engineering Applications 2013, 5, 021011.

[2] Kuravi, S.; Trahan, J.; Goswami, D.; Rahman, M.; Stefanakos, E. Thermal Energy Storage Technologies And Systems For Concentrating Solar Power Plants. Progress in Energy and Combustion Science 2013, 39, 285-319.

[3] Liu, M.; Saman, W.; Bruno, F. Review On Storage Materials And Thermal Performance Enhancement Techniques For High Temperature Phase Change Thermal Storage Systems. Renewable and Sustainable Energy Reviews 2012, 16, 2118-2132.

[4] Kaye, G.; Laby, T. Tables Of Physical And Chemical Constants And Some Mathematical Functions; Longman: [London], 1973.

[5] Hasnain, S. Review On Sustainable Thermal Energy Storage Technologies, Part I: Heat Storage Materials And Techniques. Energy Conversion and Management 1998, 39, 1127-1138.

[6] Ibrahim, D.; Marc, A. Thermal Energy Storage; Wiley: New York, 2002.

[7] Kenisarin, M. High-Temperature Phase Change Materials For Thermal Energy Storage. Renewable and Sustainable Energy Reviews 2010, 14, 955-970.

[8] Pasupathy, A.; Velraj, R. Phase Change Material Based Thermal Storage for Energy Conservation in Building Architecture. International Energy Journal 2006, 7(2), 147-159.

[9] Kumaresan, V.; Velraj, R.; Das, S. The Effect Of Carbon Nanotubes In Enhancing The Thermal Transport Properties Of PCM During Solidification. Heat Mass Transfer 2012, 48, 1345-1355.

[10] Xiao, X.; Zhang, P.; Li, M. Thermal Characterization Of Nitrates And Nitrates/Expanded Graphite Mixture Phase Change Materials For Solar Energy Storage. Energy Conversion and Management 2013, 73, 86-94.

[11] Sarı, A.; Alkan, C.; Karaipekli, A.; Uzun, O. Microencapsulated N-Octacosane As Phase Change Material For Thermal Energy Storage. Solar Energy 2009, 83, 1757-1763.

[12] Hawlader, M.; Uddin, M.; Khin, M. Microencapsulated PCM Thermal-Energy Storage System. Applied Energy 2003, 74, 195-202.

[13] Platte, D.; Helbig, U.; Houbertz, R.; Sextl, G. Microencapsulation Of Alkaline Salt Hydrate Melts For Phase Change Applications By Surface Thiol-Michael Addition Polymerization. Macromolecular Materials and Engineering 2012, 298, 67-77.

[14] Mathur, A.; Kasetty, R.; Oxley, J.; Mendez, J.; Nithyanandam, K. Using Encapsulated Phase Change Salts For Concentrated Solar Power Plant, Energy Procedia 2014, 49, 908-915.

[15] Dhau, J., Yogi Goswami, D., Chand, J., Stefanakos, E. Encapsulation of Thermal Energy Storage Media. 2013, Patent pending, United States of America Application No.-PCT/US2013/075971 and WO2014100096.

[16] Alam, T.; Dhau, J.; Yogi Goswami, D.; Stefanakos, E. Macroencapsulation And Characterization Of Phase Change Materials For Latent Heat Thermal Energy Storage Systems. Applied Energy 2015, 154, 92-101.

[17] Gil, A.; Medrano, M.; Martorell, I.; Lázaro, A.; Dolado, P.; Zalba, B.; Cabeza, L. State Of The Art On High Temperature Thermal Energy Storage For Power Generation. Part 1—Concepts, Materials And Modellization. Renewable and Sustainable Energy Reviews 2010, 14, 31-55.

[18] Zalba, B.; Marín, J.; Cabeza, L.; Mehling, H. Review On Thermal Energy Storage With Phase Change: Materials, Heat Transfer Analysis And Applications. Applied Thermal Engineering 2003, 23, 251-283.

[19] Fernandes, D.; Pitié, F.; Cáceres, G.; Baeyens, J. Thermal Energy Storage: "How Previous Findings Determine Current Research Priorities". Energy 2012, 39, 246-257.

[20] Lane, G. Solar Heat Storage; CRC Press: Boca Baton, Fla., 1983.

[21] Regin, A.; Solanki, S.; Saini, J. Heat Transfer Characteristics Of Thermal Energy Storage System Using PCM Capsules: A Review. Renewable and Sustainable Energy Reviews 2008, 12, 2438-2458.

[22] Abhat, A. Low temperature Latent Heat Thermal Energy Storage: Heat Storage Materials. Solar Energy 1983, 30, 313-332.

[23] Farid, M.; Khudhair, A.; Razack, S.; Al-Hallaj, S. A Review On Phase Change Energy Storage: Materials And Applications. Energy Conversion and Management 2004, 45, 1597-1615.

[24] Sharma, A.; Tyagi, V.; Chen, C.; Buddhi, D. Review On Thermal Energy Storage With Phase Change Materials And Applications. Renewable and Sustainable Energy Reviews 2009, 13, 318-345.

[25] Farid, M. Solar Energy Storage With Phase Change. Journal of Solar Energy Research 1986, 4, 11-29.

[26] Salyer, I.; Sircar, A.; Chartoff, R. Analysis Of Crystalline Paraffinic Hydrocarbons For Thermal Energy Storage By Differential Scanning Calorimetry; Part 1, Pure Hydrocarbons. 15th North American Thermal Analysis Society Conference, Cincinnati, OH, 1986.

[27] Hadjieva, M.; Kanev, S.; Argirov, J. Thermophysical Properties Of Some Paraffins Applicable To Thermal Energy Storage. Solar Energy Materials and Solar Cells 1992, 27, 181-187.

[28] Hadjieva, M.; Kanev, S.; Argirov, J. Thermophysical Properties Of Some Paraffins Applicable To Thermal Energy Storage. Solar Energy Materials and Solar Cells 1992, 27, 181-187.

[29] Himran, S.; Suwono, A.; Mansoori, G. Characterization Of Alkanes And Paraffin Waxes For Application As Phase Change Energy Storage Medium. Energy Sources 1994, 16, 117-128.

[30] Telkes, M. Nucleation Of Supersaturated Inorganic Salt Solutions. Industrial and Engineering Chemistry 1952, 44, 1308-1310.

[31] Cárdenas, B.; León, N. High Temperature Latent Heat Thermal Energy Storage: Phase Change Materials, Design Considerations And Performance Enhancement Techniques. Renewable and Sustainable Energy Reviews 2013, 27, 724-737.

[32] Olivares, R.; Edwards W. $LiNO_3$–$NaNO_3$–KNO_3 Salt For Thermal Energy Storage: Thermal Stability Evaluation In Different Atmospheres. Thermochimica Acta 2013, 560, 34–42.

[33] LUZ Industries Israel. Thermal Storage for Medium Temperature Solar Electric Power Plants Using PCMs: A Preliminary Assessment." Phase-Change Thermal Energy Symposium, October 19-20, California, 1988.

[34] Michels, H.; Pitz-Paal, R. Cascaded Latent Heat Storage for Parabolic Trough Solar Power Plants. Solar Energy 2007, 81, 829–837.

[35] Tufen, R; Petitet, J; Denielou, I; Le Neindre, B. Experimental Determination Of The Thermal Conductivity Of Molten Pure Salts And Salt Mixtures. International Journal of Thermophysics 1985, 6(4),315–30.

[36] Jegadheeswaran, S.; Pohekar, S. Performance Enhancement In Latent Heat Thermal Storage System: A Review. Renewable and Sustainable Energy Reviews 2009, 13, 2225-2244.

[37] Agyenim, F.; Hewitt, N.; Eames, P.; Smyth, M. A Review Of Materials, Heat Transfer And Phase Change Problem Formulation For Latent Heat Thermal Energy Storage Systems (LHTESS). Renewable and Sustainable Energy Reviews 2010, 14, 615-628.

[38] Incropera, F.; DeWitt, D. Introduction To Heat Transfer; Wiley: New York, 1996.

[39] Lacroix, M.; Benmadda, M. Numerical Simulation Of Natural Convection-Dominated Melting And Solidification From A Finned Vertical Wall. Numerical Heat Transfer Part A 1997, 31, 71–86.

[40] Shatikian, V.; Ziskind, G.; Letan, R. Numerical Investigation Of A PCM-Based Heat Sink With Internal Fins. International Journal of Heat and Mass Transfer 2005, 48, 3689-3706.

[41] Steinmann, W.; Laing, D.; Tamme, R. Development Of PCM Storage For Process Heat And Power Generation. J. Sol. Energy Eng. 2009, 131, 041009.

[42] Mesalhy, O.; Lafdi, K.; Elgafy, A.; Bowman, K. Numerical Study For Enhancing The Thermal Conductivity Of Phase Change Material (PCM) Storage Using High Thermal Conductivity Porous Matrix. Energy Conversion and Management 2005, 46, 847-867.

[43] Fiedler, T.; Öchsner, A.; Belova, I.; Murch, G. Thermal Conductivity Enhancement Of Compact Heat Sinks Using Cellular Metals. DDF 2008, 273-276, 222-226.

[44] Wang, J.; Chen, G.; Jiang, H. Theoretical Study On A Novel Phase Change Process. International Journal of Energy Research 1999, 23, 287-294.

[45] Farid, M.; Kanzawa, A. Thermal Performance Of A Heat Storage Module Using PCM'S With Different Melting Temperatures: Mathematical Modeling. ASME Journal of Solar Energy Engineering 1989, 111, 152–157.

[46] Hoover, M.; Grodzka, P.; O'Neill, M. Space Thermal Control Development. Lockheed Huntsville Research and Engineering Center Final Report, LMSC-HREC D225500, vol. 81; 1971.

[47] Khodadadi, J.; Fan, L.; Babaei, H. Thermal Conductivity Enhancement Of Nanostructure-Based Colloidal Suspensions Utilized As Phase Change Materials For Thermal Energy Storage: A Review. Renewable and Sustainable Energy Reviews 2013, 24, 418-444.

[48] Mettawee, E.; Assassa, G. Thermal Conductivity Enhancement In A Latent Heat Storage System. Solar Energy 2007, 81, 839-845.

[49] Zeng, J.; Sun, L.; Xu, F.; Tan, Z.; Zhang, Z.; Zhang, J.; Zhang, T. Study Of A PCM Based Energy Storage System Containing Ag Nanoparticles. Journal of Thermal Analysis and Calorimetry 2006, 87, 371-375.

[50] Xie, H.; Wan, J.; Chen, L. Effects On The Thase Transformation Temperature Of Nanofluids By The Nanoparticles. Journal of Materials Sciences & Technology 2008), 25, 742–744.

[51] Hong, H.; Zheng, Y.; Roy, W. Nanomaterials For Efficiently Lowering The Freezing Point Of Anti-Freeze Coolants. Journal for Nanoscience and Nanotechnology 2007, 7, 1–5.

91

[52] Weinstein, R.; Kopec, T.; Fleischer, A.; D'Addio, E.; Bessel, C. The Experimental Exploration Of Embedding Phase Change Materials With Graphite Nanofibers For The Thermal Management Of Electronics. Journal of Heat Transfer 2008, 130, 042405.

[53] Zeng, J.; Liu, Y.; Cao, Z.; Zhang, J.; Zhang, Z.; Sun, L.; Xu, F. Thermal Conductivity Enhancement Of Mwnts On The PANI/Tetradecanol Form-Stable PCM. Journal of Thermal Analysis and Calorimetry 2007, 91, 443-446.

[54] Kim, S.; Drzal, L. High Latent Heat Storage And High Thermal Conductive Phase Change Materials Using Exfoliated Graphite Nanoplatelets. Solar Energy Materials and Solar Cells 2009, 93, 136-142.

[55] Fang, X.; Fan, L.; Ding, Q.; Wang, X.; Yao, X.; Hou, J.; Yu, Z.; Cheng, G.; Hu, Y.; Cen, K. Increased Thermal Conductivity Of Eicosane-Based Composite Phase Change Materials In The Presence Of Graphene Nanoplatelets. Energy Fuels 2013, 27, 4041-4047.

[56] Yavari, F.; Fard, H.; Pashayi, K.; Rafiee, M.; Zamiri, A.; Yu, Z.; Ozisik, R.; Borca-Tasciuc, T.; Koratkar, N. Enhanced Thermal Conductivity In A Nanostructured Phase Change Composite Due To Low Concentration Graphene Additives. The Journal of Physical Chemistry C 2011, 115, 8753-8758.

[57] Li, J.; Lu, W.; Zeng, Y.; Luo, Z. Simultaneous Enhancement Of Latent Heat And Thermal Conductivity Of Docosane-Based Phase Change Material In The Presence Of Spongy Graphene. Solar Energy Materials and Solar Cells 2014, 128, 48-51.

[58] Park, S.; Ruoff, R. Chemical Methods For The Production Of Graphenes. Nature Nanotech 2009, 4, 217-224.

[59] Khodadadi, J.; Hosseinizadeh, S. Nanoparticle-Enhanced Phase Change Materials (NEPCM) With Great Potential For Improved Thermal Energy Storage. International Communications in Heat and Mass Transfer 2007, 34, 534-543.

[60] Salunkhe, P.; Shembekar, P. A Review On Effect Of Phase Change Material Encapsulation On The Thermal Performance Of A System. Renewable and Sustainable Energy Reviews 2012, 16, 5603-5616.

[61] Sarı, A.; Alkan, C.; Karaipekli, A.; Uzun, O. Microencapsulated N-Octacosane As Phase Change Material For Thermal Energy Storage. Solar Energy 2009, 83, 1757-1763.

[62] Hawlader, M.; Uddin, M.; Khin, M. Microencapsulated PCM Thermal-Energy Storage System. Applied Energy 2003, 74, 195-202.

[63] Tumirah, K.; Hussein, M.; Zulkarnain, Z.; Rafeadah, R. Nano-Encapsulated Organic Phase Change Material Based On Copolymer Nanocomposites For Thermal Energy Storage. Energy 2014, 66, 881-890.

[64] Platte, D.; Helbig, U.; Houbertz, R.; Sextl, G. Microencapsulation Of Alkaline Salt Hydrate Melts For Phase Change Applications By Surface Thiol-Michael Addition Polymerization. Macromolecular Materials and Engineering 2012, 298, 67-77.

[65] Qiu, X.; Li, W.; Song, G.; Chu, X.; Tang, G. Microencapsulated N-Octadecane With Different Methylmethacrylate-Based Copolymer Shells As Phase Change Materials For Thermal Energy Storage. Energy 2012, 46, 188-199.

[66] Qiu, X.; Lu, L.; Wang, J.; Tang, G.; Song, G. Preparation And Characterization Of Microencapsulated N-Octadecane As Phase Change Material With Different N-Butyl Methacrylate-Based Copolymer Shells. Solar Energy Materials and Solar Cells 2014, 128, 102-111.

[67] Zhang, H.; Baeyens, J.; Degrève, J.; Cáceres, G.; Segal, R.; Pitié, F. Latent Heat Storage With Tubular-Encapsulated Phase Change Materials (Pcms). Energy 2014, 76, 66-72.

[68] Zhang, G.; Li, J.; Chen, Y.; Xiang, H.; Ma, B.; Xu, Z.; Ma, X. Encapsulation Of Copper-Based Phase Change Materials For High Temperature Thermal Energy Storage. Solar Energy Materials and Solar Cells 2014, 128, 131-137.

[69] Vicente, R.; Silva, T. Brick Masonry Walls With PCM Macrocapsules: An Experimental Approach. Applied Thermal Engineering 2014, 67, 24-34.

[70] Zhao, W. Characterization of Encapsulated Phase Change Materials For Thermal Energy Storage", Theses and Dissertations, Mechanical Engineering Department, Lehigh University, 2013.

[71] Zheng, Y.; Zhao, W.; Sabol, J.; Tuzla, K.; Neti, S.; Oztekin, A.; Chen, J. Encapsulated Phase Change Materials For Energy Storage - Characterization By Calorimetry. Solar Energy 2013, 87, 117-126.

[72] Mathur, A.; Kasetty, R. Thermal Energy Storage System Comprising Encapsulated Phase Change Material. United States of America Application No.- 2012/0018116 A1, 2012.

[73] <http://www.cristopia.com/>

[74] <http://rubitherm.com/>

[75] Saitoh, T.; Hirose, K. High Performance Phase change Thermal Energy Storage Using Spherical Capsules. Chemical Engineering Communications 1986, 41, 39-58.

[76] Öztürk, H. Experimental Evaluation Of Energy And Exergy Efficiency Of A Seasonal Latent Heat Storage System For Greenhouse Heating. Energy Conversion and Management 2005, 46, 1523-1542.

[77] Felix Regin, A.; Solanki, S.; Saini, J. An Analysis Of A Packed Bed Latent Heat Thermal Energy Storage System Using PCM Capsules: Numerical Investigation. Renewable Energy 2009, 34, 1765-1773.

[78] Nithyanandam, K.; Pitchumani, R. Computational Modeling Of Dynamic Response Of A Latent Thermal Energy Storage System With Embedded Heat Pipes. ASME Journal of Solar Energy Engineering 2013, 136, 011010.

[79] Shabgard, H.; Faghri, A.; Bergman, T.; Andraka, C. Numerical Simulation Of Heat Pipe-Assisted Latent Heat Thermal Energy Storage Unit For Dish-Stirling Systems. Journal of Solar Energy Engineering 2013, 136, 021025.

[80] Valmiki, M.; Karaki, W.; Li, P.; Lew, J.; Chan, C.; Stephens, J. Experimental Investigation Of Thermal Storage Processes In A Thermocline Tank. ASME Journal of Solar Energy Engineering 2012, 134, 041003.

[81] Esakkimuthu, S.; Hassabou, A.; Palaniappan, C.; Spinnler, M.; Blumenberg, J.; Velraj, R. Experimental Investigation On Phase Change Material Based Thermal Storage System For Solar Air Heating Applications. Solar Energy 2013, 88, 144-153.

[82] Xiao, X.; Zhang, P. Experimental Investigation On Heat Storage/Retrieval Characteristics Of A Latent Heat Storage System. Heat Transfer Engineering 2014, 35, 1084-1097.

[83] Zheng, Y.; Barton, J.; Tuzla, K.; Chen, J.; Neti, S.; Oztekin, A.; Misiolek, W. Experimental And Computational Study Of Thermal Energy Storage With Encapsulated $NaNO_3$ For High Temperature Applications. Solar Energy 2015, 115, 180-194.

[84] Bellan, S.; Gonzalez-Aguilar, J.; Romero, M.; Rahman, M.; Goswami, D.; Stefanakos, E.; Couling, D. Numerical Analysis Of Charging And Discharging Performance Of A Thermal Energy Storage System With Encapsulated Phase Change Material. Applied Thermal Engineering 2014, 71, 481-500.

[85] Peng, H.; Dong, H.; Ling, X. Thermal Investigation Of PCM-Based High Temperature Thermal Energy Storage In Packed Bed. Energy Conversion and Management 2014, 81, 420-427.

[86] Nithyanandam, K.; Pitchumani, R.; Mathur, A. Analysis Of A Latent Thermocline Storage System With Encapsulated Phase Change Materials For Concentrating Solar Power. Applied Energy 2014, 113, 1446-1460.

[87] Dhaidan, N; Khodadadi, J. Melting And Convection Of Phase Change Materials In Different Shape Containers: A Review. Renewable And Suntainable Energy Reviews 2015, 43,449-477.

[88] Moore, F.; Bayazitoglu, Y. Melting Within A Spherical Enclosure. Journal of Heat Transfer 1982, 104, 19.

[89] Roy, S.; Sengupta, S. The Melting Process Within Spherical Enclosures. Journal of Heat Transfer 1987, 109, 460–462.

[90] Bareiss, M.; Beer, H. An Analytical Solution Of The Heat Transfer Process During Melting Of An Unfixed Solid Phase Change Material Inside A Horizontal Tube. International Journal of Heat and Mass Transfer 1984, 27, 739-746.

[91] Bahrami, P.; Wang, T. Analysis Of Gravity And Conduction-Driven Melting In A Sphere. Journal of Heat Transfer 1987, 109, 806-809.

[92] Roy, S.; Sengupta, S. Gravity-Assisted Melting In A Spherical Enclosure: Effects Of Natural Convection. International Journal of Heat and Mass Transfer 1990, 33, 1135-1147.

[93] Saitoh, T.; Hoshina, H.; Yamada, K. Theoretical Analysis And Experiment On Combined Close-Contact And Natural Convection Melting In Thermal Energy Storage Spherical Capsule, Energy Conversion Engineering Conference, 1997. IECEC-97, vol. 3IEEE, 1997, 1656-1661.

[94] Fomin, S.; Saitoh, T. Melting Of Unfixed Material In Spherical Capsule With Non-Isothermal Wall. International Journal of Heat and Mass Transfer 1999, 42, 4197-4205.

[95] Cho, K.; Choi, S. Thermal Characteristics Of Paraffin In A Spherical Capsule During Freezing And Melting Processes. International Journal of Heat and Mass Transfer 2000, 43, 3183-3196.

[96] Caldwell, J.; Chan, C. Spherical Solidification By The Enthalpy Method And The Heat Balance Integral Method. Applied Mathematical Modelling 2000, 24, 45-53.

[97] Ismail, K.; Henríquez, J. Solidification Of PCM Inside A Spherical Capsule. Energy Conversion and Management 2000, 41, 173-187.

[98] Khodadadi, J.; Zhang, Y. Effects Of Buoyancy-Driven Convection On Melting Within Spherical Containers. International Journal of Heat and Mass Transfer 2001, 44, 1605-1618.

[99] Eames, I.; Adref, K. Freezing And Melting Of Water In Spherical Enclosures Of The Type Used In Thermal (Ice) Storage Systems. Applied Thermal Engineering 2002, 22, 733-745.

[100] Barba, A.; Spiga, M. Discharge Mode For Encapsulated Pcms In Storage Tanks. Solar Energy 2003, 74, 141-148.

[101] Ismail, K.; Henríquez, J.; da Silva, T. A Parametric Study On Ice Formation Inside A Spherical Capsule. International Journal of Thermal Sciences 2003, 42, 881-887.

[102] Wei, J.; Kawaguchi, Y.; Hirano, S.; Takeuchi, H. Study On A PCM Heat Storage System For Rapid Heat Supply. Applied Thermal Engineering 2005, 25, 2903-2920.

[103] Chan, C.; Tan, F. Solidification Inside A Sphere—An Experimental Study. International Communications in Heat and Mass Transfer 2006, 33, 335-341.

[104] Tan, F. Constrained And Unconstrained Melting Inside A Sphere. International Communications in Heat and Mass Transfer 2008, 35, 466-475.

[105] Tan, F.; Hosseinizadeh, S.; Khodadadi, J.; Fan, L. Experimental And Computational Study Of Constrained Melting Of Phase Change Materials (PCM) Inside A Spherical Capsule. International Journal of Heat and Mass Transfer 2009, 52, 3464-3472.

[106] Rizan, M.; Tan, F.; Tso, C. An Experimental Study Of N-Octadecane Melting Inside A Sphere Subjected To Constant Heat Rate At Surface. International Communications in Heat and Mass Transfer 2012, 39, 1624-1630.

[107] Archibold, A.; Rahman, M.; Yogi Goswami, D.; Stefanakos, E. Analysis Of Heat Transfer And Fluid Flow During Melting Inside A Spherical Container For Thermal Energy Storage. Applied Thermal Engineering 2014, 64, 396-407.

[108] Archibold, A.; Yogi Goswami, D.; Rahman, M.; Stefanakos, E. Multi-Mode Heat Transfer Analysis During Freezing Of An Encapsulated Storage Medium. International Journal of Heat and Mass Transfer 2015, 84, 600-609.

[109] Kruizenga, A.; Gill, D. Corrosion Of Iron Stainless Steels In Molten Nitrate Salt. Energy Procedia 2014, 49, 878-887.

[110] Marote, P.; Matei, C.; Sigala, C.; Deloume, J. Influence Of Spectator Ions On The Reactivity Of Divalent Metal Salts In Molten Alkali Metal Nitrates. Materials Research Bulletin 2005, 40, 1-11.

[111] Kerridge, D.; Khudhari, A. Molten Lithium Nitrate-Potassium Nitrate Eutectic: The Reactions Of Compounds Of Iron. Journal of Inorganic and Nuclear Chemistry 1975, 37, 1893-1896.

[112] Burke, J.; Kerridge, D. Oxidation Of Acetate Ions By Nitrate And Nitrite Melts. Journal of Inorganic and Nuclear Chemistry 1975, 37, 751-756.

[113] Coldwell, B.; McLean, S. The Reaction Between Diphenylamine And Nitrates In Ultraviolet Light. Canadian Journal of Chemistry 1959, 37, 1637-1643.

[114] Archibold, A.; Gonzalez-Aguilar, J.; Rahman, M.; Yogi Goswami, D.; Romero, M.; Stefanakos, E. The Melting Process Of Storage Materials With Relatively High Phase Change Temperatures In Partially Filled Spherical Shells. Applied Energy 2014, 116, 243-252.

[115] Wheeler, A.; Ganji, A. Introduction To Engineering Experimentation; Prentice Hall: Englewood Cliffs, N.J., 1996.

[116] Moffat, R. Describing The Uncertainties In Experimental Results. Experimental Thermal and Fluid Science 1988, 1, 3-17.

[117] Bauer, T.; Laing, D.; Kröner, U.; Tamme, R. Sodium nitrate for high temperature latent heat storage", The 11th International Conference on Thermal Energy Storage. Effstock Stockholm, Sweden.(2009 June)

[118] < http://www.bearingworks.com/content_files/pdf/retainers/PTFE%20datasheet.pdf>

[119] Alam, T.; Dhau, J.; Yogi Goswami, D.; Rahman, M.; Stefankos, E. Experimental Investigation of a Packed-Bed Latent Heat Thermal Storage System With Encapsulated Phase Change Material. In ASME 2014 International Mechanical Engineering Congress and Exposition. Montreal, Canada (2014, November).

[120] Bird, R.; Stewart, W.; Lightfoot, E. Transport Phenomena; New York: Wiley, 1960.

[121] Jegadheeswaran, S.; Pohekar, S.; Kousksou, T. Exergy Based Performance Evaluation Of Latent Heat Thermal Storage System: A Review. Renewable and Sustainable Energy Reviews 2010, 14, 2580-2595.

[122] Stewart, T. Your Company's Most Valuable Asset: Intellectual Capital Business Pioneers Are Finding Surprising Ways To Put Real Dollars On The Bottom Line As They Discover How To Measure And Manage The Ultimate Intangible: Knowledge. Fortune. 1994, 124-128.

[123] Duarte, C. The Critical Role Of Manufacturing-Process Innovation On Product Development Excellence In High-Technology Companies. Massachusetts Institute of Technology, 2004.

97

APPENDICES

Appendix A: Nomenclature

PCM	Phase Change Material
TES	Thermal Energy Storage
LHTES	Latent Heat Thermal Energy Storage
SHTES	Sensible Heat Thermal Energy Storage
E	Total Energy (kJ)
Q	The amount of Heat Released or Absorbed (kJ)
m	The Mass of Storage Material (kg)
$\dot{m}$	Mass Flow Rate (kg/min)
C_{sp}	Specific Heat Capacity of Material in Solid State (kJ kg^{-1}K^{-1})
C_{lp}	Specific Heat Capacity of Material in Liquid State (kJ kg^{-1}K^{-1})
T	Temperature (^{o}C)
T_m	Melting Temperatures of Storage Material (°C)
T_i	Initial Temperatures of Storage (°C)
T_f	Final Temperatures of Storage (°C)
T_o	Ambient Temperature (°C)
L	Latent Heat of Fusion (kJ/kg)
PTFE	Polytetrafluoroethylene.
FEP	Fluorinated Ethylene Propylene.
$NaNO_3$	Sodium Nitrate.
PVDF	Polyvinylidene Fluoride.
$LiNO_3$	Lithium Nitrate.
KNO_3	Potassium Nitrate
$MgCl_2$	Magnesium Chloride
LiCl	Lithium Chloride
PIF	Polyimide Film.
PI-84	Polyimide 84.
FTIR	Fourier Transform Infrared Spectroscopy.
TGA	Thermogravimetric Analysis
U_c	Combined Standard Uncertainty
D_p	Capsule Diameter (m)
l	Length of the Bed (m)
ΔP	Pressure Drop (Pa)
Re_p	Particle Reynolds Number
U	Superficial Velocity (m/s)
h	Height (cm)
r	Radius (cm)

A.1 Greek Symbols

σ_{random}	Random Error
$\sigma_{systematic}$	Systematic Error
ε	Void Fraction
ρ	Density (kg/m^3)
μ	Dynamic Viscosity (N.s./m^2)

99

η	Energy Efficiency (Dimensionless)
η_{II}	Exergy Efficiency (Dimensionless)
α	Thermal diffusivity (mm^2/sec)

A.2 Subscripts

i	Initial
f	Final
sc	Single Capsule
s	Solid
l	Liquid
m	Melting
pcm	Phase change material
poly	Polymer

Appendix B. Experimental Processes and Parts

B.1 HTF Specification

Specification of the HTF used in the "capsules in the oil" test is given below.

Key Operating Temperatures			
Maximum Bulk Fluid Operating Temperature			
• Liquid Phase		750°F	400°C
• Vapor Phase		750°F	400°C
Maximum Film Temperature		800°F	427°C
Crystallizing Point		53.6°F	12°C
Physical Properties			
Composition	Stable eutectic mixture of 73% Diphenyl Oxide and 27% Biphenyl		
Flash Point (minimum)		255°F	124°C
Fire Point (minimum)		265°F	129°C
Autoignition Temperature (minimum)		1150°F	621°C
Normal Boiling Point	@760mm Hg	495°F	257°C
Critical Temperature		930.3°F	499°C
Critical Pressure	480.3 psia		
Critical Volume	0.05153 cu ft/lb		
Heat of Fusion	23.3 cal/g		
Specific Resistivity	6.4 x 10" ohm-cm @	68°F	20°C
Surface Tension in Air	36.6 dynes/cm @	77°F	25°C
Volume Contraction Upon Freezing		6.30%	
Volume Expansion Upon Melting		6.66%	
Moisture	300 ppm (maximum)		
Density	8.83 pounds per gallon @	77°F	25°C
Specific Gravity	1.050 to 1.075 @	77°F	25°C
Average Molecular Weight	166		
* Data represents typical laboratory samples and are not guaranteed for all samples.			

B.2 Electroless and Electroplating Materials and Process
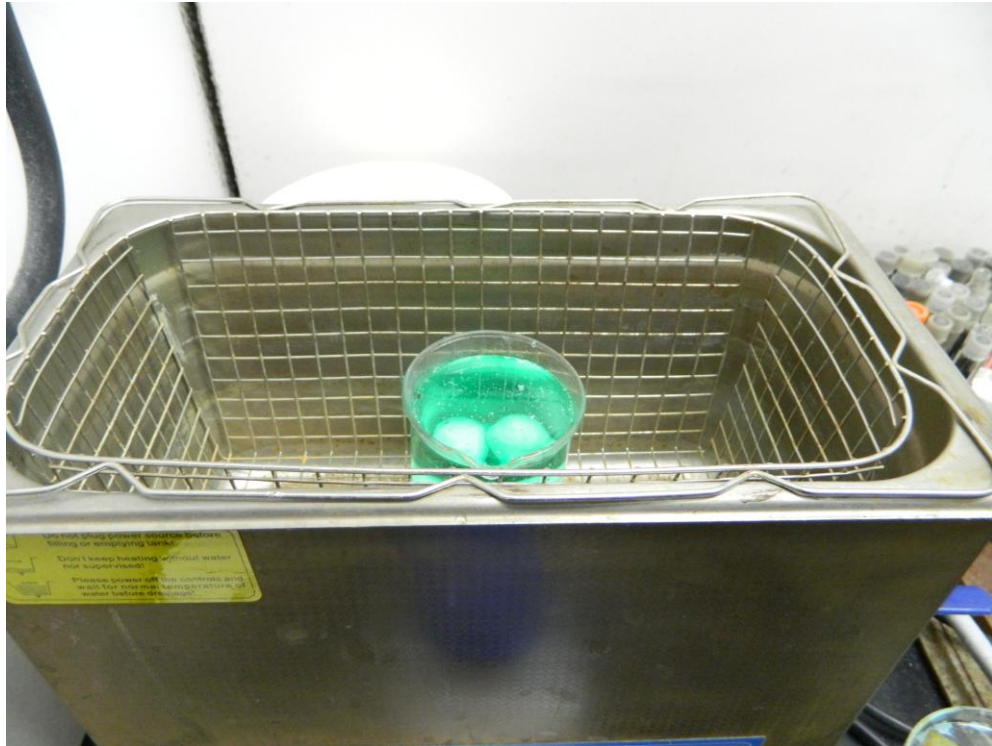

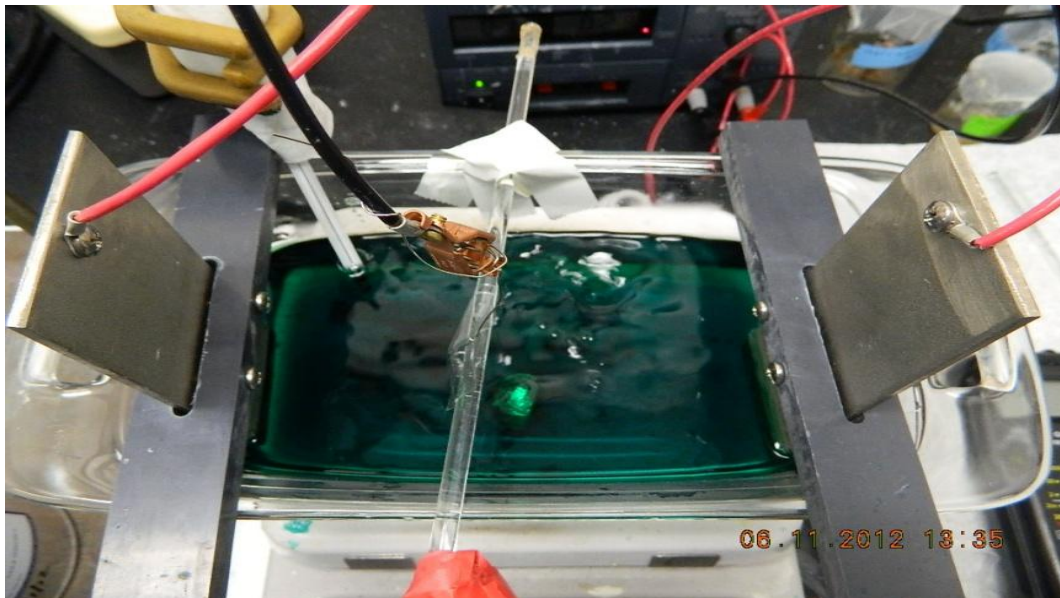Figure B-1: Electroless plating in ultra sonicator
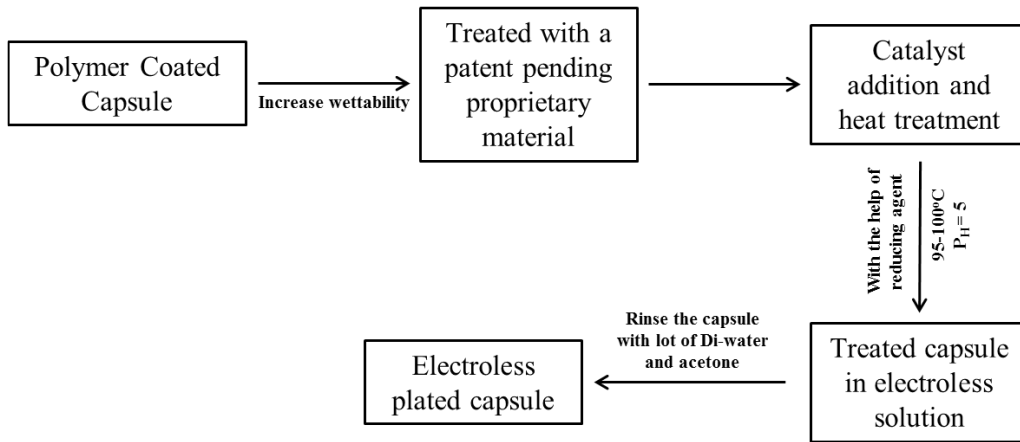

Figure B-2: Electroplating setup

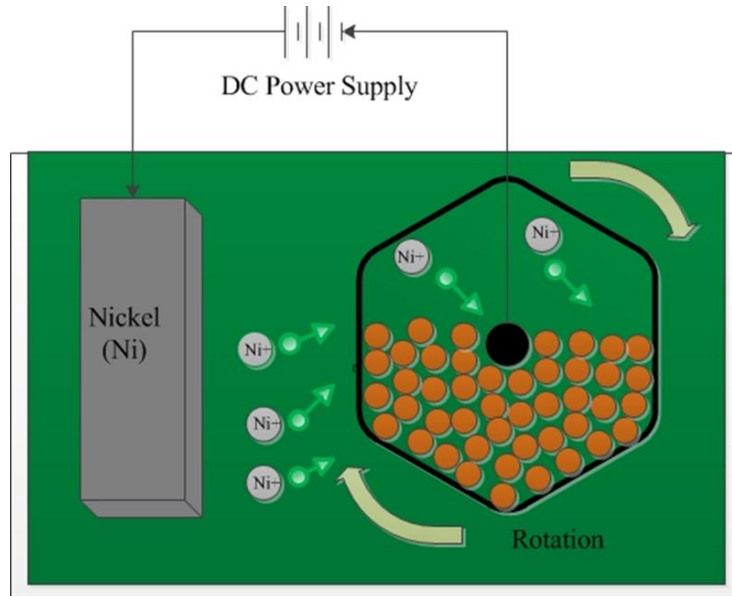Figure B-3: Flow chart of electroless plating process

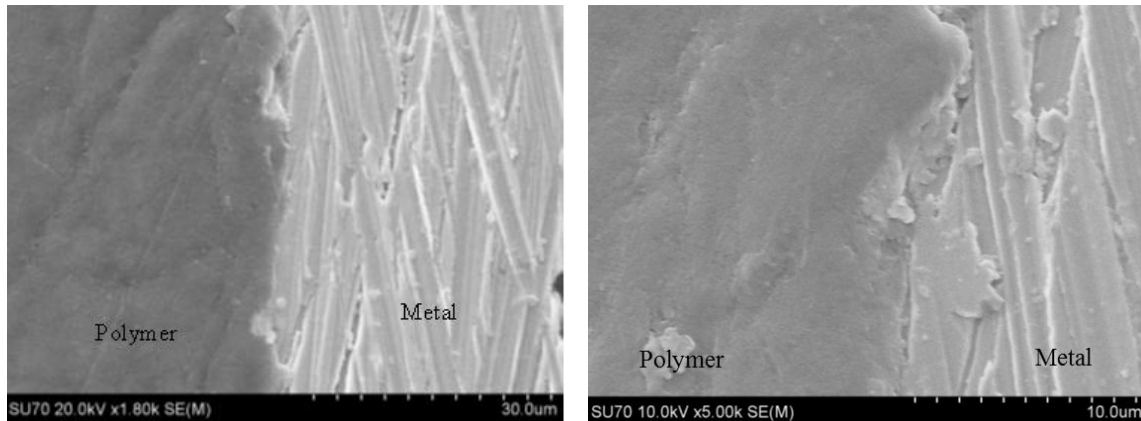Figure B-4: Schematic of electroplating process

Figure B-5: SEM image showing the bond between PTFE and plated metal layer

103

Product specification of electroless nickel is given below.

Product Number: Improved Electroless Nickel Plating Ammonia Free

Product: 44070

This solution is a vastly improved, electroless nickel (EN) preparation, formulated specifically for semiconductor use. The composition is based upon ions of a nickel complex and hypophosphite together in solution with a catalytic accelerator and a stabilizer. The solution is buffered at the optimum pH for EN catalysis. This formula is a very stable product, free of ammonia, and ready for use. Fume problems are eliminated. Also, it is not subject to undesirable changes in composition during use.

The reaction progresses catalytically with nickel deposition occurring at the operating temperature of 95 – 100 ºC. The nascent hydrogen evolved insures an oxide free nickel deposit. In addition, some NiP formed in a side reaction improves corrosion resistance and solderability. The nickel deposit is highly conductive, remains unstressed, particularly after suitable heat treatment, and shows good adherence.

Operating conditions
Appearance:	Green Solution
pH:	5
pH Control:	None needed
Operating Temperature:	90 – 98 ºC
Platable Materials:	Si, Ge, GaAs, CdS, Ni, Kovar
Plating Capacity:	1400 square inches/micron/gallon
Deposition Rate:	2000 Angstroms/minute at 95 ºC on Silicon
Shelf Life:	6 months
Storage:	Room Temperature

Physical Properties of Deposit
Composition of Deposit:	99+% Ni, 1% phosphide
Melting Point:	890 ºC
Specific Gravity:	7.85
Coefficient Of Expansion:	0.000130 in/in/ ºC
Reflectivity:	65%
Electrical Conductivity:	60 micro-ohm-cm
Thermal Conductivity:	0.01 cal/sq.cm/cm/ ºC/sec
Hardness (as plated):	500 Vickers
Solderability:	Excellent Flux not required above 500 ºC in hydrogen or forming gas atmosphere

Product specification of electroplating solution is given below.

Bath Composition Barrett SN Ready Mix* Option 1

	100 Gallon Bath	100 Liter Bath
Barrett SN*	100 gallons	100 liters

*The Barrett SN bath is supplied as a purified, ready-to-use solution that requires no dilutions, additions other than boric acid, or treatments prior to use. The composition of the Barrett SN solution is:

Nickel Sulfamate* (anhydrous)	327 g/L (43.6 oz/gal)
**Equivalent nickel metal concentration	76.5 g/L (10.2 oz/gal)
Boric acid	30 g/L (4.0 oz/gal)
Barrett Additive 'A' *	3 g/L (0.4 oz/gal)
Barrett SNAP® A/M (anti-pit agent)	0.3% by volume
Water	Balance

*Additive A is a chloride-bearing corrosion aid. If a bromide-bearing aid is preferred, Additive B can be used instead at a concentration of 1-3% by volume (2% typical).

Boric Acid

The boric acid concentration should be increased at operating temperatures above 32°C (90°F) as shown in the following chart:

Temperature	Boric Acid Conc.
32°C (90°F)	31.9 g/L (4.25 oz/gal)
43°C (100°F)	37.5 g/L (5 oz/gal)
49°C (120°F)	45 g/L (6 oz/gal)
54°C (130°F)	47 g/L (6.25 oz/gal)
60°C (140°F)	49 g/L (6.5 oz/gal)

NOTE: If operating temperatures are lower or allowed to vary after initial additions, the excess boric acid will precipitate out and must be filtered from the solution to prevent deposit roughness.

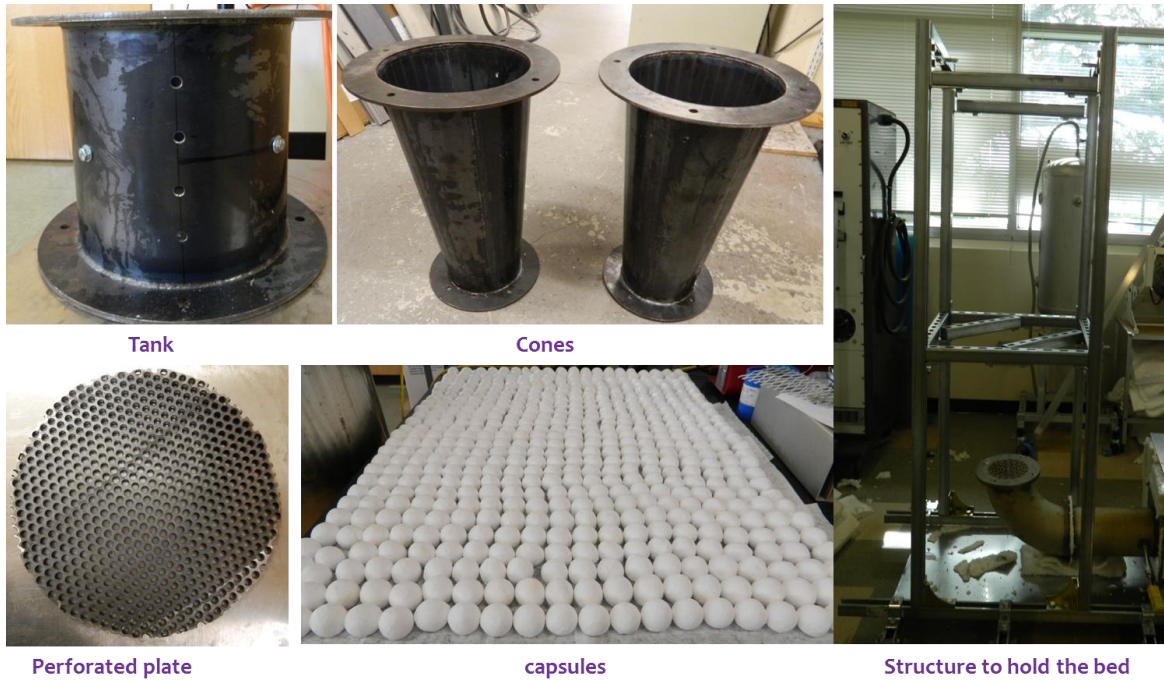## B.3 Supplemental Information on the LHS Packed-Bed Prototype System

Tank	**Cones**	
Perforated plate	**capsules**	**Structure to hold the bed**

Figure B-6: Different parts used in packed-bed setup

Figure B-7: Polymer encapsulated PCM

106

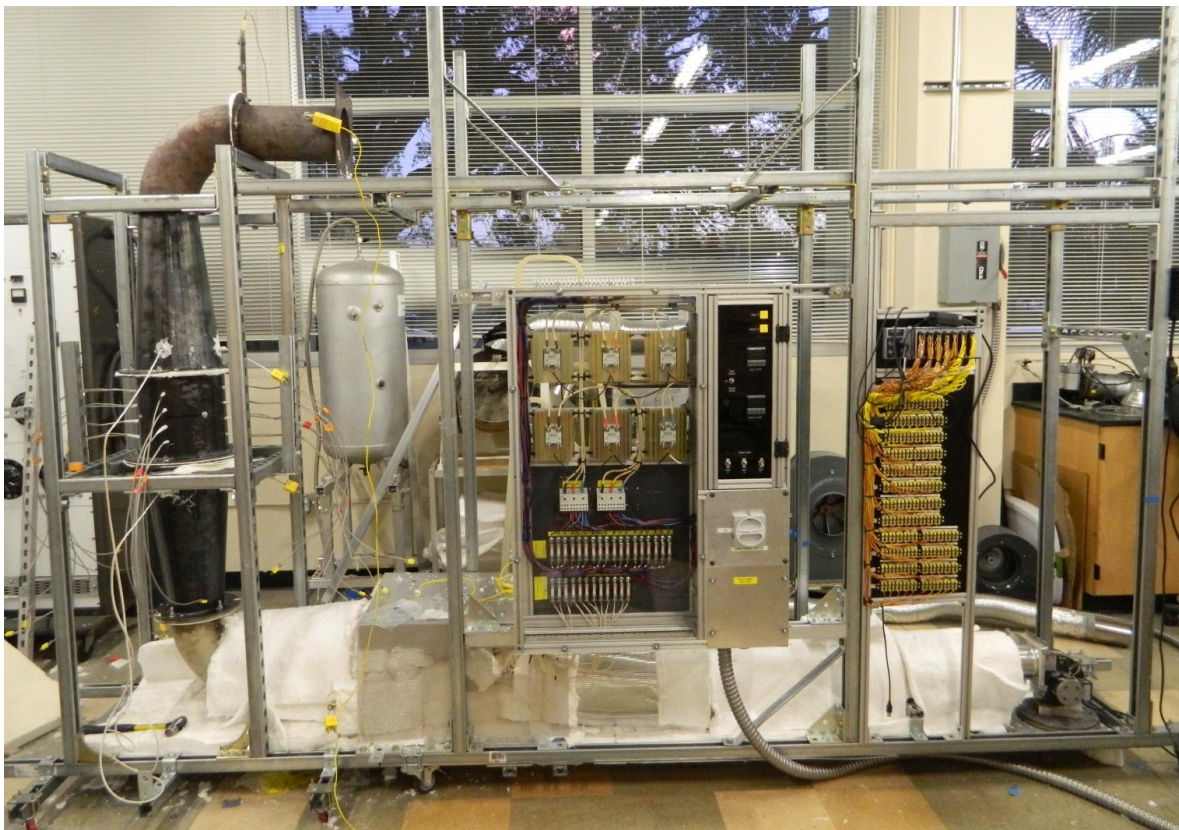Figure B-8: Randomly packed capsules inside the packed-bed

Figure B-9: Packed-bed setup without insulation

Appendix C. Copyright Permissions

Below is permission for the use of figure 2-3.

Order Completed

Thank you very much for your order.

This is a License Agreement between Tanvir E Alam ("You") and Elsevier ("Elsevier"). The license consists of your order details, the terms and conditions provided by Elsevier, and the payment terms and conditions.

Get the printable license.

License Number	3636161046261
License date	May 25, 2015
Licensed content publisher	Elsevier
Licensed content publication	Renewable and Sustainable Energy Reviews
Licensed content title	A review of materials, heat transfer and phase change problem formulation for latent heat thermal energy storage systems (LHTESS)
Licensed content author	Francis Agyenim,Neil Hewitt,Philip Eames,Mervyn Smyth
Licensed content date	February 2010
Licensed content volume number	14
Licensed content issue number	2
Number of pages	14
Type of Use	reuse in a thesis/dissertation
Portion	figures/tables/illustrations
Number of figures/tables/illustrations	1
Format	electronic
Are you the author of this Elsevier article?	No
Will you be translating?	No
Original figure numbers	figure 3
Title of your thesis/dissertation	Experimental Investigation of Encapsulated Phase Change Materials for Thermal Energy Storage
Expected completion date	Aug 2015
Estimated size (number of pages)	120
Elsevier VAT number	GB 494 6272 12
Permissions price	0.00 USD
VAT/Local Sales Tax	0.00 USD / 0.00 GBP
Total	0.00 USD

108

Below is permission for the use of material in chapter 3.

Order Completed

Thank you very much for your order.

This is a License Agreement between Tanvir E Alam ("You") and Elsevier ("Elsevier"). The license consists of your order details, the terms and conditions provided by Elsevier, and the payment terms and conditions.

Get the printable license.

License Number	3636170427701
License date	May 25, 2015
Licensed content publisher	Elsevier
Licensed content publication	Applied Energy
Licensed content title	Macroencapsulation and characterization of phase change materials for latent heat thermal energy storage systems
Licensed content author	None
Licensed content date	15 September 2015
Licensed content volume number	154
Licensed content issue number	n/a
Number of pages	10
Type of Use	reuse in a thesis/dissertation
Portion	full article
Format	both print and electronic
Are you the author of this Elsevier article?	Yes
Will you be translating?	No
Title of your thesis/dissertation	Experimental Investigation of Encapsulated Phase Change Materials for Thermal Energy Storage
Expected completion date	Aug 2015
Estimated size (number of pages)	120
Elsevier VAT number	GB 494 6272 12
Permissions price	0.00 USD
VAT/Local Sales Tax	0.00 USD / 0.00 GBP
Total	0.00 USD

Below is permission for the use of material in chapter 4.

Below is permission for the use of figure 5-4.

Order Completed

Thank you very much for your order.

This is a License Agreement between Tanvir E Alam ("You") and Elsevier ("Elsevier"). The license consists of your order details, the terms and conditions provided by Elsevier, and the payment terms and conditions.

Get the printable license.

License Number	3638731189276
License date	May 30, 2015
Licensed content publisher	Elsevier
Licensed content publication	International Communications in Heat and Mass Transfer
Licensed content title	Constrained and unconstrained melting inside a sphere
Licensed content author	F.L. Tan
Licensed content date	April 2008
Licensed content volume number	35
Licensed content issue number	4
Number of pages	10
Type of Use	reuse in a thesis/dissertation
Portion	figures/tables/illustrations
Number of figures/tables/illustrations	1
Format	both print and electronic
Are you the author of this Elsevier article?	No
Will you be translating?	No
Title of your thesis/dissertation	Experimental Investigation of Encapsulated Phase Change Materials for Thermal Energy Storage
Expected completion date	Aug 2015
Estimated size (number of pages)	120
Elsevier VAT number	GB 494 6272 12
Permissions price	0.00 USD
VAT/Local Sales Tax	0.00 USD / 0.00 GBP
Total	0.00 USD

ABOUT THE AUTHOR

Tanvir E Alam was born in Dhaka, Bangladesh on April 14, 1986. He completed his bachelor's degree in 2009 from Bangladesh University of Engineering and Technology. After receiving his bachelor's in Mechanical Engineering, he moved on to complete his higher education at University of South Florida. There, he completed his master's degree with a specialization in Material Science and his research focus was based on removing organic material and heavy metal from water by using graphene/metal oxide nanoparticles. In the summer of 2012, he joined the Clean Energy Research Center at the University of South Florida and started his doctoral program in Mechanical Engineering. In his PhD, he developed encapsulation techniques of high temperature phase change materials (PCMs) with polymer and metal coating for thermal energy storage system and constructed a packed-bed latent heat storage of ~1KWh$_{th}$.

Tanvir E Alam and Farhana Rahman were married on July 4, 2013 in Dhaka, Bangladesh.